Sustainable selective oxidations in confined spaces

Denekamp, I.M.

Publication date
2021
Document Version
Final published version

Sustainable selective oxidations in confined spaces

Ilse M. Denekamp

Sustainable selective oxidations in confined spaces

Ilse Maria Denekamp

ISBN: 978-94-6416-427-5

Cover: Yasmin Katlich, Ridderprint

Printing: Ridderprint, The Netherlands

Sustainable selective oxidations in confined spaces

ACADEMISCH PROEFSCHRIFT

ter verkrijging van de graad van doctor

aan de Universiteit van Amsterdam

op gezag van de Rector Magnificus

prof. dr. ir. K.I.J. Maex

ten overstaan van een door het College voor Promoties ingestelde commissie,

in het openbaar te verdedigen

op woensdag 7 april 2021, te 10.00 uur

door

Ilse Maria Denekamp

geboren te Purmerend

Promotiecommissie

Promotores:	prof. dr. G. Rothenberg	Universiteit van Amsterdam
	dr. D. Dubbeldam	Universiteit van Amsterdam
Overige leden:	prof. dr. E.J. Meijer	Universiteit van Amsterdam
	prof. dr. J.H. van Maarseveen	Universiteit van Amsterdam
	prof. dr. G.J.M. Gruter	Universiteit van Amsterdam
	prof. dr. S. Woutersen	Universiteit van Amsterdam
	prof. dr. ir. L. Lefferts	University of Twente
	prof. dr. S. Calero	Eindhoven University of Technology

Faculteit der Natuurwetenschappen, Wiskunde en Informatica

The research reported in this thesis was carried out at the Van't Hoff Institute for Molecular Sciences, Faculty of Science, University of Amsterdam and is part of the Sustainable Chemistry Research Priority Area. This work is part of the TOP-PUNT project *Catalysis in Confined Spaces* (718.015.004) with financial support of Nederlandse Organisatie voor Wetenschappelijk Onderzoek (NWO).

Het probleem is alleen als je heel veel van iets weet,
houd je geen verstand meer over
om het ook nog eens te begrijpen

De voorstelling 'na de pauze'
Herman Finkers

Table of Contents

List of abbreviations

BDMA	Butyldimethylamine
BHT	2,6-di-tert-butyl-4-methylfenol
C_2	Oxalyl chloride
C_6	Adipoyl chloride
C_{10}	Sebacoyl chloride
C_{TPA}	Terephthaloyl chloride
Ccit	Carbon prepared from citric acid precursor
Cr_xO_y	Chromium oxide
DBU	1,8-diazabicyclo[5.4.0]undec-7-ene
EXAFS	Extended X-ray absorption fine structure
FAU	Faujasite
FTIR	Fourier-transform infrared spectroscopy
H_2O_2	Hydrogen peroxide
H_2Pc	Metal-free phthalocyanine
H_2SO_4	Sulphuric acid
HCD	High current density
HNO3	Nitric acid
HRMS	High resolution mass spectrometry
KMnO4	Potassium permanganate
LCD	Low current density
LSV	Linear sweep Voltammetry
LTA	Linde type A
MALDI-TOF	Matrix-assisted laser desorption/ionisation-Time of Flight
MeCN	Acetonitrile
MPc	Metal phthalocyanine
NaOCl	Sodium hypochlorite
N:C	Nitrogen doped carbon
NMR	Nuclear magnetic resonance
NTA	Nitrolotriacetic acid

O_2	Oxygen
O_3	Ozone
OsO_4	Osmium tetraoxide
ORR	Oxygen Reduction Reaction
Pc	Phthalocyanine
PCA	Principal component analysis
PcF16	Fluorinated phthalocyanine
PPh3	Triphenylphosphine
p-XRD	Powder X-ray diffraction
RDS	Rate-Determining step
RRDE	Rotating ring-disk electrode
SBU	Secondary building block
SDA	Structure directing agent
SEC	Size exclusion chromatography
SEM	Scanning Electron Microscopy
SOD	Sodalite
SPM	Scanning probe microscopy
TBA	Tributylamine
TEM	Transmission electron microscopy
TGA	Thermal gravimetric analysis
TPR	Temperature-programmed reduction
XAS	X-ray absorption spectroscopy
XPS	X-ray photoelectron spectroscopy

Introduction

Chapter 1

1.1 Global to local production

Sustainable chemistry is now more important than ever, especially since the beginning of the 21st century, as worldwide trade has advanced rapidly, spurred by ever-growing cheap and fast internet access. Besides technical advances, tariffs and other trade barriers were reduced, opening up global trade. Using airfreight and the Internet, transport of international goods became more commonplace and efficient. This enabled producers to locate each stage of their production processes in countries where production costs are the lowest. The low-cost/long-distance trade has been the key to global economic growth. Thanks to this growth, most people are better off in the 21st century compared to the 20th, with less poverty and an overall increase in life quality. Notably, China's economy has grown quickly, closing the gap with Europe and North America.[1–3]

However, economic growth has been put on a sudden hold due to the COVID-19 pandemic. With forced lockdowns, the gathering of raw materials, the production of goods and its shipping have all taken a hard hit. The pandemic has complicated shipping globally and this will have lasting effects. The largest market affected is the oil industry. Future contract prices fell in April 2020, for the first time in history, to negative values, due to suppliers' fear of not being able to store their oil. Border closures reduced flight and road traffic, lowering the demand for oil. With COVID-19 containment measures remaining in place for months to come, the world economy won't return quickly to its pre-pandemic activity level.

Besides the effect of COVID-19 on the oil price and the transport industry, there are other signs of changing economics. The economies of China and India are growing at a fast but unsustainable pace.[4] China is expected to dominate the global economy by 2030, resulting in an increase of both work opportunities and average wealth there. This means higher salaries, better working conditions and in general more expensive end products. With overall processes becoming more expensive, producers might choose to relocate, saving on shipping and/or seeking lower cost production locations, such as

Africa. The final point that is influencing the global economy is the political climate. We see many conflicting countries and regions, such as China vs the US, Europe dealing with Brexit, and tensions between Russia and the Middle East.[5] These conflicts already have made marks in countries moving their production. Asian companies fear the tariffs war between China and the US. These aren't small companies either. Japanese giants Mitsubishi Electric and Toshiba Machine Co. started relocating in July 2018.[6] Others, such as Compal (Taiwan) and LG Electronics (South Korea) have emergency plans ready in the event that this conflict escalates further.

The pandemic is pushing de-globalisation further. With the paralysis of production and global transport industries, some countries are moving manufacturing back home. Many do not wish to rely on authoritarian governments for essential goods. Local industry and food production will increase, giving independence to countries and ecological benefits. Japan has announced a €2Bn stimulus package to shift manufacturing out of China, avoiding the effect the virus has on supply chains. Higher tariffs and sanctions will push other foreign companies out of China. The US is building an Economic Prosperity Network, a network of trusted partners which develop common standards in areas such as digital business, energy, education and commerce. This includes Australia, India, Japan, New Zealand, South Korea and Vietnam, with a goal to prevent a trade disruption like the current one from repeating.[7]

This shift in production will change how products are manufactured. Expect more use of local resources, local production and local consumption. All of these bring their own challenges to the table. Using local resources means not all raw materials will be available for certain processes, but it can also lead to new technologies.[8,9] One well-known example is the shortage of crude oil in South Africa due to the international embargo during the Apartheid period. To overcome this shortage, Sasol became the world leader in coal gasification and synthetic fuel production via the Fischer-Tropsch synthesis. Eventually, this development benefitted the whole world.

Local production and local consumption would lead to higher labour costs, but also to less transport. This decrease in transport will reduce oil demand. Some energy companies might shift their focus more towards chemicals, where they can still obtain high value. For example, Saudi Aramco and Sabic are planning a new complex in Yanbu, Saudi Arabia, for making petrochemicals. This complex will make 9 million metric tons of petrochemicals from 400,000 barrels of oil per day. Roughly 45% of the output of the facility will be chemicals, such as olefins, aromatics, glycols and polymers.[10,11]

This shift in production, processes and materials opens opportunities to redesign more sustainable processes. Indeed, the pandemic is showing us how we can improve our world by traveling less. In 2020, air quality levels in major world cities have improved considerably, with lower CO_2, NO_x, ozone and particulate matter.

1.2 Defining green and sustainable chemistry

Sustainability is extremely important in this discussion. The desired change in the chemical industry relies on green chemistry. Sustainability and green chemistry are often described together, with sustainability being a wider concept, applicable to any science. Green chemistry, defined by Anastas and Warner in 1991,[12] shows how chemistry can contribute to sustainable processes. The **12 principles of green chemistry** give guidelines for analysing the potential for environmental improvement, as follows:

1. *Prevent waste*; It is better to prevent waste than to treat or clean up waste after it has been created.
2. *Atom economy*; Synthetic methods should be designed to maximize incorporation of all materials used in the process into the final product.
3. *Less hazardous synthesis*; Wherever practicable, synthetic methods should be designed to use and generate substances that possess little or no toxicity to human health and the environment.
4. *Design benign chemicals*; Chemical products should be designed to preserve efficacy of function while reducing toxicity.

5. *Benign solvents & auxiliaries*; The use of auxiliary substances (e.g., solvents, separation agents) should be made unnecessary wherever possible and, innocuous when used.
6. *Design for energy efficiency*; Energy requirements should be recognized for their environmental and economic impacts and should be minimized. Synthetic methods should be conducted at ambient temperature and pressure.
7. *Use renewable feedstocks*; A raw material or feedstock should be renewable rather than depleting whenever technically and economically practicable.
8. *Reduce the number of derivatives*; Unnecessary derivatization (use of blocking groups, protection/deprotection, temporary modification of physical/chemical processes) should be minimized or avoided if possible, because such steps require additional reagents and can generate waste.
9. *Catalyst*; Catalytic cycles using benign reagents (as selective as possible) are superior to wasteful non-catalytic processes.
10. *Design for degradation*; Chemical products should be designed so that at the end of their function they break down into innocuous degradation products and do not persist in the environment.
11. *Real Time analysis for pollution prevention*; Analytical methodologies need to be further developed to allow for real-time, in-process monitoring and control prior to the formation of hazardous substances.
12. *Inherently benign chemistry for accident prevention*; Substances and the form of a substance used in a chemical process should be chosen to minimize the potential for chemical accidents, including releases, explosions, and fires.

Note that these guidelines were formulated for a linear production chain, whereas today we aim more and more towards circular processes. In a circular process, materials are fed back into the process to be reused, getting the most out of the resource and preserving restock. The principles of circular chemistry focus on a closed-loop, waste-free chemical industry, with principles such as collect and use waste, enhance process efficiency and target optimal design.[13]

Sustainable chemistry covers the avoidance of hazardous materials (benign chemicals), using renewable resources (optimize resource efficiency), minimising negative environmental effects (no out-of-plant toxicity) and gives technologies that are economically competitive for and advantageous to industry. Taking this into account for the redesign of processes, local production is taking advantage of local resources. Local resources will heavily influence the possible production process we can use for them. New processes are often less optimised compared to the older ones, because either they are brand new, or never optimised. We can design processes that fit the green chemistry guidelines, making it sustainable and interesting for industry.

Where many of the 12 principles suggest safer chemical design and the use of renewable resources, using catalysts should be highlighted more. Sustainable production requires better processes and for numerous catalytic processes this means a better catalyst. The dictionary defines a catalyst as a substance that increases the rate of a chemical reaction without itself undergoing any permanent chemical change. This means a catalyst can either change the selectivity of a reaction and/or its yield. The selectivity is the ratio between the products of the reaction. In an ideal world, only one wanted product would be made, but unfortunately, more often than not, multiple unwanted by-products are created. The yield is the product of selectivity x conversion. Ideally, we want a yield of 100%, but in practice this is rarely the case.

1.3 Controlling reactions through catalysis

Here catalysts can make a big difference. Roughly 80% of the industrial chemical synthesis depends on heterogeneous catalysis for bulk chemical production. With a few exceptions such as hydroformylation and the Shell Higher Olefins Process, homogeneous catalysis is more common in small-volume synthesis, such as fine-chemicals and pharmaceuticals manufacturing. The advantage of a heterogeneous catalyst is that it can easily be removed or recovered from a synthesis, saving on separation costs and energy. Moreover, heterogeneous catalysts can often be reactivated simply through a chemical or heat treatment.

What we want to achieve are processes with less waste, a higher selectivity (product ratio) and not compromising on yield (desired product formed). We can reach these goals by having less separation of different products and using a smaller recycling stream to achieve a higher selectivity. Catalysts can help with obtaining a higher selectivity and or a higher yield. Catalysts typically speed up a reaction by reducing activation energies or changing the reaction mechanism.

The need for catalysts is evident for most reactions, but oxidation reactions are a special case. These reactions are necessary in many chemical processes. Roughly 60% of all industrial chemical reactions are oxidation reactions, with almost all chemical products or intermediates containing an oxygen functional group.[14] The problem with oxidative reactions is that oxygen is very stable. While this is a good thing for our normal daily lives, it is bad news for those who want to do oxidative chemistry. In order to do oxidative reactions, we either have to use stronger oxidants, with all their hazards and environmental consequences, or a catalyst to activate oxygen. However, this isn't the only issue. Oxidation reactions are challenging, with low selectivity being a big problem. Common causes include over-oxidation of the material due to harsh reaction conditions, a too-powerful oxidant and the final product of a reaction being usually easier to oxidise than the starting material. This is because the activation energy of the final product being lower compared to the starting material, making a final product more sensitive to being oxidised. A good example of this is the synthesis of methanol from methane, a reaction that has sparked much scientific interest for many years. Currently methanol is obtained through an indirect, energy-intensive route via syngas. This is done on huge scale in even larger plants, see **Figure 1**. The direct oxidation of methane to methanol could fix this problem. However, this solution has a big thermodynamic challenge.

Figure 1: Methanol plant from Atlantic Methanol in West Africa that produces 1,000,000 metric tons of methanol per year. Photo from atlanticmethanol.com reproduced with permission.

Methane is a very stable molecule, having a low electron and proton affinity, low polarity and a strong C–H bond of roughly 440 kJ mol^{-1}.[15] It can be oxidised to methanol, but methanol has a C–H bond of a little below 410 kJ mol^{-1},[16] making this a weaker bond compared to methane, and also easily oxidised, going to formaldehyde, continuing to formic acid and ending up in being completely oxidized to carbon dioxide.[17] Simply stated; the reaction conditions required to oxidise methane to methanol will result in over-oxidation to CO_2 and water.[18] As shown in **Figure 2**, the further oxidation of methanol to formaldehyde, formic acid and CO_2 are all strongly exothermic, increasing the likelihood of over-oxidation. Controlling these reactions is difficult, and where nature is capable of performing some of these reactions, we scientists struggle.

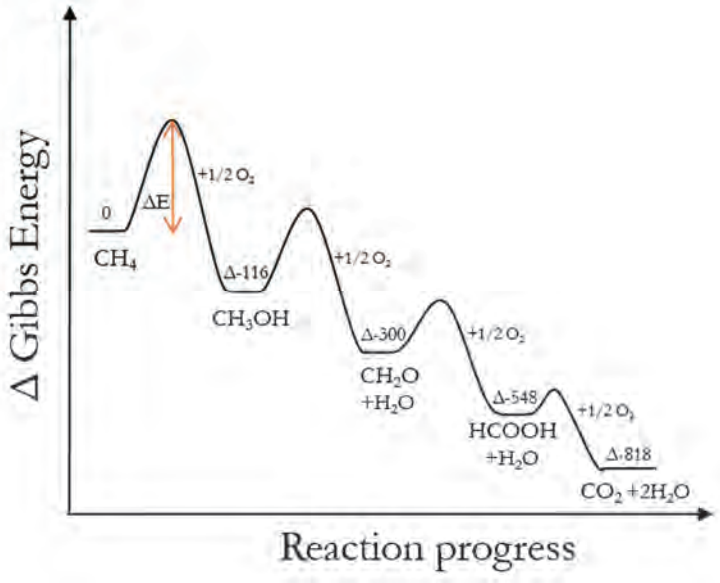

Figure 2: Energy diagram of the oxidation of methane to methanol, formaldehyde, formic acid and CO_2.

1.4 Controlling reactions through oxidative agents

With oxidation reactions being so important for the production of materials, how can we gain control over these reactions and end up with a high selectivity and yield? We need to control two aspects, one of which is the oxidant used. There are many oxidative agents, so it should be possible to find at least a few sustainable options. However, some will be very strong and will oxidise everything, causing a lot of unnecessary waste or toxic side products. Others may be too selective, useful only in a few specific reactions. Here we will compare multiple oxidative agents, on their availability (are they available locally), cost (dollar per ton), environmental impact (energy and CO_2 footprint), adaptability (how universal are they) and their reactivity (how easily are they activated). Here, we use oxidants as compounds that can donate an oxygen atom and accept electrons. **Figure 3** shows a comparison between the several options: oxygen, ozone, sodium hypochlorite, sulphuric acid, nitric acid, permanganate, osmium tetraoxide and hydrogen peroxide. In this type of graph, the longer the axes (larger web), the better the result for that category.

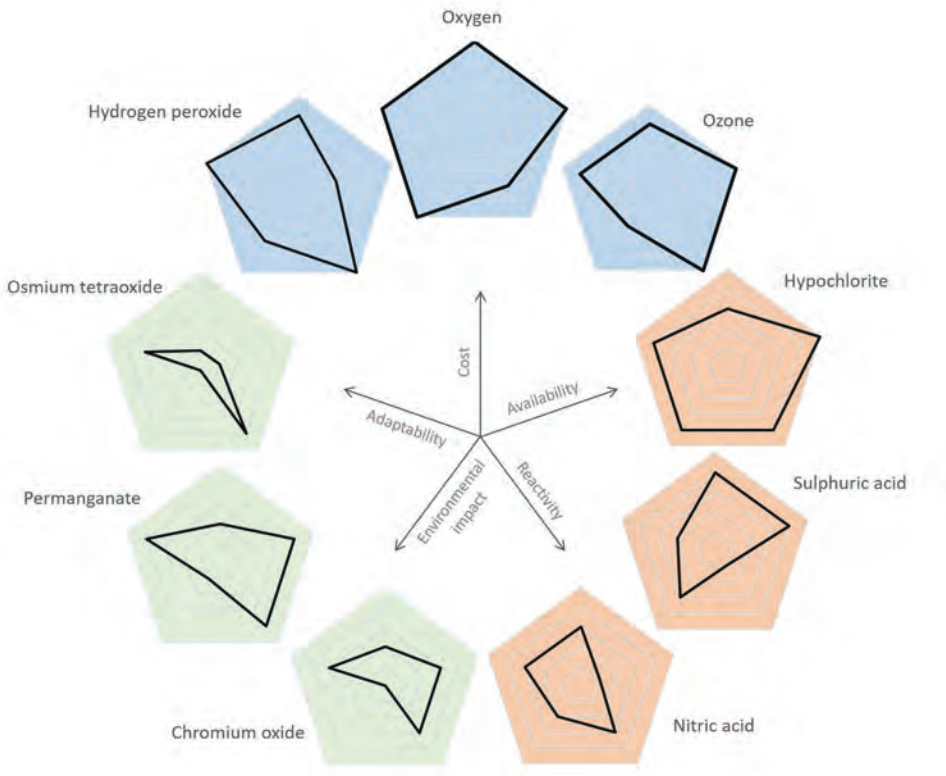

Figure 3: Comparative overview of different oxidative agents. The further the point on the web, the better the catalyst is in that category. Blue webs represent the pure oxygen oxidants, green webs denote metal-based ones and orange webs denote acid/base oxidants.

Oxygen (O_2) is freely available in the air, making it the cheapest and most abundant oxidant. For its environmental impact, we can split oxygen up in two cases; one is air (20.95 vol% of oxygen), the other is pure oxygen. Pure oxygen has a downside in that it needs to be diluted before use. This is to scavenge free radicals, to adsorb and desorb the reactant from the catalyst and to acts as a heat-transfer medium. The nitrogen in the air already acts as the diluent, even though it doesn't scavenge radicals well and is not a good heat-transfer medium. The upside of pure oxygen is that it is a pure reactant, giving a smaller footprint, and a better reactor space/time yield. When air is used, a larger reactor is required to compensate for the nitrogen volume.[19] For the production

of pure oxygen there are factors to consider, such as energy input. However, commercial oxygen is one of the most significant chemicals. It can be manufactured wherever needed and is therefore not traded on the international market, and making it requires roughly 2.8 kWh/kg.[20] In general, using oxygen from air does not form a hazard, and even pure oxygen is not as dangerous compared to other oxidative agents. It has no GHS labels and a release into the environment is not a problem. A downside for oxygen is its high activation barrier, due to its resonance stability.[21] However, once it is activated it can react using free-radicals with many compounds. The downside here is that over-oxidation is frequent.

Ozone (O_3) can be made from water and air, making it a process that can be conducted everywhere with different methods. One kg of ozone requires roughly 10 kWh of energy and 8.3 kg of oxygen,[20] which is quite cheap, on the same level of pure oxygen and hydrogen peroxide. It is adaptable for many reactions and easily produced. The most common method of making ozone is by dissociating oxygen, either photochemically or electrically. The latter is practical, efficient for large scale quantities and can be made on location. Using pure oxygen for the generation of ozone is preferred, due to the absence of by-products, the lack of corrosion due to the moisture content in atmospheric air and the smaller generator required. However, ozone is highly reactive and therefore forms a risk to work with, having 4 GHS labels; oxidizers, carcinogen, toxic to aquatic environment and acute toxic. An ozone spill will affect the surrounding area, particularly the plant life, however because it naturally decomposes any effect will be limited and bioaccumulation does not occur.

Sodium hypochlorite (NaOCl), also known as bleach, is made by the Hooker process, where chlorine gas is passed into a cold sodium hydroxide solution. The chlorine is prepared by electrolysis and the entire process is not limited by any hard-to-get chemicals and uses ~3.5 kWh/kg.[20] Sodium hypochlorite is often used to oxidise primary and secondary alcohols. Besides this, it is easily stored and safe to transport.

However, the GHS classification shows that it burns skin and is toxic to the environment, especially to aquatic life.

Sulphuric acid (H_2SO_4) is produced from sulphur, oxygen and water via the contact process. Sulphur trioxide is made using a vanadium(V)oxide catalyst, the vanadium being sourced from South Africa, Russia and China. Countries can also make the catalyst from local resources. Vanadium is also a by-product of the oil industry, so its availability is guaranteed in the coming decades (although sulphur is not prominent in every country). However, to use sulphuric acid as an oxidative agent you need a concentrated solution, and is often used to oxidise metals. It is a corrosive material and should not be released into the environment.

For the production of **nitric acid (HNO_3)**, ammonia, oxygen and a platinum and rhodium catalyst are necessary. Platinum is mined in Canada, Russia, South Africa, USA, Zimbabwe and Australia, and Rhodium in South Africa and North America. As an oxidative agent, nitric acid reacts violently with many organic materials, and is even used as a rocket propellant. It is often used to oxidise primary alcohols. However, it is difficult to handle and can break down the catalyst. On top of this, the fumes of nitric acid are toxic and cause injury or even death.

Chromium oxide (Cr_xO_y) is only mined in South Africa and the Middle East. However, there are many species of chromium oxide, ranging from chromium(II)oxide to chromium(VI). For this, we are focussing on chromium trioxide, since this is the most stable form and a strong oxidizing agent.[22] Again used for mostly primary and secondary alcohols, it will explode on contact with organic compounds and solvents. Therefore, it is also quite dangerous to work with, having GHS labels oxidizing, acutely toxic, corrosive and carcinogen, scoring the lowest number possible on environmental impact. Chemical companies avoid using Cr(VI), and many shun all chromium species.

Potassium permanganate ($KMnO_4$) is made of manganese and potassium hydroxide, both widely available. Other methods include the MnO_2 ore fusion followed by electrolysis, however this has a high energy consumption (15 kWh/kg).[20] Potassium

permanganate is a very powerful oxidizing agent. This oxidative agent has the unique property that it functions as one on all pH levels and in most solvents, making it very adaptable and often used for the oxidation of double bonds, olefins and aromatic side chains.

Osmium tetroxide (OsO_4) is made of osmium and not easily accessible for all countries. However, it is a dirty oxidiser, with short exposure leading to serious injury. It has the GHS labels for deadly, toxic and dangerous to the touch. It is a hard to handle compound and not used very often.

The last one is **hydrogen peroxide (H_2O_2)**, which must be made in bulk to be profitable, and can be made by the anthraquinone process, which is energy efficient (>3.5 kWh/kg).[20,23] In this process, 2-alkyl-9,10-anthraquinones reacts with hydrogen to form hydroquinones. This is oxidized to quinones using air and yield hydrogen peroxide. The quinones is recycled back into the feed loop.[24,25] H_2O_2 is even made in living organisms using enzymes. While its toxicity is low, it can cause skin irritation and burns.

Comparing the above oxidants, oxygen is clearly preferable. It is the only one that is abundant, free, suitable for most oxidative reactions and forms no environmental risk. Oxygen sounds like the ideal option, but it has limitations. It is thermodynamically stable and yet is capable reacting exothermically with almost all other elements.[21,26,27] This is prevented due to the large activation barrier.[28] Once this barrier is crossed, oxygen reacts violently. This causes over-oxidation, leading to CO_2 and H_2O as products. Using oxygen in a controlled selective manner is a challenge and ideas on how to do this can be found in nature. Every life-form uses oxygen and therefore is capable of doing very selective oxidative reactions.

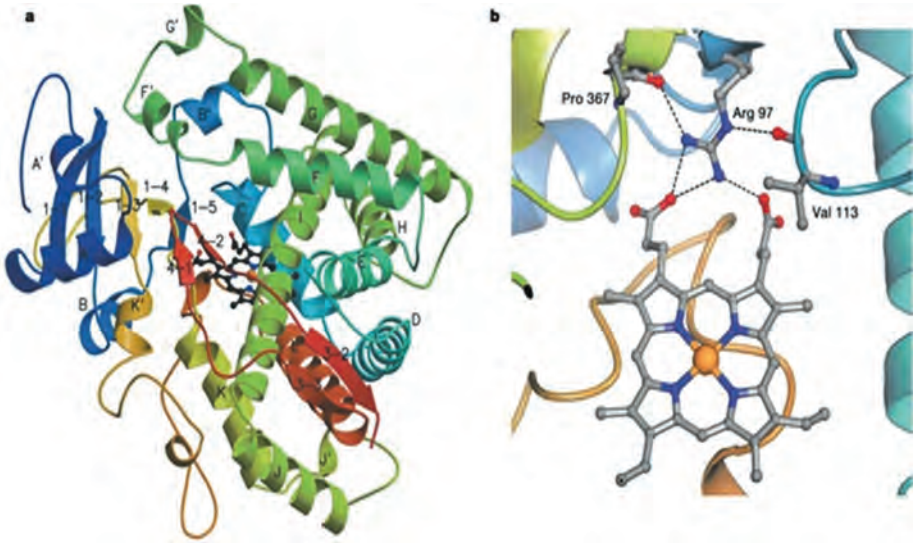

Figure 4: a. Overall fold of P450 CYP2C9. The haem group is depicted as a ball-and-stick model in the centre of the molecule, flanked by helices I and L. b. The haem group, with in orange the iron centre. Reprinted from ref. [29] *with permission from Nature.*

The biological answer to selective oxidation reactions are enzymes. In all forms of life, it is cytochromes P450, a family of enzymes that catalyse monooxygenase reactions. This entails the binding and splitting of dioxygen, after which the enzyme inserts a single oxygen atom into an organic substrate and reduces the other oxygen atom to water. The oxygen activation is performed by the single metal centre in the haem, located in the centre of P450. This haem is a porphyrin containing often a single iron atom. Porphyrin, shown in **Figure 4** on the left, is a ligand containing a metal centre surrounded by four nitrogen atoms.[29] This ring around the single-atom centre is crucial to the process, since it donates an electron during the process of the cleaving of the O–O bond.[30,31] However, the porphyrin cannot do the entire process alone. It is the enzyme protecting the haem centre and helping it achieve controllable oxygen activation. P450 comprises multiple α-helices, two of which are in contact with the haem group. One of these delivers a proton to stabilize the peroxo intermediate formed in the oxidative process. Another amino acid spatially close to haem, containing a thiol group, works together with the iron centre to selectively create a Fe–S bond, able to "push and pull", helping

in the activation of the O–O bond splitting and C–H activation. .[32] This "push and pull" system is done by having an strong electron donation ("push") from the thiol, increasing the electron density on the ferryl oxygen and this enhances the reactivity for the C–H bond activation ("pull").[33–35] It is clear from the functioning of haem, that the active site needs help from its environment. The haem group offers protection, necessary protons and a "pull and push" system, all nestled in perfectly within the enzyme. The confinement effect haem has is the key to high yield and selectivity in oxidation reactions.

1.5 Confinement effects in heterogeneous catalysis

Confinement effects can be found in nature, and we can mimic them in our materials. Since metal active site optimisation is often limited, it is beneficial to develop confinement effect to increase the activity of the catalyst. This confinement can be done in three different ways, geometric confinement, chemical confinement and space confinement, all with their own respective advantages and challenges.

Geometric confinement is the physical confinement around an active site. There are simple ways this can be achieved, one of them making a material with small pores, meaning a larger surface area per g of catalyst, which will increase the contact between substrate and catalytic surface. This will increase the yield of a reaction, but not the selectivity. To achieve geometric confinement, the size of the pores can be of great influence.[36]

An example of a geometric confinement effect can be found in several zeolites, also known as "molecular sieves". These have microporous channels that interconnect with cavities, with sizes of 2–20 Å, in the range of many molecular diameters.[37]

Zeolites are used in many different areas, mostly in the oil industry, but also as water softeners. They are easily modified to contain Brønsted and/or Lewis acid sites. However, the property that makes them interesting is their shape selectivity.[38] The active site inside the zeolite can only convert the substrate that can actually fit inside.

This can be divided in 3 categories; reactant selectivity, product selectivity, and transition-state selectivity (**Figure 5a**, **5b**, and **5c**, respectively).[39] The first excludes larger reactants from entering the pore, resulting in specific smaller reactants reacting. This mass-transfer effect ensures that in a mixture, only the desired reactant reacts. Shape selectivity will occur not only when a reactant doesn't fit into the pore, but also when the diffusion is sufficiently smaller than the smaller species.[40] The second category, product selectivity, occurs when the products form inside the pores, however only specific product shapes can exit the pore. The zeolite limits the formation of high mass-transfer limited products. This gives a very selective reaction, but it is only useful when the undesired products can convert to the desired product. Otherwise, these large and incorrectly shaped final products will block pores and therefore deactivate the catalyst.[41] The final category, transition-state selectivity, limits the shape of the transition state, prohibiting certain larger transition states and therefore allow only specific products.[42–48] All three categories of confinement increase the selectivity simply by changing the geometry of the catalyst.

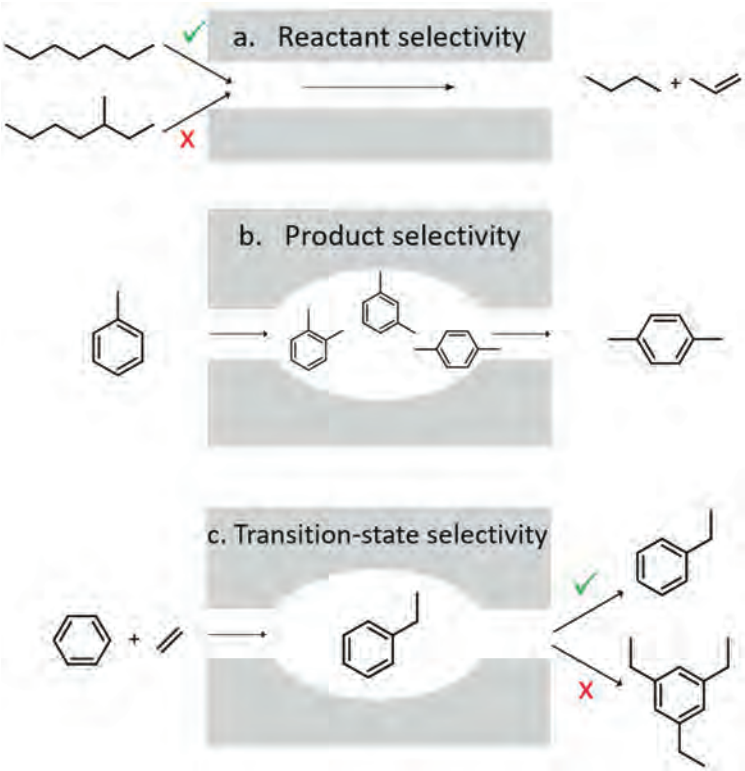

Figure 5: Shape selectivity in zeolites with examples of reactions. (a) Reactant selectivity: cleavage of hydrocarbons. (b) Product selectivity: methylation of toluene. (c) Restricted transition-state selectivity: disproportionation of m-xylene.

The second type of confinement that influences a reaction is **chemical confinement**. In this case, the surface of the catalytic material influences the binding of the substrate. This can either be that the reactant can only selectively bind, meaning only one side of the molecule can react. Another option is that the entire surface prevents binding at all. One of the advantages enzymes have is that they have binding pockets, causing a reactant to bind in a specific orientation to the active site.[49] We can try to recreate this, as done by Medlin *et al.* by adding thiolate self-assembled monolayers to substrates.[50] Changing the functional group of the hydrocarbon tails influences the interactions close to the surface, similar to the enzyme binding pockets. By doing this, reactants can only bind at the active site. Other examples can be found in homogeneous catalysis, where noncovalent interactions between reactant and catalyst occur. In this way small chiral

catalysts with specific ligands show enantioselectivity by reducing the ways the reactant can react with the active site.[51–53] Another option is changing the entire surface of an catalyst, i.e. very hydrophilic or hydrophobic.[54] This effect can be used in any reaction where reactant and product have different hydrophilicity, for example the methane to methanol reaction, where excess oxidation of the methanol might be prevented this way.

Finally, there is **spatial confinement**. This category differs from the other confinements since it is a unique interaction between the active sites and its direct surroundings; otherwise the reaction could not occur. One example is the "active doughnut" concept, where an active particle supported on an active site work together to create a doughnut-shaped volume around the active particle.[55] Here, the oxygen gets activated on the surface, and immediately reacts further using the active particle. This prevents the very reactive oxygen going into solution and prevents over-oxidation, therefore increasing the selectivity. Other examples are tandem reactions, where you make the reagent close to the active site, after which it can react further with the active site. The last example is solvent pockets, which can occur when a variety of solvents are used. Solvents can nestle inside the pores, creating small spaces that are more reactive than others.[46,56] Besides this specific effect, solvents have an influence on reactions, and choosing the right solvent is important.[57] All these effects can either help the yield of a reaction, and or the selectivity of products.

1.6 Objective and scope of this thesis

The previous sections showed the importance of sustainable production in our changing world. In my opinion, a key solution to these problems is to design catalysts for specific reactions. By optimising catalysts, we can achieve maximum selectivity and yield. This is tricky, especially in oxidative chemistry, where the right type of oxidant must be found and the chance of over-oxidation is always present.

The design of oxidation catalysts is the metaphorical red thread running throughout my thesis. Chapter 2 is about the selective oxidation of cyclohexene using metal oxides on nitrogen-doped carbon. The different reaction pathways are discussed, and how the surface and active site interact with each other and affect the selective oxidation of cyclohexene. The catalyst design combines nitrogen-doped carbon, that can activate oxygen, and metal particles, achieving high selectivity and yield. On top of this, it gives us insight into oxidative chemistry which we can use later on.

The third chapter discloses a novel synthesis of phthalocyanine, a catalyst related to haem. This catalyst is purposely chosen for oxidative chemistry. The single atom catalyst gives optimum use of the metal, and the ligand around it is suitable for industrial conditions. The synthesis procedure described in chapter 3 is then further applied in chapter 4. Here, the catalyst building blocks are further designed into a polymer, through a mix & match approach. By varying the distance between the active sites in the polymer, we can see the intermetal distance influencing the reaction. As we can easily change metal, active site distance and environmental effects in this catalyst, we control the confinement of the metal in the reaction. True design power is shown here.

Finally, in the fifth chapter we apply the knowledge that we gained on synthesis and design of catalysts to a new related problem. This is the synthesis and design of zeolites, a different type of confinement catalyst. The purpose here is to see if the approach we have developed over the previous chapters is translatable to new type of materials. Overall, I hope to show the you, the reader, that the design of catalysts is a right step into making our world more sustainable.

1.7 References

[1] A pillar of the European economy - cefic.org https://cefic.org /our-industry/a-pillar-of-the-european-economy/.

[2] Catalyzing growth and addressing our world's sustainability challenges, https://www.oxfordeconomics.comrecent-releases /the-global-chemical-industry-catalyzing-growth-and-addressing-our-world-sustainability-challenges.

[3] Chemicals 2025: Will the industry be dancing to a very different tune? | McKinsey, https://www.mckinsey.com/industries /chemicals/our-insights/chemicals-2025-will-the-industry-be-dancing-to-a-very-different-tune.

[4] The Indian chemical industry | McKinsey, https://www.mckinsey.com/industries/chemicals/our-insights/indias-chemical-industry-unleashing-the-next-wave-of-growth.

[5] Analysis | The U.S. and China finally signed a trade agreement. Who won?, *Wash. Post*.

[6] Japanese and other Asian firms shifting production from China as U.S. tariffs take toll, J. Park, M. Yamazaki, https://www.japantimes.co.jp/news/2018/09/23 /business/corporate-exodus-china-underway-fresh-u-s-tariffs-hit/, **2018**.

[7] Trump administration pushing to rip global supply chains from China: officials, *Reuters* **2020**.

[8] Grand challenges for catalysis in the Science and Technology Roadmap on Catalysis for Europe: moving ahead for a sustainable future, P. Lanzafame, S. Perathoner, G. Centi, S. Gross, E.J.M. Hensen, *Catal. Sci. Technol.* **2017**, *7*, 5182–5194.

[9] Sustainable Industrial Chemistry: Principles, Tools and Industrial Examples, F. Cavani, G. Centi, S. Perathoner, F. Trifirò, *Sustainable Industrial Chemistry: Principles, Tools and Industrial Examples*, John Wiley & Sons, **2009**.

[10] Why the future of oil is in chemicals, not fuels, https://cen.acs.org/business/ petrochemicals/future-oil-chemicals-fuels/97/i8.

[11] Aramco and SABIC advance oil-to-chemicals, https://cen.acs.org /articles/95/i48/Aramco-SABIC-advance-oilchemicals.html.

[12] "Happy silver anniversary": Green Chemistry at 25, P. Anastas, B. Han, W. Leitner, M. Poliakoff, *Green Chem.* **2015**, *18*, 12–13.

[13] Circular chemistry to enable a circular economy, T. Keijer, V. Bakker, J.C. Slootweg, *Nat. Chem.* **2019**, *11*, 190–195.

[14] New concepts and new strategies in selective oxidation, G. Centi, F. Cavani, F. Trifirò, in *Sel. Oxid. Heterog. Catal.* (Eds.: G. Centi, F. Cavani, F. Trifirò), Springer US, Boston, MA, **2001**, pp. 325–362.

[15] Platinum catalysts for the high-yield oxidation of methane to a methanol derivative, R.A. Periana, D.J. Taube, S. Gamble, H. Taube, T. Satoh, H. Fujii, *Science* **1998**, *280*, 560–564.

[16] Theoretical study of the bond dissociation energies of methanol, C.W. Bauschlicher, S.R. Langhoff, S.P. Walch, *J. Chem. Phys.* **1992**, *96*, 450–454.

[17] Recent progress in direct conversion of methane to methanol over copper-exchanged zeolites, M.B. Park, E.D. Park, W.S. Ahn, *Front. Chem.* **2019**, *7*, DOI 10.3389/fchem.2019.00514.

[18] Misconceptions and challenges in methane-to-methanol over transition-metal-exchanged zeolites, M. Ravi, V.L. Sushkevich, A.J. Knorpp, M.A. Newton, D. Palagin, A.B. Pinar, M. Ranocchiari, J.A. van Bokhoven, *Nat. Catal.* **2019**, *2*, 485–494.

[19] Oxygen, M.J. Kirschner, A. Alekseev, S. Dowy, M. Grahl, L. Jansson, P. Keil, G. Lauermann, M. Meilinger, W. Schmehl, H. Weckler, et al., in *Ullmanns Encycl. Ind. Chem.* (Ed.: Wiley-VCH Verlag GmbH & Co. KGaA), Wiley-VCH Verlag GmbH & Co. KGaA, Weinheim, Germany, **2017**, pp. 1–32.

[20] Environmental fate and effects of pulp and paper: Mill Effluents, M.R. Servos, *Environmental Fate and Effects of Pulp and Paper: Mill Effluents*, CRC Press, **2020**.

[21] Dioxygen: what makes this triplet diradical kinetically persistent?, W.T. Borden, R. Hoffmann, T. Stuyver, B. Chen, *J. Am. Chem. Soc.* **2017**, *139*, 9010–9018.

[22] Stability of chromium oxides, M.A. Mosesman, *J. Am. Chem. Soc.* **1954**, *76*, 295–296.

[23] Energy efficiency in ECF and TCF bleaching, T. Laxen, K. Henricson, *Pulp Pap. Can.* **1996**, *97*, 58–62.

[24] Hydrogen peroxide, G. Goor, J. Glenneberg, S. Jacobi, in *Ullmanns Encycl. Ind. Chem.*, American Cancer Society, **2007**.

[25] Oxygen activation and oxygen toxicity, E.F. Elstner, *Annu. Rev. Plant Physiol.* **1982**, *33*, 73–96.

[26] The role of oxygen in catalysis, J. Haber, E.M. Serwicka, *React. Kinet. Catal. Lett.* **1987**, *35*, 369–379.

[27] Oxygen activation, C.R. Jefcoate, V. Ullrich, E. Antonini, A. Cimino, J.E. Germain, R.D. Gillard, J.A. Ibers, R. Lontie, A. Martell, R. Ugo, in *Catal. Prog. Res.* (Eds.: F. Basolo, R.L. Burwell), Springer US, Boston, MA, **1973**, pp. 155–164.

[28] Why combustions are always exothermic, Yielding About 418 kJ per mole of O_2, K. Schmidt-Rohr, *J. Chem. Educ.* **2015**, *92*, 2094–2099.

[29] Crystal structure of human cytochrome P450 2C9 with bound warfarin, P.A. Williams, J. Cosme, A. Ward, H.C. Angove, D. Matak Vinković, H. Jhoti, *Nature* **2003**, *424*, 464–468.

[30] Cytochrome P450: Structure, Mechanism, and Biochemistry, P.R.O. de Montellano, *Cytochrome P450: Structure, Mechanism, and Biochemistry*, Springer Science & Business Media, **2005**.

[31] How do enzymes activate oxygen without inactivating themselves?, J.P. Klinman, *Acc. Chem. Res.* **2007**, *40*, 325–333.

[32] Oxygen activation by cytochrome P450 monooxygenase, D. Hamdane, H. Zhang, P. Hollenberg, *Photosynth. Res.* **2008**, *98*, 657–666.

[33] Using push to get pull, J.T. Groves, *Nat. Chem.* **2014**, *6*, 89–91.

[34] Synthesis of novel push- pull unsymmetrically substituted alkynyl phthalocyanines, E.M. Maya, C. García, E.M. García-Frutos, P. Vázquez, T. Torres, *J. Org. Chem.* **2000**, *65*, 2733–2739.

[35] Rewiring the "Push-Pull" catalytic machinery of a heme enzyme using an expanded genetic code, M. Ortmayer, K. Fisher, J. Basran, E.M. Wolde-Michael, D.J. Heyes, C. Levy, S.L. Lovelock, J.L.R. Anderson, E.L. Raven, S. Hay, et al., *ACS Catal.* **2020**, *10*, 2735–2746.

[36] Adsorption and catalysis: The effect of confinement on chemical reactions, E.E. Santiso, A.M. George, C.H. Turner, M.K. Kostov, K.E. Gubbins, M. Buongiorno-Nardelli, M. Sliwinska-Bartkowiak, *Appl. Surf. Sci.* **2005**, *252*, 766–777.

[37] Catalysis: An Integrated Textbook for Students, U. Hanefeld, L. Lefferts, *Catalysis: An Integrated Textbook for Students*, Wiley-VCH, **2018**.

[38] Adsorption and tautomerization reaction of acetone on acidic zeolites: The confinement effect in different types of zeolites, B. Boekfa, P. Pantu, M. Probst, J. Limtrakul, *J. Phys. Chem. C* **2010**, *114*, 15061–15067.

[39] Shape-selective catalysis: Zeolites, in *Ind. Catal.*, Wiley-VCH Verlag GmbH & Co. KGaA, Weinheim, Germany, **2015**, pp. 239–260.

[40] Molecular shape selective catalysis, P.B. Weisz, *Pure Appl. Chem.* **1980**, *52*, 2091–2103.

[41] Shape-selective catalysis in zeolites, S.M. Csicsery, *Zeolites* **1984**, *4*, 202–213.

[42] Determining the topology of zeolites by adsorption microcalorimetry of organic molecules. Dedicated to Professor Lovat V.C. Rees in recognition and appreciation of his lifelong devotion to zeolite science and his outstanding achievements in this field. J.M. Guil, R. Guil-López, J.A. Perdigón-Melón, A. Corma, *Microporous Mesoporous Mater.* **1998**, *22*, 269–279.

[43] The confinement effect in zeolites, G. Sastre, A. Corma, *J. Mol. Catal. Chem.* **2009**, *305*, 3–7.

[44] Surface curvature effects in physisorption and catalysis by microporous solids and molecular sieves, E.G. Derouane, J.M. Andre, A.A. Lucas, *J. Catal.* **1988**, *110*, 58–73.

[45] Diffusion of alkanes in molecular sieves evidence for confinement effects, E.G. Derouane, J.B. Nagy, C. Fernandez, Z. Gabelica, E. Laurent, P. Maljean, *Appl. Catal.* **1988**, *40*, L1–L10.

[46] Molecular simulations of zeolites: Adsorption, diffusion, and shape selectivity, B. Smit, *Chem. Rev.* **2008**, *108*, 4125–4184.

[47] Shape-selective catalysis in zeolites, S.M. Csicsery, *Prepr Pap - Am Chem Soc Div Fuel Chem U. S.* **1983**, *28:2*.

[48] Industrial catalysis: A practical approach, J. Hagen, *Industrial Catalysis: A Practical Approach*, **2015**.

[49] Computational design of an enzyme catalyst for a stereoselective bimolecular Diels-Alder reaction, J.B. Siegel, A. Zanghellini, H.M. Lovick, G. Kiss, A.R. Lambert, J.L. St.Clair, J.L. Gallaher, D. Hilvert, M.H. Gelb, B.L. Stoddard, et al., *Science* **2010**, *329*, 309–313.

[50] Control of metal catalyst selectivity through specific noncovalent molecular interactions, K.R. Kahsar, D.K. Schwartz, J.W. Medlin, *J. Am. Chem. Soc.* **2014**, *136*, 520–526.

[51] π Stacking effects in asymmetric synthesis, G.B. Jones, B.J. Chapman, *Synthesis* **1995**, *1995*, 475–497.

[52] Enantiofacially selective binding of prochiral olefins to a chiral catalyst via simultaneous face−face and edge−face aromatic interactions, R.W. Quan, Z. Li, E.N. Jacobsen, *J. Am. Chem. Soc.* **1996**, *118*, 8156–8157.

[53] The origin of greater than 200:1 enantioselectivity in a catalytic Diels-Alder reaction as revealed by physical and chemical studies, E.J. Corey, T.P. Loh, T.D. Roper, M.D. Azimioara, M.C. Noe, *J. Am. Chem. Soc.* **1992**, *114*, 8290–8292.

[54] Confinement effects of metal–organic framework on the formation of charge-transfer tetrathiafulvalene dimers, T. Chen, P. Huo, J.-L. Hou, J. Xu, Q.-Y. Zhu, J. Dai, *Inorg. Chem.* **2016**, *55*, 12758–12765.

[55] Cooperative catalysis for selective alcohol oxidation with molecular oxygen, T.K. Slot, D. Eisenberg, D. van Noordenne, P. Jungbacker, G. Rothenberg, *Chem. – Eur. J.* **2016**, *22*, 12307–12311.

[56] Zeolites as solid solvents Paper presented at the International Symposium `Organic Chemistry and Catalysis' on the occasion of the 65th birthday of Prof. H. van Bekkum, Delft, Netherlands, 2–3 October 1997. E.G. Derouane, *J. Mol. Catal. Chem.* **1998**, *134*, 29–45.

[57] Confinement effects in catalysis using well-defined materials and cages, V. Mouarrawis, R. Plessius, J.I. van der Vlugt, J.N.H. Reek, *Front. Chem.* **2018**, *6*, 623.

Selective catalytic oxidation of cyclohexene with molecular oxygen

Chapter 2

Abstract

We study the allylic oxidation of cyclohexene with O_2 under mild conditions in the presence of transition-metal catalysts. The catalysts comprise nanometric metal oxide particles supported on porous N-doped carbons (M/N:C, M=V, Cr, Fe, Co, Ni, Cu, Nb, Mo, W). Most of these metal oxides give only moderate conversions, and the majority of the products are over-oxidation products. Co/N:C and Cu/N:C, however, give 70–80 % conversion and 40–50 % selectivity to the ketone product, cyclohexene-2-one. Control experiments in which we used free-radical scavengers show that the oxidation follows the expected free-radical pathway in almost all cases. Surprisingly, the catalytic cycle in the presence of Cu/N:C does not involve free-radical species in solution. Optimisation of this catalyst gives >85 % conversion with >60 % selectivity to the allylic ketone at 70 °C and 10 bar O_2. We used SEM, X-ray photoelectron spectroscopy and XRD to show that the active particles have a cupric oxide/cuprous oxide core–shell structure, giving a high turnover frequency of approximately 1500 h^{-1}. We attribute the high performance of this Cu/N:C catalyst to a facile surface reaction between adsorbed cyclohexenyl hydroperoxide molecules and activated oxygen species.

Part of this work has been published as "Selective Catalytic Oxidation of Cyclohexene with Molecular Oxygen: Radical Versus Nonradical Pathways", I.M. Denekamp, M. Antens, T.K. Slot, G. Rothenberg, *ChemCatChem* **2018**, *10*, 1035–1041.

2.1 Introduction

The allylic oxidation of alkenes is an important chemical reaction. It allows us to keep the double bond and at the same time create a new alcohol or carbonyl function.[1,2] As such, it is useful across the board, from bulk chemicals and agrochemicals,[3,4] all the way to fine-chemicals and fragrances.[5–7] In theory, allylic oxidation is a straightforward exothermic reaction. It requires only O_2, a free, eco-friendly and widely available reagent. However, there is a trade-off: O_2 has a high activation barrier because of its resonance stabilisation.[8] Once this barrier is overcome, the active oxygen species often react with hydrocarbons via free-radical intermediates. These wreak havoc in solution and cause side reactions that all-too-often lead to unwanted over-oxidation products.[9–11]

Recently, we showed that this problem can be solved for the specific case of the oxidation of activated alcohols to aldehydes and ketones by using a bifunctional catalyst.[12] Yet this oxidation was "only" a dehydrogenation reaction. It involved the transfer of protons and electrons without the addition of a new O atom to the substrate. Allylic oxidation is tricky because it is an oxygenation that involves the cleavage of at least one C–H bond and the creation of new C–O or C=O bonds. This requires a direct interaction between the substrate and an active oxygen species, which must then be stopped at the allylic alcohol/ketone stage before "burning" further to carboxylic acids, CO and CO_2.

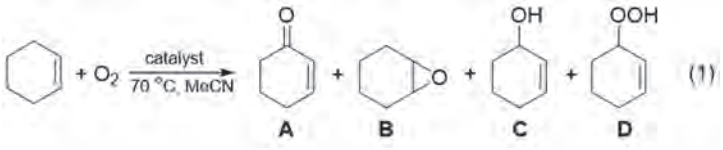

Here we examine the catalytic oxidation of cyclohexene with O_2 under mild conditions [**Eq. (1)**]. Cyclohexene is a good model compound for two reasons: first, it is a small and symmetric molecule, similar to many starting compounds in chemical synthesis. Second, it is itself industrially important and participates in the synthesis cycles of key

C_6 chemicals such as adipic acid and caprolactone.[13,14] Building on our preliminary communication on alcohol oxidation,[12] we designed a set of metal oxide catalysts supported on N-doped carbons. We used no noble metals and we focussed on abundant transition metal oxides as catalysts.

There are several reports on the allylic oxidation of cyclohexene catalysed by abundant transition metals. In general, the use of O_2 as an oxidant requires additional activation, either by adding 5–10% of a free-radical initiator such as H_2O_2 or by using elevated temperatures. Zhang and Tang[15] reported a Cu catalyst on expanded graphite that gave 99% conversion and 65% selectivity to 2-cyclohexene-1-one. Yin *et al.*[16] and Rossi *et al.*[17] used Co-based catalysts to obtaining 94% conversion and 44% selectivity and 90% conversion and 61% selectivity, respectively. Peng *et al.*[18] used metal-free N-doped carbon nanotubes as catalysts. They tested 22 organic solvents and found that acetonitrile gave the best results of 60% conversion and 39% selectivity to the 2-cyclohexene-1-one.

Our initial hypothesis was that the allylic oxidation reaction would follow a pathway similar to alcohol oxidation with oxygen activation at the support surface followed by a reaction at the oxide particle. Based on the reports, we expected the reaction to involve free-radical intermediates.[10,17,19] Surprisingly, we found that at least in one case, namely if we used copper oxide particles supported on N-doped carbon, there are no free-radicals in the solution. In this study, we try to resolve the different pathways that lead to allylic oxidation, with the goal of gaining a better understanding of this important reaction.

2.2 Results and Discussion

Catalyst synthesis and testing. We began by preparing and testing a set of nine *d*-block metal oxides supported on the same batch of hierarchically porous N-doped carbons[20] (1.2 mmolg^{-1} M/N:C, M = V, Cr, Fe, Co, Ni, Cu, Nb, Mo, and W). The catalysts were prepared using vacuum pore impregnation (see experimental section for details). To this set of catalysts, we added two blanks: a clean N:C support and a carbon

prepared from a citric acid precursor (denoted C_{cit}), which has a similar surface area to N:C (≈1500 m^2/g^{-1}) but contains no N. All catalysts were then tested in cyclohexene oxidation by using an autoclave under 10 bar O_2 and 55 bar Ar, within safe explosion limits. Typically, each autoclave was charged with approximately 25 mmol of cyclohexene, 10 mg of catalyst (a nominal substrate/metal oxide ratio of 2000:1) and 15 mL of MeCN as solvent. Reactions were stirred for 16 h at 1000 rpm and analysed by GC.

Table 1. Cyclohexene oxidation in the presence of different catalysts.[a]

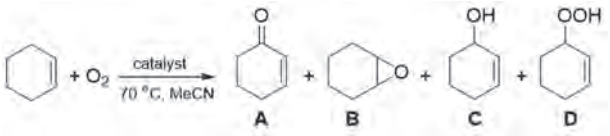

Entry	Catalyst	Conversion (%)	Selectivity (%)				
			A	**B**	**C**	**D**	other
1	None	22	8	2	0	10	80
2	C_{cit}	23	14	2	0	17	67
3	N:C	49	28	3	0	5	64
4	W@N:C	43	17	4	0	12	67
5	Ni@N:C	44	17	3	0	17	63
6	Mo@N:C	45	17	5	0	11	69
7	Fe@N:C	53	23	3	0	3	74
8	Nb@N:C	58	25	6	0	8	61
9	V@N:C	64	20	15	0	2	63
10	Cr@N:C	66	32	7	1	4	56
11	Cu@N:C	71	47	9	16	4	24
12	Co@N:C	80	38	6	6	6	44

[a] Reaction conditions: 10 bar O_2; 2,5 mL (24,7 mmol) cyclohexene; 0.5 mL (1.85 mmol) cyclohexane (IS); 10 mg catalyst; 15 mL MeCN; stirred in an autoclave (1000 rpm); 70 °C; 16 h.

Cyclohexene is oxidised to four main products (**Table 1**): 2-cyclohexene-1-one (**A**), cyclohexene oxide (**B**), 2-cyclohexene-1-ol (**C**) and 2-cyclohexene-1-hydroperoxide (**D**; herein the ketone, epoxide, alcohol and hydroperoxide, respectively). The rest of the products were over-oxidation products, mainly CO and CO_2. Products **A–C** were determined directly by GC. The hydroperoxide **D** could not be observed by GC and was quantified by reacting each sample with PPh3 (see Experimental Section for details). Control experiments confirmed that the internal standard, cyclohexane, showed no conversion under these reaction conditions. Further, in the absence of any catalyst, the background reaction at 70 °C gives only 22 % conversion, most of it to CO and CO_2 (**Table 1, entries 1–3**). The addition of porous carbon does not change the conversion but reduces the amount of over-oxidation slightly, possibly because of radical-scavenging by the carbon surface sites.[21] In the presence of pristine N:C, the conversion more than doubles to approximately 50 %. Moreover, the selectivity to the ketone **A** increases to 28 %, at the expense of the hydroperoxide **D**. Indeed, we showed recently that these porous N:C materials are excellent oxygen reduction catalysts,[20] yet these results also point to a N:C-catalysed route from **D** to **A** *(vide infra)*.

The addition of W, Ni, Mo, Fe or Nb does not change the results significantly (**Table 1, entries 4–8**). For some of these catalysts, the selectivity to **A** is lower than that of the pristine N:C support, which may reflect the blocking of labile sites on the support by metal oxide particles. However, the catalysts that contain V, Cr, Cu and Co showed a significant increase in conversion (entries 9–12). Vanadium oxide (V/N:C), which is known as a good epoxidation catalyst,[22,23] gives a high selectivity to the epoxide **B** . The remaining three catalysts are interesting: they are the only ones to give measureable yields of the alcohol **C** . All three give less hydroperoxide compared with the blanks, which indicates a pathway from **D** to **C**. Cobalt oxide gives the highest conversion. However, copper oxide gives the highest selectivity to the ketone **A** with a remarkably low amount of over-oxidation products. Even at this un-optimised stage, the Cu/N:C catalyst gives a combined ketone + alcohol yield of nearly 45 % with a minimum turnover number (TON) >1400 and turnover frequency (TOF) >88 h^{-1}

(the actual TON and TOF per site are much higher because most of the copper oxide is not accessible, see discussion below). Therefore, we focussed our investigation on these two catalysts.

Table 2. Oxidation of cyclohexene with various copper oxide and cobalt oxide catalysts.[a]

Entry	Catalyst	Temp (°C)	Conversion (%)	Selectivity (%)				
				A	**B**	**C**	**D**	other
1	Co@N:C	70	80	38	6	6	6	44
2	Co@Alu	70	56	20	3	0	3	74
3	Co@N:C	70	87	43	6	11	nd[c]	40
4	Co@N:C	80	87	41	12	5	nd[c]	42
5	Cu@N:C	70	71	47	9	16	4	24
6	Cu@N:C	70	86	61	15	8	nd[c]	16
7	Cu@N:C	80	85	53	10	17	nd[c]	20

[a] Reaction conditions: 10 bar O_2; 2.5 mL (24.7 mmol) cyclohexene; 0.5 mL (1.85 mmol) cyclohexane (IS); 10 mg carbon catalyst, 73 mg alumina catalyst; 15 mL MeCN; stirred in an autoclave (1000 rpm); 16 h. [b] 1.0 mL H2O2 added (10 wt %, 3.3 mmol, 13 mol % based on cyclohexene). [c] Not determined.

Control reactions in which we used equivalent amounts of cobalt oxide supported on γ-alumina showed lower conversions and more side-products, which confirms the importance of the N:C support (**Table 2, entry 2**). Copper oxide supported on γ-alumina shows a good conversion but with a lower selectivity and more side-products than that supported on N:C, making the γ-alumina-supported catalyst less favourable (entry 6). Notably, the difference in the surface area between the carbon and the γ-alumina was corrected for by increasing the catalyst amount accordingly. To boost the number of free radicals at the start of the reaction, we added H_2O_2 (13 mol % relative to the substrate, entry 3).[5,7]

Table 3. Effects of adding free-radical scavengers.[a]

Entry	Catalyst	Addition	Conversion (%)	Selectivity (%)			
				A	**B**	**C**	**other**
1[b]	N:C	-	49	28	3	0	69
2[b,c]	N:C	BHT	0	0	0	0	0
3	Co@N:C	-	87	41	12	5	42
4[c]	Co@N:C	BHT	0	0	0	0	0
5	Cu@N:C	-	85	53	10	17	20
6[c]	Cu@N:C	BHT	76	46	10	20	24

[a] Reaction conditions: 10 bar O_2; 2.5 mL (24.7 mmol) cyclohexene; 0.5 mL (1.85 mmol) cyclohexane (IS); 10 mg carbon catalyst; 15 mL MeCN; stirred in an autoclave (1000 rpm); 80 °C; 16 h. [b] Reaction temperature 70 °C. [c] 354 mg BHT added (7 mol% based on cyclohexene).

H_2O_2 can decompose into water and oxygen under these reaction conditions. The water molecules themselves do not change the conversion and selectivity (the H_2O_2 solution is already 90 % water), but the decomposition of H_2O_2 affects the reaction by releasing free radicals into the solution. The addition of H_2O_2 increased the conversion but did not change the selectivity significantly. A similar increase was observed if the reaction was performed at 80 °C. With copper oxide, however, the addition of H_2O_2 or an increase of the reaction temperature affected both the conversion and the selectivity (entries 7 and 8). The conversion increased to 85 %, and the combined selectivity to **A** + **C** increased to 70 %. Importantly, this increase in selectivity came at the expense of the over-oxidation products (unlike with Co, with which there was still a lot of over-oxidation products). To our minds, this was counter-intuitive: we would assume that the addition of an initiator such as H_2O_2 or an increase of the temperature would lead to more CO and CO_2. These results led us to think that perhaps the copper oxide catalysed reaction is not a simple free-radical process. Previous reports in which the oxidation kinetics of cyclohexene and [D10]cyclohexene are compared show a clear primary isotope effect (k_H:k_D =8.2), which indicates that the rate-determining step involves C−H bond scission.[10] Moreover, the addition of a radical scavenger

quenched the reaction.[10,15] To check if this also applies our system, we ran additional control experiments in the presence of 6 mol % of 2,6-di-tert -butyl-4-methylphenol (BHT; see details in the Experimental Section). The addition of BHT to the reaction mixture that contained the N:C support or the Co/N:C catalyst stopped the reaction completely (**Table 3**, *cf.* entries 2 and 4 with 1 and 3). However, if we added BHT to the Cu/N:C-catalysed reaction, there was only a slight decrease in the conversion and selectivity (from 85 to 76 % and from 53 to 46 %, respectively; entries 5 and 6). This shows that although the reactions catalysed by metal-free N:C and by Co/N:C are definitely free-radical processes, the Cu/N:C-catalysed reaction is not affected by free-radical scavengers (these experiments were repeated multiple times by different people to ensure their repeatability and reproducibility). Therefore, we conclude that in the Cu-catalysed system, there are no free radicals in solution.

SEM images (**Figure 1**) of the Cu/N:C catalyst showed spherical copper oxide particles of approximately 200–250 nm in diameter distributed evenly across the surface. Unlike the support, the particles are non-porous. Consequently, most of the copper oxide is "inside" the particle and unavailable for catalysis. If we consider that the active outer shell is approximately five atomic layers (≈2 nm in thickness), the actual active catalyst comprises only 0.1 wt %. Accordingly, the actual TON of this catalyst would be >24 000 with a corresponding TOF of >1500 h^{-1}.

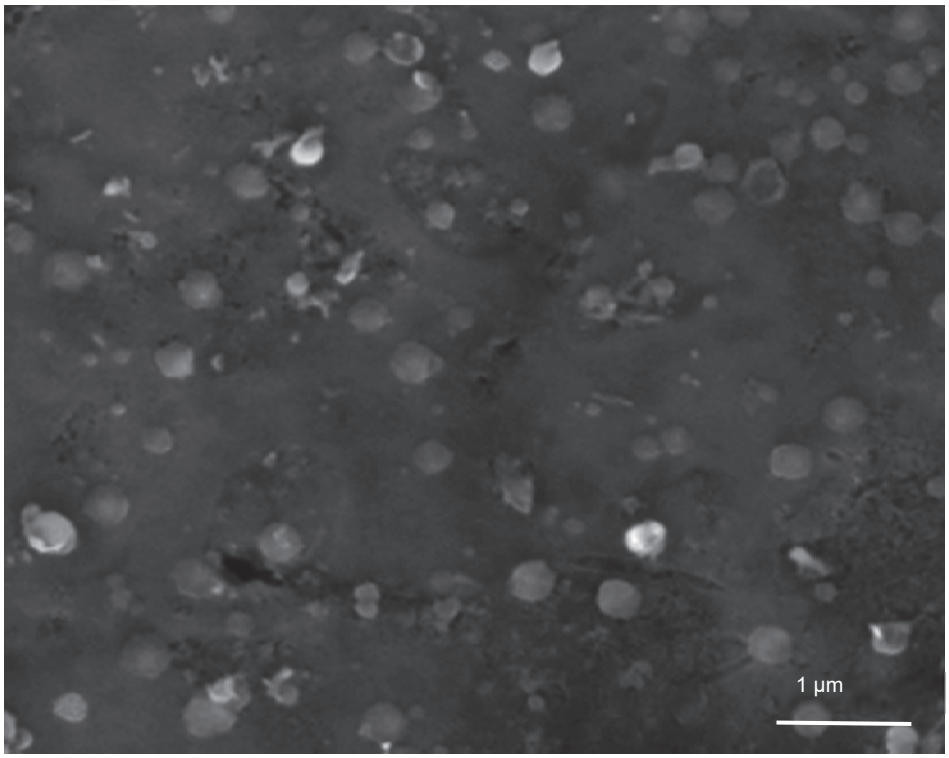

Figure 1: Scanning electron micrograph of Cu/N:C at ×15 000 magnification (an image with particle measurements is included in the Appendix).

We used X-ray photoelectron spectroscopy (XPS; **Figure 2**) to show that the impregnation of the N:C surface with copper oxide does not affect the N binding energy. This suggests that the copper oxide is not coordinated to surface N atoms. The impregnation increases the intensity of the O 1s peak, which indicates a higher oxygen content in the sample. For Cu, the XPS spectrum shows the typical Cu $2p_{1/2}$ and Cu $2p_{3/2}$ peaks, which can be assigned to both Cu^{+} and Cu^{2+}. Yet the characteristic CuO peak at a binding energy of 945 eV is absent, which supports the presence of Cu_2O[24] (metallic Cu is unlikely at such low treatment temperatures[25] and if we consider the increase in the O signal).

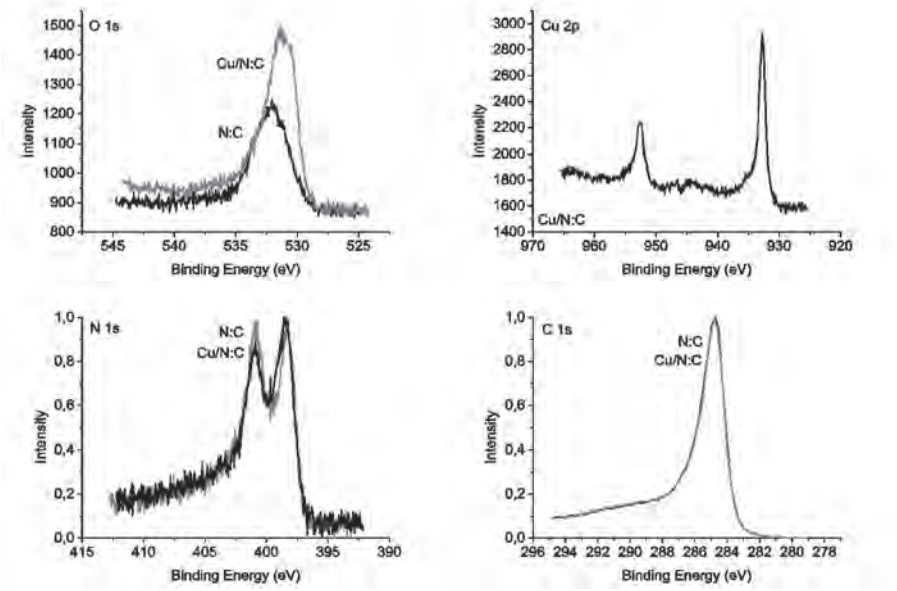

Figure 2: XPS spectra of Cu/N:C and pristine N:C that show the O 1s, Cu 1/2p and 3/2p, N 1s and C 1s binding energies. Impregnation of copper oxide on the N:C increases the O content but does not affect the N or C peaks. The N and C spectra are normalised for clarity.

The carbon peak is not affected by impregnation with Cu. However, powder XRD patterns of the catalyst show CuO as the major component in the particles (see details in the Appendix). These results are consistent with a CuO–CuO_2 core–shell structure as XRD measures the entire particle, whereas XPS penetrates only a few atomic layers.[26] Therefore, we suggest that during the thermal treatment following the impregnation step, the adsorbed $Cu(NO_3)_2$ precursor is first converted to CuO and $NO_{2(g)}$. As the temperature approaches 300 °C, the Cu_2O shell starts to form. Indeed, temperature-programmed reduction measurements indicate the presence of multiple copper oxides (details in Appendix). Similarly, thermogravimetric analysis of the pristine N:C and the Cu/N:C samples shows that the latter decomposes at a lower temperature (400 vs. 500 °C, respectively). This supports the hypothesis that Cu partially oxidises the surface to create more labile sites (see details in the Appendix).

Mechanistic considerations. From these results, we propose two alternatives for the catalytic allylic oxidation of cyclohexene with O_2. The first follows the traditional free-radical route and pertains to the Co, Fe, Cr, Mo, V, Ni, Nb and W/N:C catalysts. Here, O_2 is either activated thermally or in a redox process on the N:C surface. The insertion of this activated oxygen into the allylic C−H bond gives the cyclohexenyl hydroperoxide **D** . This can then either rearrange to give the ketone **A** or undergo scission to give oxo and peroxo radicals that propagate a chain oxidation reaction.[2,15] Accordingly, this pathway, which involves free-radicals in the bulk solution, is quenched readily if BHT is added.

Conversely, in the presence of Cu/N:C, there are no free radicals in the bulk solution. Oxygen can still be activated at the N:C surface sites but now there are two options: the small amounts of short-lived activated oxygen species (e.g., $O_2^{-\cdot}$ radical anions) that travel into solution will be quenched by BHT (**Figure 3a**, *cf.* also the difference in conversion between entries 5 and 6 in **Table 3**). The BHT molecules are too bulky to enter the micropores. Therefore, they will quench only the radicals in the solution. Conversely, the activated oxygen species that are close enough to diffuse to a supported copper oxide particle,[27] and react there with cyclohexene to form an adsorbed hydroperoxide (**Figure 3b**). This adsorbed hydroperoxide can undergo two reactions.

The first is rearrangement and dehydration to give the ketone **A** and a molecule of water (**Figure 3c**).[9,28] The second is a disproportionation reaction with another cyclohexene molecule to give two molecules of cyclohexene-1-ol **C** (**Figure 3d**). Compared with the other metal oxides, the scission of the RO−OH bond on the copper oxide surface is apparently much slower. This means that fewer free radicals are released into the solution, which gives enough time for the rearrangement and disproportionation reactions.

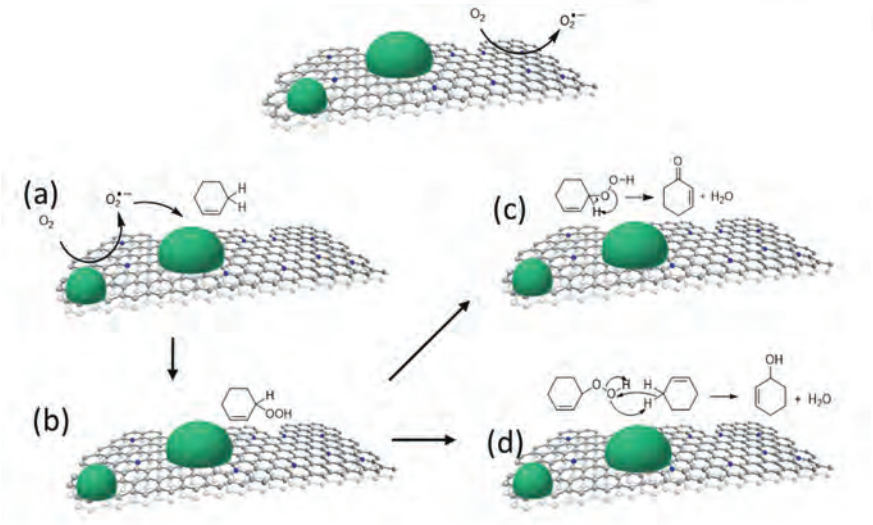

Figure 3: Proposed reaction pathways for the catalytic oxidation of cyclohexene with O2 in the presence of Cu/N:C. a) Oxygen activation at the support surface followed by radical migration into solution. b) Insertion of activated oxygen into the allylic C−H bond to give the adsorbed hydroperoxide ***D*** *followed by either c) rearrangement to the ketone* ***A*** *and water or d) reaction with another cyclohexene molecule to give two molecules of the alcohol* ***C****.*

Interestingly, there is a marked difference between the oxidation of activated alcohols, which we reported earlier,[12] and that of cyclohexene. With an activated alcohol substrate such as cinnamyl alcohol, the N:C support is required for oxygen activation. There, no reaction was observed for copper oxide particles supported on C_{cit}, an analogous porous carbon with no N dopants. Cyclohexene oxidation, however, does proceed in the presence of Cu/C_{cit}, which shows that the allylic oxidation in this case is easier. This is supported by the results of Gray and co-workers,[10] who showed that the allylic C–H bond scission is rate-determining, and by the fact that this bond is weaker than the alcohol C–H bond (83 and 96 kcal mol^{-1}, respectively[29,30]).

In all cases, the epoxide **B** probably forms via another pathway.[4,31] Cyclohexene molecules can interact with M=O groups on the particle surface to give the epoxide and a labile surface site which is then re-oxidised by incoming oxygen.[24]

2.3 Conclusions

The catalytic oxidation of cyclohexene with O_2 can follow different pathways that depend on the type of catalyst. In the presence of transition metal oxide nanoparticles supported on N-doped carbons, the key step is the insertion of O_2 into the allylic C−H bond to give the cyclohexenyl hydroperoxide. This reaction can be enhanced by oxygen activation at the N-doped carbon surface. In most cases, the allylic oxidation follows a free-radical pathway. However, in the presence of Cu/N:C the reaction does not release free radicals into solution. This enables a more selective reaction at the copper oxide surface, which probably involves cuprous oxide sites.

2.4 Experimental Section

Materials and instrumentation. GC was performed by using a PerkinElmer Clarus 580 instrument. This system was equipped with a flame ionisation detector and autosampler (G4513A). A 30 m×32 mm I.D. Rxi-5 ms fused silica crossbond diphenyl dimethyl polysiloxane column with a film thickness of 0.25 μm was used. The injector volume was 1 μL, and the flow was 100 mL min^{-1} of He carrier gas. The temperature program was 40 °C, 20 °C min^{-1}, 160 °C for 2 min. SEM was performed by using a Verios-460 microscope (FEI) at an accelerating voltage of 5 kV with a working distance of 2–5 mm. Powder XRD patterns were obtained by using a MiniFlex II diffractometer by using Ni-filtered CuK_α radiation. The X-ray tube was operated at 30 kV and 15 mA with a 0.01° step and 1 s dwell time. XPS measurements were performed by using a PHI VersaProbe II scanning XPS microprobe (Physical Instruments AG, Germany) using a monochromatic AlK_α X-ray source with a power of 24.8 W and a beam size of 100 μm. The spherical capacitor analyser was set at a 45° take-off angle with respect to the sample surface. The pass energy was 46.95 eV to yield a full width at half maximum of 0.91 eV for the Ag $3d_{5/2}$ peak. Peaks were calibrated using the C 1s position. Curve fitting was performed using the XPSPeak 4.1 software package. All chemicals were obtained from commercial sources (>99 % pure) and were used as received. Temperature-programmed reduction (TPR) was performed by placing 25 mg of sample sandwiched between two quartz wool plugs in a quartz tube reactor (4 mm i.d.). After purging with N_2, a flow of 5 % H_2 in N_2 was applied. The system was allowed to equilibrate and then heated at 5 °Cmin^{-1} to 800 °C (no hold time).

Preparation of the N-doped carbon support. The N:C support samples were prepared following the procedure published by Eisenberg *et al.*[20] Briefly, nitrilotriacetic acid (NTA) was mixed in a 1:1 ratio with magnesium carbonate. This was dissolved in de-ionised water, stirred for 10 min at 85 °C, and cooled to RT. The

solid was then precipitated by adding an excess of ethanol and chilling in an ice bath for 2 h. The white solid was scraped out, dried at 40 °C for 48 h, and ground into a fine white powder. This powder was then pyrolysed in Ar at 900 °C. The MgO particles were washed with 3×500 mL of 0.5 M citric acid. The resulting crude N:C sample was dried at 120 °C for 2 h and treated under Ar at 1000 °C for 1 h.

Preparation of M/N:C catalysts. This is a modification of the procedure published by Slot *et al.*[12] The N-doped carbon support (100 mg) was placed in a small vial with a septum. The air was removed carefully by using a needle, and an aqueous solution of the desired metal precursor salt (0.2 mL, which corresponds to a nominal loading of 1 mmol m^{-2}) was added to the vial under continuous stirring. The vial was shaken vigorously for 2–3 min to create a uniform solid paste, which was then dried at 85 °C for 12 h. Each catalyst was then heat-treated at 300 °C under Ar (except for Nb/N:C, which was treated at 700 °C) and cooled to RT. The different M/N:C catalysts were prepared from their respective precursors salts: $Co(NO_3)_2{\cdot}6\,H_2O$, $Cu(NO_3)_2{\cdot}3\,H_2O$, $Fe(NO_3)_3{\cdot}9\,H_2O$, NH_4VO_3 (dissolved using 2 equiv. of oxalic acid), $Cr(NO_3)_3{\cdot}9\,H_2O$, $(NH_4)_6Mo_7O_{24}{\cdot}4\,H_2O$, $Ni(NO_3)_2{\cdot}6\,H_2O$, $C_{10}H_5NbO_{20}{\cdot}x\,H_2O$ and $(NH_4)_{10}W_{12}O_{41}{\cdot}5\,H_2O$. The Co/alumina catalyst sample was prepared similarly from γ-Al_2O_3 (Ketjen; ground and sieved to 200–400 nm) and $Co(NO_3)_2{\cdot}6\,H_2O$ stock solution (0.8 mL, 0.55 M).

Catalytic oxidation of cyclohexene. This is a modification of the procedure published by Cao *et al.*[32] A 75 mL autoclave lined with a 50 mL Teflon insert was loaded with cyclohexene (2.5 mL, 24.7 mmol), cyclohexane (0.5 mL, internal standard), acetonitrile (solvent, 15 mL), catalyst (10 mg M/N:C carbon or 73 mg Co/alumina) and a stirring bar (30 mm). The autoclave was sealed, flushed with Ar and O_2 twice before the final O_2 (10 bar) and Ar (55 bar) atmosphere was applied. The autoclave was then heated to 70 °C for 16 h with stirring at 1000 rpm. After 16 h, the autoclave was cooled to ambient temperature. Acetone (5 mL) was added to the

sample, and the reaction mixture was filtered using 0.45 μm PTFE syringe filters and analysed by using GC.

The presence of free radicals in solution was tested by adding BHT (354 mg, 6 mol %) to the reaction at $t = 0$ and then following the above procedure. Reactions were performed in triplicate, and all GC analyses were performed in duplicate.

Quantification of the cyclohexenyl hydroperoxide D. The hydroperoxide **D** cannot be measured directly by using GC because of its instability. Instead, we quantified it by comparing a control reaction sample to one in which triphenylphosphine (PPh_3, 30 mg, 1 mol %) was added. The sample was shaken for 1 min, and heat was generated as the PPh_3 reacts with the hydroperoxide **D** to give PPh_3O and the alcohol **C [Eq. 2]**. After this reaction, the sample was analysed by GC and compared to its untreated counterpart. The subtraction of the initial amount of the alcohol formed in the control reaction from the amount of the alcohol after the addition of PPh_3 gives the amount of hydroperoxide **D** in the original sample.[6,33]

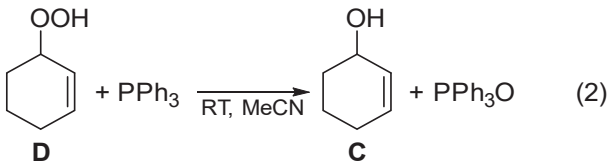

(2)

2.5 References

[1] CuNi/Co composites prepared by electroless deposition: structure and catalytic activity for the oxidation of cyclohexene with oxygen, J. Hao, X. Jiao, L. Han, Q. Suo, A. Ma, J. Liu, X. Lian, L. Zhang, *RSC Adv.* **2015**, *5*, 13809–13817.

[2] Polymer-supported Schiff base complexes in oxidation reactions, K.C. Gupta, A. Kumar Sutar, C.-C. Lin, *Coord. Chem. Rev.* **2009**, *253*, 1926–1946.

[3] Tunable gold catalysts for selective hydrocarbon oxidation under mild conditions, M.D. Hughes, Y. J. Xu, P. Jenkins, P. McMorn, P. Landon, D.I. Enache, A.F. Carley, G.A. Attard, G.J. Hutchings, F. King, et al., *Nature* **2005**, *437*, 1132–1135.

[4] Efficient allylic oxidation of olefins catalyzed by polymer supported metal schiff base complexes with peroxides, S.M. Islam, A.S. Roy, P. Mondal, N. Salam, *J. Inorg. Organomet. Polym. Mater.* **2012**, *22*, 717–730.

[5] Enhanced catalytic activity and unexpected products from the oxidation of cyclohexene by organic nanoparticles of 5,10,15,20-Tetrakis-(2,3,4,5,6-pentafluorophenyl)porphyrinatoiron(III) in water by using O_2, G. Smeureanu, A. Aggarwal, C.E. Soll, J. Arijeloye, E. Malave, C.M. Drain, *Chem. Weinh. Bergstr. Ger.* **2009**, *15*, 12133–12140.

[6] Oxidation mechanism of molecular oxygen over cyclohexene catalyzed by a cobalt l - glutamic acid complex, Y. N. Wei, H. Li, F. Yue, Q. Xu, J. D. Wang, Y. Zhang, *RSC Adv.* **2016**, *6*, 107104–107108.

[7] Highly selective oxidation of cyclohexene to 2-cyclohexene-1-one over polyoxometalate/metal–organic framework hybrids with greatly improved performances, J. Tong, W. Wang, L. Su, Q. Li, F. Liu, W. Ma, Z. Lei, L. Bo, *Catal. Sci. Technol.* **2017**, *7*, 222–230.

[8] Dioxygen: what makes this triplet diradical kinetically persistent?, W.T. Borden, R. Hoffmann, T. Stuyver, B. Chen, *J. Am. Chem. Soc.* **2017**, *139*, 9010–9018.

[9] Uncatalysed oxidation of cyclohexene, S.M. Mahajani, M.M. Sharma, T. Sridhar, *Chem. Eng. Sci.* **1999**, *54*, 3967–3976.

[10] On the mechanism of catalytic alkene oxidation by molecular oxygen and halogenated iron porphyrins, E.R. Birnbaum, M.W. Grinstaff, J.A. Labinger, J.E. Bercaw, H.B. Gray, *J. Mol. Catal. Chem.* **1995**, *104*, L119–L122.

[11] Aerobic catalytic oxidation of cyclohexene over TiZrCo catalysts, T. Liu, H. Cheng, W. Lin, C. Zhang, Y. Yu, F. Zhao, *Catalysts* **2016**, *6*, 24.

[12] Cooperative catalysis for selective alcohol oxidation with molecular oxygen, T.K. Slot, D. Eisenberg, D. van Noordenne, P. Jungbacker, G. Rothenberg, *Chem. – Eur. J.* **2016**, *22*, 12307–12311.

[13] A "green" route to adipic acid: direct oxidation of cyclohexenes with 30 percent hydrogen peroxide, K. Sato, M. Aoki, R. Noyori, *Science* **1998**, *281*, 1646–1647.

[14] Effect of texture and structure on the catalytic activity of mesoporous niobosilicates for the oxidation of cyclohexene, I. Nowak, M. Ziolek, *Microporous Mesoporous Mater.* **2005**, *78*, 281–288.

[15] Expanded graphite supported copper catalyst for effective oxidation of cyclohexene with molecular oxygen under mild conditions, R. Zhang, R. Tang, *J. Mater. Sci.* **2016**, *51*, 5802–5810.

[16] Allylic oxidation of cyclohexene with molecular oxygen using cobalt resinate as catalyst, C. Yin, Z. Yang, B. Li, F. Zhang, J. Wang, E. Ou, *Catal. Lett.* **2009**, *131*, 440–443.

[17] Magnetically recoverable copper oxide catalysts for aerobic allylic oxidation of cyclohexene, F.P. da Silva, R.V. Gonçalves, L.M. Rossi, *J. Mol. Catal. Chem.* **2017**, *426*, 534–541.

[18] Solvent effect on the allylic oxidation of cyclohexene catalyzed by nitrogen doped carbon nanotubes, Y. Cao, H. Yu, H. Wang, F. Peng, *Catal. Commun.* **2017**, *88*, 99–103.

[19] Generalized reaction mechanism for the selective aerobic oxidation of aryl and alkyl alcohols over nitrogen-doped graphene, V.S. Jeyaraj, M. Kamaraj, V. Subramanian, *J. Phys. Chem. C* **2015**, *119*, 26438–26450.

[20] A simple synthesis of an N-doped carbon ORR catalyst: hierarchical micro/meso/macro porosity and graphitic shells, D. Eisenberg, W. Stroek, N.J. Geels, C.S. Sandu, A. Heller, N. Yan, G. Rothenberg, *Chem. – Eur. J.* **2016**, *22*, 501–505.

[21] Titania-catalysed oxidative dehydrogenation of ethyl lactate: effective yet selective free-radical oxidation, E.V. Ramos-Fernandez, N.J. Geels, N.R. Shiju, G. Rothenberg, *Green Chem* **2014**, *16*, 3358–3363.

[22] Vanadium-catalyzed epoxidation of cyclic allylic alcohols. Stereoselectivity and stereocontrol mechanism, T. Itoh, K. Jitsukawa, K. Kaneda, S. Teranishi, *J. Am. Chem. Soc.* **1979**, *101*, 159–169.

[23] Vanadium-catalyzed epoxidations. I. A new selectivity pattern for acyclic allylic alcohols, E.D. Mihelich, *Tetrahedron Lett.* **1979**, *20*, 4729–4732.

[24] Electronic and optical properties of Cu, CuO and Cu2O studied by electron spectroscopy, D. Tahir, S. Tougaard, *J. Phys. Condens. Matter* **2012**, *24*, 175002.

[25] Thermal decomposition of hydrated copper nitrate $Cu(NO_3)x3H_2O$ on activated carbon fibers, S.K. Ryu, W.K. Lee, S.J. Park, *Carbon Lett.* **2004**, *5*, 180–185.

[26] Angle-resolved XPS depth-profiling strategies, P.J. Cumpson, *Appl. Surf. Sci.* **1999**, *144*, 16–20.

[27] The mechanism of methanol synthesis on copper/zinc oxide/alumina catalysts, M. Bowker, R.A. Hadden, H. Houghton, J.N.K. Hyland, K.C. Waugh, *J. Catal.* **1988**, *109*, 263–273.

[28] Mechanistic study of cyclohexene oxidation and its use in modification of industrial waste organics, S. Mukherjee, S. Samanta, A. Bhaumik, B. Ray, *Appl. Catal. B Environ.* **2006**, *68*, 12–20.

[29] Bond dissociation energies of organic molecules, S.J. Blanksby, G.B. Ellison, *Acc. Chem. Res.* **2003**, *36*, 255–263.

[30] Hydrocarbon bond dissociation energies, D.F. McMillen, and D.M. Golden, *Annu. Rev. Phys. Chem.* **1982**, *33*, 493–532.

[31] Highly selective epoxidation of cyclohexene by reductive activation of molecular dioxygen using hexylviologen as catalyst, Y. Tsuda, S. Matsui, K. Takahashi, *J. Mol. Catal. Chem.* **1999**, *148*, 183–187.

[32] Selective allylic oxidation of cyclohexene catalyzed by nitrogen-doped carbon nanotubes, Y. Cao, H. Yu, F. Peng, H. Wang, *ACS Catal.* **2014**, *4*, 1617–1625.

[33] The reaction of hydroperoxides with triphenylphosphine, R. Hiatt, R.J. Smythe, C. McColeman, *Can. J. Chem.* **1971**, *49*, 1707–1711.

[34] Nanostructured CuO thin film electrodes prepared by spray pyrolysis: a simple method for enhancing the electrochemical performance of CuO in lithium cells, J. Morales, L. Sánchez, F. Martín, J.R. Ramos-Barrado, M. Sánchez, *Electrochimica Acta* **2004**, *49*, 4589–4597.

Appendix - The supporting information for Chapter 2

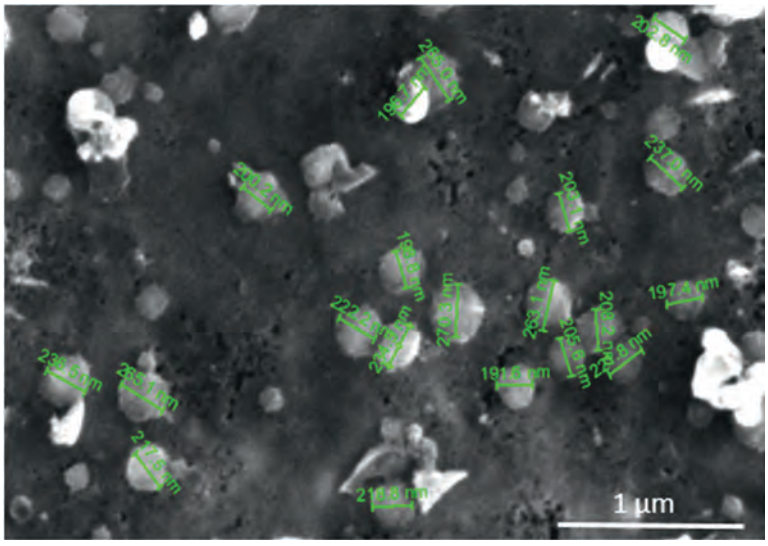

Figure A1: Scanning electron micrographs of Cu/N:C. The size of the copper oxide is ca. 200–250 nm.

Scanning electron microscopy (SEM) of Cu/N:C catalyst with particle measurements. The average size of the copper oxide spherical particles is ca. 200-250 nm. Furthermore, the clusters are evenly distributed onto the support surface.

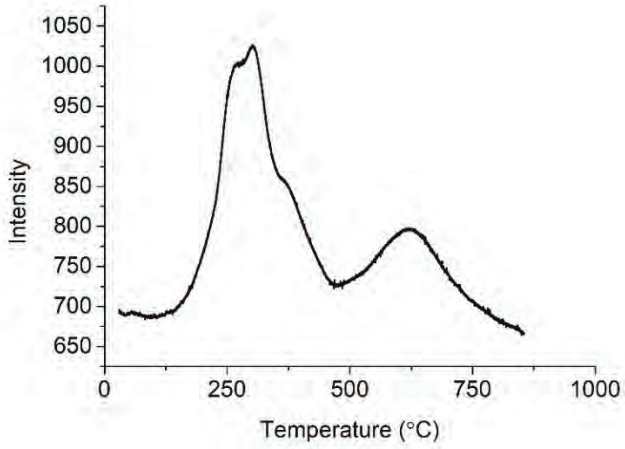

Figure A2: Temperature programmed reduction (TPR) spectrum for Cu/N:C.

The temperature programmed reduction (TPR) shows multiple copper oxide species presence inside the copper oxide catalyst. At 300 °C copper oxide is reduced, where multiple peaks indicate multiple copper oxide species. At 600 °C the support N:C is reduced.[1]

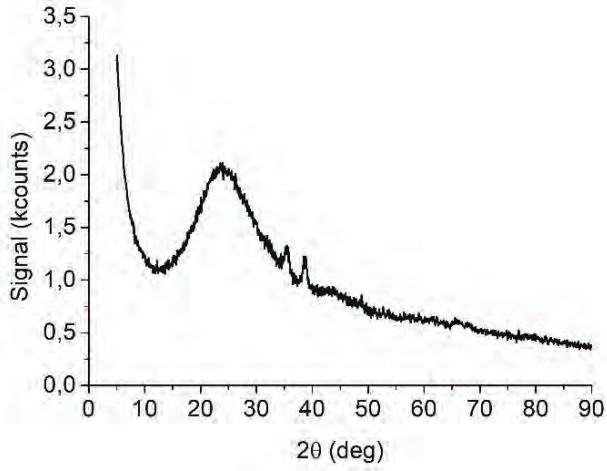

Figure A3: X-ray powder diffraction (XRD) spectrum for Cu/N:C.

X-ray diffraction showed a broad peak at 25° which is typical for carbon. The small peaks at 36.1° (–111) and at 39° (111) are typical for CuO.[2]

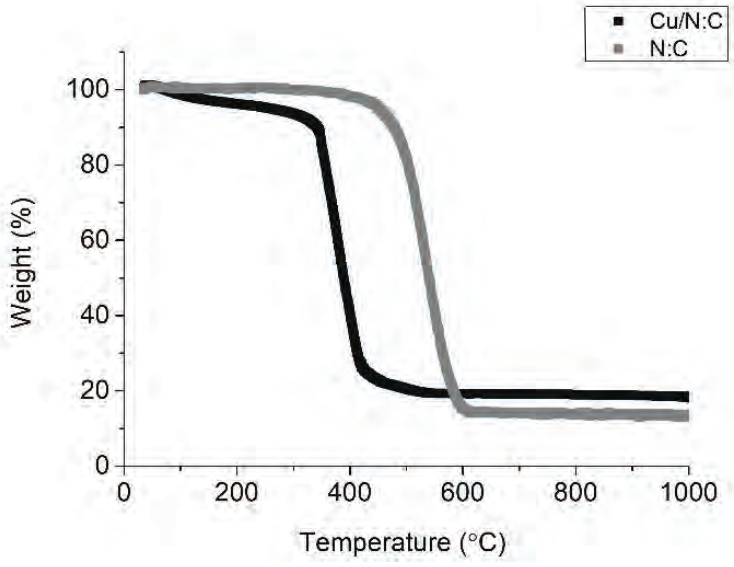

Figure A4: Thermal gravimetric analysis (TGA) curves of Cu/N:C and plain N:C.

TGA showed the mass loss of N:C at 500°C, whereas the Cu/N:C has a mass loss at a lower temperature. This difference indicates that the copper oxidises the nitrogen-doped surface during the treatment, thereby lowering the temperature of the mass loss. The difference in weight percentage at the end of the measurement around 600 °C is the copper oxide that is present in the Cu/N:C sample.

References

[1] Cooperative catalysis for selective alcohol oxidation with molecular oxygen, T.K. Slot, D. Eisenberg, D. van Noordenne, P. Jungbacker, G. Rothenberg, *Chem. – Eur. J.* **2016**, *22*, 12307–12311.

[2] Nanostructured CuO thin film electrodes prepared by spray pyrolysis: a simple method for enhancing the electrochemical performance of CuO in lithium cells, J. Morales, L. Sánchez, F. Martín, J.R. Ramos-Barrado, M. Sánchez, *Electrochimica Acta* **2004**, *49*, 4589–4597.

A simple synthesis of phthalocyanines as oxidative catalysts

Chapter 3

Abstract

We report a simple synthesis protocol for making phthalocyanines (Pcs) starting from phthalonitriles. This method is general and requires no specialised equipment. The complexes are isolated and characterised using X-ray diffraction, NMR, FTIR and Raman spectroscopy and high-resolution mass spectrometry. First, we study and present a one-step synthesis route to a metal-free Pc (H_2PcH_{16}), as well as to the corresponding $MPcH_{16}$ complexes of Mn, Fe, Co, Ni, Cu and Zn. Then, we show that this route can also be used to make the fluorinated Pc analogues ($MPcF_{16}$). Finally, we present a new and useful procedure for inserting a metal ion into a metal-free H_2PcH_{16} ring, by direct metalation, yielding the corresponding $MPcH_{16}$ complex. This last method is especially useful if you want to make different $MPcH_{16}$ complexes.

Part of this work has been published as "A simple synthesis of symmetric phthalocyanines and their respective perfluoro and transition-metal complexes", I.M. Denekamp, F.L.P. Veenstra, P. Jungbacker, G. Rothenberg, *Appl. Organomet. Chem.* **2019**, *33*, e4872.

3.1 Introduction

Nature excels at evolving complex catalytic systems that can carry out "simple" chemical reactions cleanly and efficiently. The best (and to us chemists, most frustrating) examples are the enzymes nitrogenas[1] and methane monooxygenase,[2] which can fix nitrogen from the air and oxidise methane to methanol under ambient conditions, respectively. Another example is the activation of dioxygen, which is particularly challenging owing to its resonance stabilisation.[3] Here, one of nature's tools is the heme porphyrin molecule, which is embedded in vivo within the protective shell of the haemoglobin protein. This combined system shows many features of an ideal catalyst, operating efficiently at ambient temperature and pressure and using only a single iron atom per site. However, transferring this activity to in vitro and ultimately to industrial setups is far from trivial.

As part of our ongoing research into selective oxidation with molecular oxygen,[4–6] we tried building synthetic porphyrin analogues that could serve as good single-atom catalysts *in vitro* . For this, we turned to phthalocyanines (Pcs), which are highly stable two-dimensional macrocycles with a structure analogous to that of porphyrins (**Scheme 1**). Pcs are by no means new compounds. They were first characterized in 1934 by Linstead, after their discovery at Scottish Dyes Ltd., in Grangemouth.[7] Today, Pcs have a broad range of applications due to their strong colour and long-term stability. The copper phthalocyanine pigment is the single largest-volume colorant sold worldwide (mainly thanks to its availability and low price).[8,9] Pcs are applied as colour pigments for cars, due to their strong blue colour, insolubility in water, high dispersability and high heat stability.[10,11] They are also found in printing inks,[12] pen inks,[13,14] general dye applications, biomedical applications and in catalysis.[15–19]

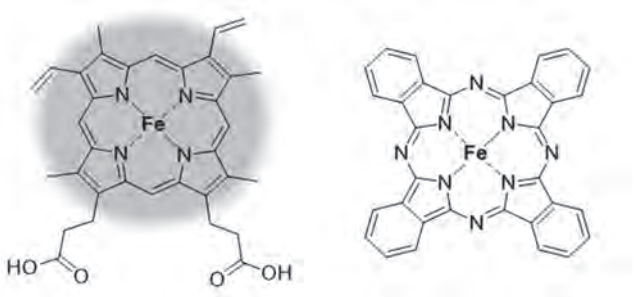

Scheme 1: left: Heme B, within the porphyrin highlighted in gray. Right: $FePcH_{16}$.

Pcs can be made by the cyclisation of phthalonitriles in the presence of an organic base.[18,20–22] However, all these procedures include cumbersome and/or difficult synthesis or separation steps. The reactions require high temperature, typically above 180 °C,[23–25] leading to side products and lowering yields.[26] Other protocols require high pressure,[27] ionic liquids,[28] gaseous ammonia[26] or long reaction times (>150 h).[29]

Notwithstanding the synthetic achievements of the above reports, one would prefer a simple, short and general synthesis protocol that requires no specialised equipment. In this chapter, we present a one-step synthetic route to metal-free Pcs (hereafter noted as H_2PcH_{16}), their corresponding Mn, Fe, Co, Ni, Cu and Zn complexes ($MPcH_{16}$), and the perfluorinated analogues ($MPcF_{16}$). Furthermore, we present a new and facile procedure for making the same complexes by metalation of a metal-free H_2PcH_{16} ring.

3.2 Results and Discussion

First, we tried synthesising the metal-free H_2PcH_{16} ring following the procedures of Ogawa,[22] Wöhrle[30] and Kharisov.[21] These protocols give a good basis, advising the use of 1,8-diazabicyclo[5.4.0]undec-7-ene (DBU) as the base and alcohol solvents. They are based on the cyclisation of phthalonitrile (**Scheme 2**) but should be done under inert atmosphere, as moisture from the air can hydrolyse the nitrile groups,

forming unwanted side products. The reaction proceeds best in an alcohol solvent, and is quite solvent-dependent.[22] We found that *n*-pentanol is the optimal choice because it also enables the solvation of various MPcs thanks to its higher boiling point. The reaction can be monitored visually, as dissolving the phthalonitrile in *n*-pentanol gives a milky liquid, which turns orange on addition of DBU. When this mixture is heated, it turns a dark blue-purple, indicating the formation of the Pc ring, which can then be washed and isolated (see experimental section for details).

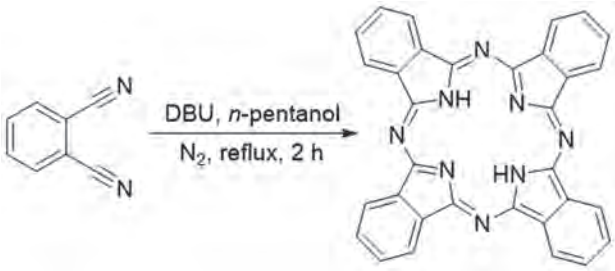

Scheme 2: Cyclisation of phthalonitrile gives the symmetric phthalocyanine.

We then turned to the metal-Pc complexes, or $MPcH_{16}$. In principle, these complexes can be made in two ways. One can either synthesise them in a single step from the metal precursor and phthalonitrile, or one can first synthesise H_2PcH_{16} ligand, and then complex it with the metal salt precursor. The first method is most commonly used, and here we present only a simplified variation. To the best of our knowledge, the second method is new.

The direct route to $MPcH_{16}$ is very similar to the synthesis of the H_2PcH_{16} ring. The reaction should be run under an inert atmosphere, not only to prevent the hydrolysis of the nitrile groups, but also to avoid unwanted oxidation of the metal cation (manganese, for example, will only form the complex as Mn^{2+}).[31] The choice of solvent is critical, because the reaction is run under reflux. Low-boiling point solvents such as pentane, cyclohexane, and even *n*-butanol gave only trace amounts of product. Control experiments showed that *n*-pentanol, which boils at 138 °C, gave the highest yields, with quantitative conversion of the phthalonitrile precursor after 2 h.

We first optimised this protocol for $CuPcH_{16}$, and then applied it to the synthesis of the manganese, iron, cobalt, nickel and zinc analogues. All six complexes were characterised by IR, Raman, XRD and high-resolution MS (see experimental section and the appendix chapter 3 for details).

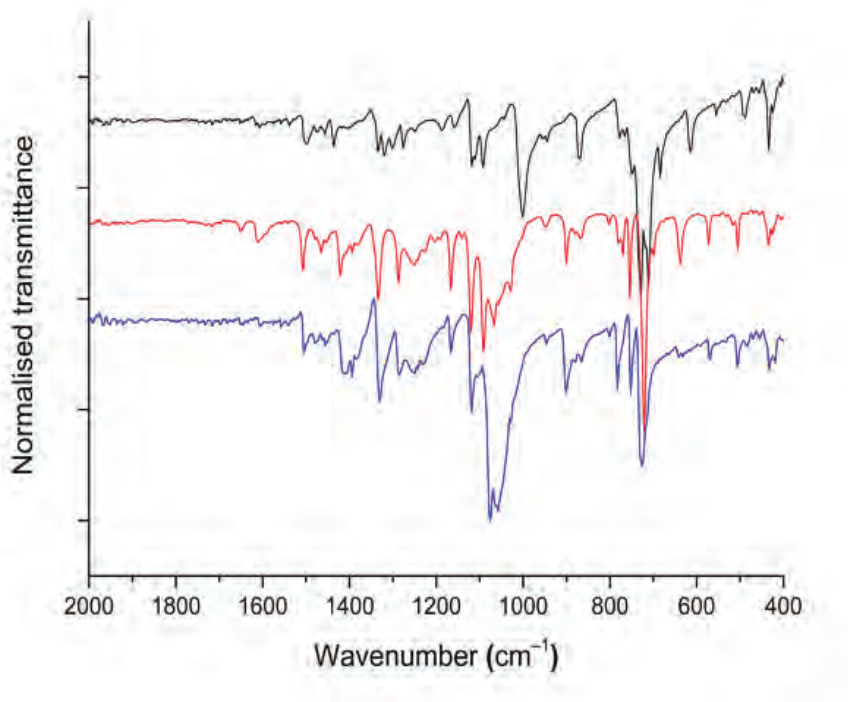

Figure 1: FTIR spectra of H_2PcH_{16} (black), CuPcH16 (red) and $MnPcH_{16}$ (blue).

The FTIR spectra of H_2PcH_{16}, $CuPcH_{16}$ and $MnPcH_{16}$, **Figure 1**, show distinctive peaks. Small shifts between the Pcs are expected due to the different metals. The peak at ca. 428 cm^{-1} shows the in-plane C–C–H bend, while that at ca. 717 cm^{-1} pertains to the out-of-plane C–C–H bend. Further, we observe the N–H bend at 752 cm^{-1}, the C–N stretch at 1118 cm^{-1}, the C–H bend (or possibly C–N stretch) at 1164 cm^{-1}, a strong C–C stretch peak at 1333 cm^{-1}, and the C=N stretch at 1508 cm^{-1}.[32–34]

The structure of $ZnPcH_{16}$ was also confirmed by ^{1}H-NMR, shown in **Figure 2**. The NMR clearly shows the formation of the highly symmetric complex, with only two types of chemically different hydrogen atoms, noted in the figure as α and β. The two double doublets at δ_H = 9.46–9.43 and at δ_H = 8.15–8.12 have coupling constants of 3.0 and 5.6 Hz, respectively, indicating meta and ortho coupling. This is in good agreement with what is expected for aromatic systems.[35]

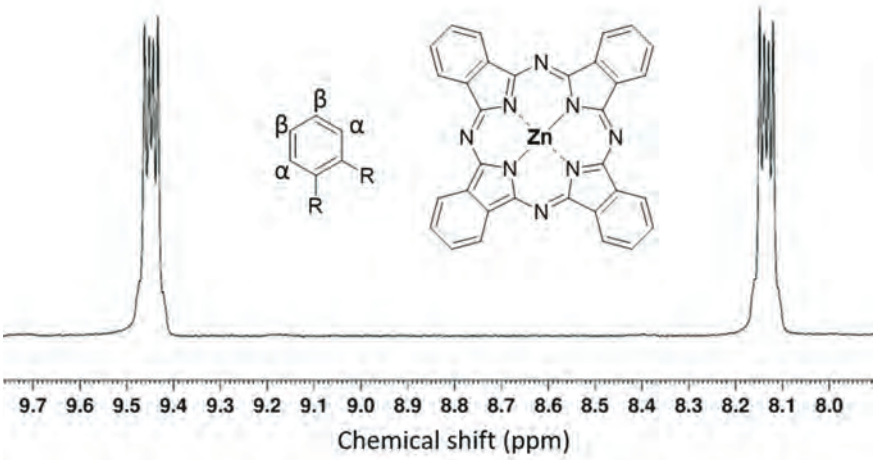

Figure 2: ^{1}H-NMR of $ZnPcH_{16}$ (300 MHz, $CDCl_3$). The a and β designations correspond to the two types of chemically different hydrogen atoms. Chemical shifts are reported relative to $CDCl_3$.[36]

The second route to $MPcH_{16}$ involves the insertion of a metal ion into a metal-free H_2PcH_{16} ring, giving the $MPcH_{16}$ product plus two equivalents of protons (**Scheme 3**). This is a new procedure, which we feel has merit, especially if you want to make several different $MPcH_{16}$ complexes. The main barrier to this reaction is the general insolubility of H_2PcH_{16} (it does dissolve in methylnaphthalene, even at room temperature, but unfortunately the metalation does not occur). However, we found that H_2PcH_{16} dissolves slightly under reflux in *n*-pentanol, giving an opportunity for the metal insertion to proceed. Once this starts, the reaction runs readily. Quantitative yield is reached after 2 h, and the product isolation is simple and straightforward (see

experimental section for details). This reaction doesn't require inert atmosphere (control experiments showed that the metalation of $CuPcH_{16}$ proceeds readily under air).[36]

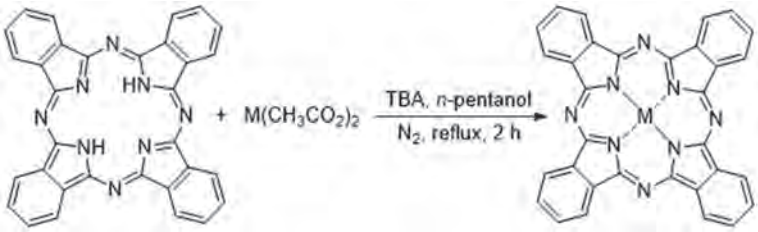

Scheme 3: Complexation of the "empty" Pc with various metals; M = Mn, Fe, Co, Cu, Zn.

This metalation requires an organic base to remove the acidic protons from the centre of the Pc ring. The reaction proceeds well with either tributylamine (TBA) or butyldimethylamine (BDMA), but no conversion was observed in the presence of DBU. We hypothesise that the 3D bulkiness of TBA and BDMA helps in unstacking the Pc rings, which are bound to each other by π–π interactions. At the end of the reaction, any excess base is easily removed by washing with dilute HCl.

The metalation was confirmed by powder X-Ray diffraction studies, which show a clear difference between the metal-free H_2PcH_{16} and the metalated $MPcH_{16}$. **Figure 3** shows the diffraction patterns for three samples: an H_2PcH_{16} (black), a $CuPcH_{16}$ made using the direct route (red) and a $CuPcH_{16}$ made by the two-step method (blue). The H_2PcH_{16} sample shows four peaks in the region $2\theta = 10–20°$, namely at 13.6°, 14.95°, 15.95° and 16.8°. Conversely, both of the $CuPcH_{16}$ samples show peaks at 10.65°, 12.6°, 14.2°, 18.25° and 18.65°, which are distinct from those of H_2PcH_{16}. This also confirms that both metalation protocols result in the same $MPcH_{16}$ product.

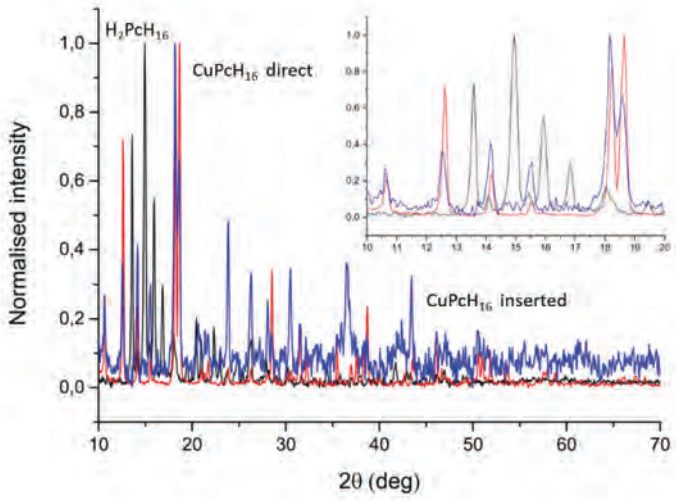

Figure 3: Powder x-ray diffraction pattern of H_2PcH_{16} (black), $CuPcH_{16}$ (red) prepared via the direct route and $CuPcH_{16}$ (blue) made in the two-step method. The inset shows the zoomed-in spectra for the region 2θ = 10-20°.

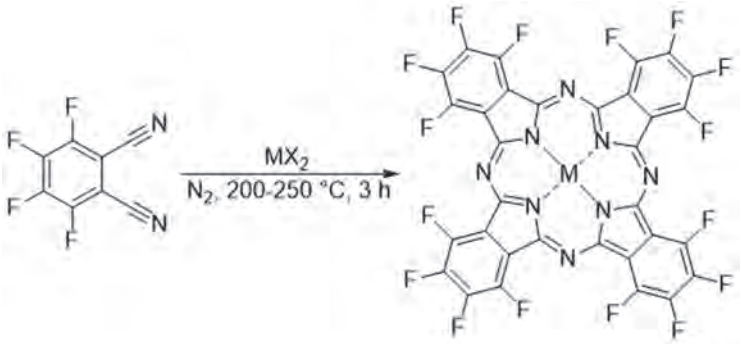

Scheme 4: MX_2 = $Co(OAc)_2{\cdot}4H_2O$, $Mn(OAc)_2{\cdot}4H_2O$, $Fe(OAc)_2$, $CuCl_2$, $Zn(OAc)_2{\cdot}2H_2O$.

The first route, starting from the phthalonitrile, can also be used for making the perfluorinated metal-Pc complexes $MPcF_{16}$ (**Scheme 4**). These are interesting because the perfluorinated ring creates a 'protective shell' around the complex that can prevent its oxidation and degradation. As an added bonus, the perfluorinated metal-Pc complexes are much more readily soluble in several organic solvents. Here we combined two different procedures, from van Lier *et al.*[37] and Morley and co-workers.[38]

Using 2,3,4,5-tetrafluorophthalonitrile as our starting material, we ran the reactions at higher temperatures, typically 200 °C for $CuPcF_{16}$ and 250 °C for $CoPcF_{16}$, $ZnPcF_{16}$, $FePcF_{16}$ and $MnPcF_{16}$, without any solvent (the reagent itself melts at ca. 85 °C, so in practice it serves as its own solvent). The synthesis is straightforward, giving the crude $MPcF_{16}$ complexes as dark blue/black solids. After crushing the hard black solids, any leftover metal salt is washed away with water. The product is then Soxhlet extracted using acetone and checked in NMR for starting material. Note that the type and the size of the reaction vessel is important here, because if you use a too-large round-bottomed flask the tetrafluoro-phthalonitrile will sublime on the top part of the flask, effectively separating your reagents from each other.Powder X-Ray diffraction studies of the different $MPcF_{16}$ compounds show one main single peak (**Figure 4**), which shifts slightly depending on the metal ion. In general, complexes of heavier metals show this peak at higher 2θ values: {$MnPcF_{16}$, 26.90°}; {$FePcF_{16}$, 27.65°}; {$CoPcF_{16}$, 27.70°}; {$CuPcF_{16}$, 28.45°}; and {$ZnPcF_{16}$, 28.6°}.

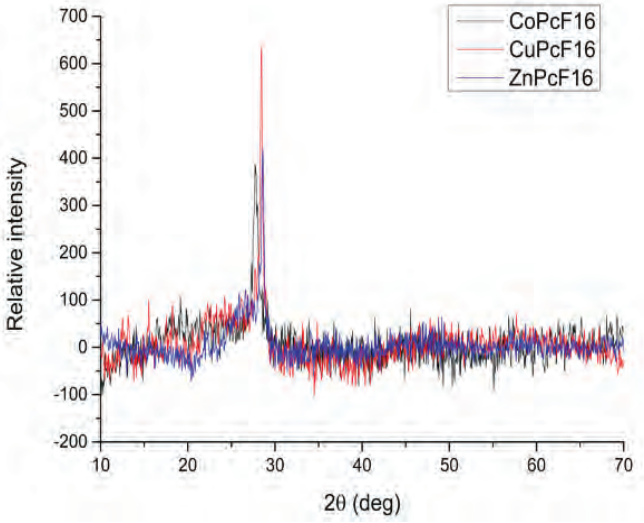

Figure 4: Powder x-ray diffraction of $MPcF_{16}$ complexes. The data for the iron and manganese complexes are omitted for clarity.

3.3 Conclusions

We successfully developed the synthesis of H_2PcH_{16}, $MPcH_{16}$ and $MPcF_{16}$, for a variety of metals. Furthermore, we succeeded in inserting a metal into the H_2PcH_{16} structure. The synthetic protocols are easy, general and can be performed with standard lab equipment. We trust and hope that these simple and effective routes will help researchers who are interested in making phthalocyanines, increasing their variety of applications even further.

3.4 Experimental Section

Materials and instrumentation. All chemicals were purchased from either VWR chemicals, Fluorochem or Merck and were used without further purification, except for solvents, which were dried prior to reaction over 3 Å molecular sieves. All experiments were performed under nitrogen atmosphere, unless stated otherwise.

NMR spectra [^{1}H, ^{19}F] were measured on a Bruker AV 300 spectrometer. IR spectra (4000–400 cm^{-1}, resol. 0.5 cm^{-1}) were recorded on a Varian 660 FTIR spectrometer using ATR and the transmission technique. X-Ray diffraction (XRD) patterns were obtained with a MiniFlex II diffractometer using Ni-filtered CuKα radiation. The X-ray tube was operated at 30 kV and 15 mA, with a 0.01° step and 1 s dwell time. Raman spectra were recorded using a Renishaw InVia system (532 and 632.8 nm) and a Kaiser Optical Systems RXN-4 system (785 nm) coupled with fibre optics to an immersion probe with a short focal length.

Mass spectra were collected on two instruments: (A) AccuTOF LC, JMS-T100LP Mass spectrometer (JEOL, Akishima, Tokyo, Japan). ESI source, positive-ion mode; needle voltage 2500 V, orifice 1 voltage 120 V, orifice 2 voltage 9 V; ring Lens voltage 22 V; orifice 180 °C, desolvating chamber 250 °C. The samples were measured using flow injection with a flow rate of 0.01 mL/min, and the spectra were recorded with an average duration of 0.5 min. (B) AccuTOF GC v 4 g, JMS-T100GCV Mass spectrometer (JEOL, Japan). FD emitter, Carbotec or Linden (Essen, Germany), FD 13 μm. Current rate 51.2 mA/min over 1.2 min.

Procedure for synthesising the metal-free phthalocyanine (H_2PcH_{16}).

Phthalonitrile (0.50 g, 3.9 mmol) was dissolved in *n*-pentanol (2 mL). Then 1,8-diazabicyclo(5.4.0)undec-7-ene (0.1 mL, 0.7 mmol, DBU) was added and the mixture was heated for 2 h at 140 °C, forming a dark blue/purple solution (adding more DBU

is unadvisable as this creates problems in the workup). The reaction was cooled down to ambient temperature, filtered and washed first with water (5 × 10 mL) and then with EtOH (5 × 10 mL) and dried in air at 20 °C. This yielded the product as dark blue/purple small needles, 0.33 gram (66 mol% based on phthalonitrile). HRMS (FD+) m/z calculated $C_{32}H_{18}N_8$, 514.165, found, 514.167. FTIR (cm^{-1}): 1110, 1095, 995, 717; Raman shift/cm^{-1}: 682, 723, 795, 1141, 1337, 1541. XRD (2θ °): 13.6, 14.95, 15.95, 16.8.

General procedure for synthesising metal-containing phthalocyanines ($MPcH_{16}$) via the direct route.

Phthalonitrile and the corresponding metal salt were dissolved in *n*-pentanol after which the DBU was added. The mixture was heated for 2 h at 140 °C, forming a dark coloured solution. The reaction mixture was cooled down to ambient temperature, forming a solid. This was filtered under vacuum and washed with water (5 × 10 mL) and then with EtOH (5 × 10 mL). The residue was dried under air.

Example 1: $CuPcH_{16}$: Phthalonitrile (0.50 g, 3.9 mmol) and $Cu(OTf)_2$ (362 mg, 1.0 mmol) were dissolved in *n*-pentanol (2 mL). DBU (0.1 mL, 0.7 mmol) was added and the mixture was heated at 140 °C for 2 h, forming a dark blue solution. The reaction was cooled down to ambient temperature, filtered under vacuum and washed with water (5 × 10 mL) and then with EtOH (5 × 10 mL). This gave the $CuPcH_{16}$ as a blue powder, 0.40 gram (70 mol% based on phthalonitrile). HRMS (FD+) m/z calculated $C_{32}H_{16}CuN_8$, 575.079, found, 575.107. FTIR (cm^{-1}): 1612, 1508, 1334, 1118, 1095, 717; Raman shift/cm^{-1}: 592, 680, 1142, 1340, 1449, 1523.

Example 2: $ZnPcH_{16}$: Phthalonitrile (0.50 g, 3.9 mmol) and ZnCl2 (136 mg, 1.0 mmol) were dissolved in *n*-pentanol (2 mL). DBU (0.1 mL, 0.7 mmol) was added and the mixture was heated for 2 h at 140 °C, forming a dark green

solution. The reaction was cooled down to ambient temperature, filtered under vacuum and washed with water (5 × 10 mL) and then with EtOH (5 × 10 mL). This gave a green powder, weighing 263 mg (45 mol% based on phthalonitrile). HRMS (FD+) m/z calc. $C_{32}H_{16}N_8Zn$, 576.078, found 576.085. ^{1}H-NMR (300 MHz, $CDCl_3$) δ 9.46–9.43 (8H, double doublet), 8.15–8.12 (8H, double doublet). FTIR (cm^{-1}):1594, 1482, 1328, 1112, 1083, 1058, 885, 746, 728; Raman shift/cm^{-1}: 160, 591, 674, 1330, 1495.

The syntheses of $FePcH_{16}$, $MnPcH_{16}$, $CoPcH_{16}$ and $NiPcH_{16}$ was similarly performed, using: $FeCl_2 \cdot 4H_2O$ (199 mg, 1 mmol, 16 mol% based on phthalonitrile), $MnCl_2 \cdot 2H_2O$, (162 mg, 1 mmol, 73 mol%), $CoCl_2 \cdot 6H_2O$ (238 mg, 1 mmol, 21 mol%), $Ni(OTf)_2$ (357 mg, 1 mmol, 66 mol%).

Procedure for metalation of the H_2PcH_{16} (the two-step method).

The H_2PcH_{16} and the metal salt (1:2.5 equiv) were dissolved in *n*-pentanol. Tributylamine (TBA) was added and the mixture was heated for 2 h at 160 °C and then cooled down to ambient temperature. The dark coloured mixture was filtered under ambient pressure, giving a dark-coloured cake. This was washed first with water (2 x 10 mL), then with 0.6 M HCl (1 × 10 mL), again with water (1 × 10 mL) and finally with EtOH (3 x 10 mL). The dark powder was dried in open air.

Example 1: $CuPcH_{16}$: The H_2PcH_{16} (20 mg, 0.04 mmol) and $Cu(OAc)_2 \cdot H_2O$ (20 mg, 0.1 mmol) were dissolved in *n*-pentanol (3.0 mL) together with the TBA (0.05 mL, 2 mmol). The mixture was heated for 2 h at 160 °C, forming a dark blue solution. This was allowed to cool down to ambient temperature and then filtered, giving a dark-blue cake. The cake was washed first with water (2 × 10 mL), then with 0.6 M HCl (1 × 10 mL), again with water (1 × 10 mL) and finally with EtOH (3 × 10 mL). The resulting

blue powder was dried in air, yielding 40 mg (100 mol% based on the H_2PcH_{16}). XRD (2θ°): 10.65, 12.6, 14.15, 18.25, 18.62, 23.8, 26.2.

Example 2: $MnPcH_{16}$: The H_2PcH_{16} (15 mg, 0.03 mmol) and $Mn(OAc)_2{\cdot}4H_2O$ (25 mg, 0.1 mmol) were dissolved in *n*-pentanol (3.0 mL) after which the TBA (0.05 mL, 2 mmol) was added. The reaction was heated at 160 °C for 2 h, forming a green solution. The mixture was cooled down to ambient temperature and then filtered, giving a dark green cake. The cake was washed first with water (2 × 10 mL), then with 0.6 M HCl (1 × 10 mL), again with water (1 × 10 mL) and finally with EtOH (3 × 10 mL). While washing, the product lost its green colour, turning into a dark blue powder, which was air dried. This gave 12 mg (70 mol% based on the H_2PcH_{16}). XRD (2θ°): 14.1, 15.5, 18.2, 23.75, 26.2.

The syntheses of $FePcH_{16}$, $ZnPcH_{16}$ and $CoPcH_{16}$ were performed similarly, starting from $Fe(OAc)_2$ (17 mg, 0.1 mmol, 100 mol% yield based on the H_2PcH_{16}), $Zn(OAc)_2{\cdot}2H_2O$ (26 mg, 0.12 mmol) and $Co(OAc)_2{\cdot}4H_2O$ (20 mg, 0.1 mmol, 57 mol% yield based on the H_2PcH_{16}).

General procedure for the synthesis of metal-containing fluorophthalocyanine ($MPcF_{16}$).

Tetrafluorophthalonitrile and the corresponding metal salt were mixed and heated at 250 °C (200 °C in the case of copper) for 3 h in a closed 10 mL round bottom flask. The reaction mixture was cooled down to ambient temperature, forming a black solid. This was crushed, filtered and washed with water (5 × 10 mL) and extracted by soxhlet using acetone. The acetone filtrate was collected and evaporated, yielding the product.

Example 1: $CuPcF_{16}$: Tetrafluorophthalonitrile (0.20 g, 1 mmol) and CuCl2 (0.135 g, 1 mmol) were added and heated for 3 h at 200 °C, forming a dark

blue/green solid. After it was allowed to cool down to ambient temperature, it was vacuum filtrated and washed with water (5 × 10 mL), EtOH (5 × 10 mL) and acetone (10 × 10 mL), respectively. The acetone filtrate was evaporated and gave 95 mg, (45 mol% based on tetrafluorophthalonitrile). HRMS (FD+) m/z calc. $C_{32}CuF_{16}N_8$, 862.928, found, 862.974. FTIR (cm^{-1}): 1737, 1488, 1384, 1321, 1151, 962; Raman shift/cm^{-1}: 587, 734, 1360, 1480, 1525. XRD (2θ°): 28.45.

Example 2: $CoPcF_{16}$: Tetrafluorophthalonitrile (0.5 g, 2.5 mmol) and Co $(OAc)_2 \cdot 4H_2O$ (0.623 g, 2.5 mmol) were mixed and heated at 250 °C for 3 h, forming a black solid. The solid was cooled down to ambient temperature, crushed, filtered and washed with water (5 × 10 mL). Soxhlet extraction using acetone gave a blue liquid. Filtration and evaporation of the acetone gave the product in 66 mg, (12 mol% based on tetrafluorophthalonitrile). HRMS (FD+) m/z calculated $C_{32}CoF_{16}N_8$, 858.932, found, 858.949. FTIR (cm^{-1}): 1471, 1261, 1097, 1027, 802; Raman shift/cm^{-1}: 587, 729, 1400, 1530, 1614. XRD (2θ°): 27.7.

The syntheses of $FePcF_{16}$, $ZnPcF_{16}$ and $MnPcF_{16}$ were performed similarly, starting from $Fe(OAc)_2$ (435 mg, 2.5 mmol, 15 mol% based on tetrafluorophthalonitrile), $Zn(OAc)_2 \cdot 2H_2O$ (550 mg, 2.5 mmol, 33 mol% yield) and $Mn(OAc)_2 \cdot 4H_2O$ (613 mg, 1 mmol, 16 mol% yield).

3.5 References

[1] Nitrogenase and homologs, Y. Hu, M.W. Ribbe, *JBIC J. Biol. Inorg. Chem.* **2015**, *20*, 435–445.

[2] A tale of two methane monooxygenases, M.O. Ross, A.C. Rosenzweig, *JBIC J. Biol. Inorg. Chem.* **2017**, *22*, 307–319.

[3] Dioxygen: What makes this triplet diradical kinetically persistent?, W.T. Borden, R. Hoffmann, T. Stuyver, B. Chen, *J. Am. Chem. Soc.* **2017**, *139*, 9010–9018.

[4] Selective autooxidation of ethanol over titania-supported molybdenum oxide catalysts: Structure and reactivity, C. Caro, K. Thirunavukkarasu, M. Anilkumar, N.R. Shiju, G. Rothenberg, *Adv. Synth. Catal.* **2012**, *354*, 1327–1336.

[5] Cooperative catalysis for selective alcohol oxidation with molecular oxygen, T.K. Slot, D. Eisenberg, D. van Noordenne, P. Jungbacker, G. Rothenberg, *Chem. – Eur. J.* **2016**, *22*, 12307–12311.

[6] Selective catalytic oxidation of cyclohexene with molecular oxygen: Radical versus nonradical pathways, I.M. Denekamp, M. Antens, T.K. Slot, G. Rothenberg, *ChemCatChem* **2018**, *10*, 1035–1041.

[7] 212. Phthalocyanines. Part I. A new type of synthetic colouring matters, R.P. Linstead, *J. Chem. Soc. Resumed* **1934**, *0*, 1016–1017.

[8] Industrial applications of phthalocyanines, P. Gregory, *J. Porphyr. Phthalocyanines* **2000**, *4*, 432–437.

[9] Phthalocyanines, G. Löbbert, in *Ullmanns Encycl. Ind. Chem.*, American Cancer Society, **2000**.

[10] Direct identification of various copper phthalocyanine pigments in automotive paints and paint smears by laser desorption ionization mass spectrometry, T. Mukai, H. Nakazumi, S. Kawabata, M. Kusatani, S. Nakai, S. Honda, *J. Forensic Sci.* **2008**, *53*, 107–115.

[11] Raising the performance of copper-phthalocyanine pigments, V.N.G.& C. KG, found under http://www.european-coatings.com/Raw-materials-technologies/Applications/Automotive-coatings/Raising-the-performance-of-copper-phthalocyanine-pigments.

[12] What's Inside: Inkjet Cartridges, P.D. Justo, *Wired* **2011**, *19*.

[13] Identification of colorants in pigmented pen inks by laser desorption mass spectrometry, K. Papson, S. Stachura, L. Boralsky, J. Allison, *J. Forensic Sci.* **2008**, *53*, 100–106.

[14] The Ink in your ballpoint pen is full of interesting chemistry, J. Chaussee, *Wired* **2016**.

[15] Preparation of a water-soluble fluorinated zinc phthalocyanine and its effect for photodynamic therapy, K. Oda, S. Ogura, I. Okura, *J. Photochem. Photobiol. B* **2000**, *59*, 20–25.

[16] Synthesis and photodynamic activity of novel asymmetrically substituted fluorinated phthalocyanines, W.M. Sharman, J.E. van Lier, *Bioconjug. Chem.* **2005**, *16*, 1166–1175.

[17] Fluorination of copper phthalocyanines: Electronic structure and interface properties, H. Peisert, M. Knupfer, T. Schwieger, G.G. Fuentes, D. Olligs, J. Fink, Th. Schmidt, *J. Appl. Phys.* **2003**, *93*, 9683–9692.

[18] Phthalocyanine metal complexes in catalysis, A.B. Sorokin, *Chem. Rev.* **2013**, *113*, 8152–8191.

[19] Metal phthalocyanines as electrocatalysts for redox reactions, P. Vasudevan, N. Phougat, A.K. Shukla, *Appl. Organomet. Chem.* **1996**, *10*, 591–604.

[20] Electrosynthesis of phthalocyanines: Influence of solvent, B.I. Kharisov, L.M. Blanco, L.M. Torres-Martinez, A. García-Luna, *Ind. Eng. Chem. Res.* **1999**, *38*, 2880–2887.

[21] Low-temperature synthesis of phthalocyanine and its metal complexes, B.I. Kharisov, U. Ortiz Mendez, J. Rivera de la Rosa, *Russ. J. Coord. Chem.* **2006**, *32*, 617–631.

[22] Synthesis of phthalocyanines from phthalonitrile with organic strong bases, H. Tomoda, S. Saito, S. Ogawa, S. Shiraishi, *Chem. Lett.* **1980**, *9*, 1277–1280.

[23] Phthalocyanine Compounds, F.H. Moser, A.L. Thomas, *Phthalocyanine Compounds*, Reinhold Publishing Corporation, New York, **1963**.

[24] Ruthenium phthalocyanine: structure, magnetism, electrical conductivity properties, and role in dioxygen activation and oxygen atom transfer to 1-Octene, A. Capobianchi, A.M. Paoletti, G. Pennesi, G. Rossi, R. Caminiti, C. Ercolani, *Inorg. Chem.* **1994**, *33*, 4635–4640.

[25] Synthesis and characterization of highly soluble hexadecachloro- and hexadecafluorophthalocyanine ruthenium(II) complexes, D. Christendat, M.A. David, S. Morin, A.B.P. Lever, K.M. Kadish, J. Shao, *J. Porphyr. Phthalocyanines* **2005**, *09*, 626–636.

[26] Improved synthesis of metal-free phthalocyanines, P.J. Brach, S.J. Grammatica, O.A. Ossanna, L. Weinberger, *J. Heterocycl. Chem.* **1970**, *7*, 1403–1405.

[27] High-pressure conditions for improved synthesis of phthalocyanines, S. J. Edmondson, J. S. Hill, N. S. Isaacs, P.C. H. Mitchell, *J. Chem. Soc. Dalton Trans.* **1990**, *0*, 1115–1118.

[28] Phthalocyanine synthesis in ionic liquids: Preparation of differently substituted phthalocyanines in tetrabutylammonium bromide, P.C. Lo, D.Y.Y. Cheng, D.K.P. Ng, *Synthesis* **2005**, *7*, 1141–1147.

[29] The solid phase, room-temperature synthesis of metal-free and metallophthalocyanines, particularly of 2,3,9,10,16,17,23,24-octacyanophthalocyanines, V.N. Nemykin, N. Kobayashi, V.M. Mytsyk, S.V. Volkov, *Chem. Lett.* **2000**, *29*, 546–547.

[30] Efficient synthesis of phthalocyanines and related macrocyclic compounds in the presence of organic bases, D. Wöhrle, G. Schnurpfeil, G. Knothe, *Dyes Pigments* **1992**, *18*, 91–102.

[31] Synthesis, structure, and optical properties of manganese phthalocyanine thin films and nanostructures, L. Meng, K. Wang, Y. Han, Y. Yao, P. Gao, C. Huang, W. Zhang, F. Xu, *Prog. Nat. Sci. Mater. Int.* **2017**, *27*, 329–332.

[32] Molecular orientation and spectral investigations of Langmuir–Blodgett films of selected copper phthalocyanines, B. Barszcz, A. Bogucki, A. Biadasz, B. Bursa, D. Wróbel, A. Graja, *J. Photochem. Photobiol. Chem.* **2011**, *218*, 48–57.

[33] Synthesis and characterization of copper phthalocyanine and tetracarboxamide copper phthalocyanine deposited mica-titania pigments, B.B. Topuz, G. Gündüz, B. Mavis, Ü. Çolak, *Dyes Pigments* **2013**, *96*, 31–37.

[34] Molecular organization in the thin films of chloroaluminium hexadecafluorophthalocyanine revealed by polarized Raman spectroscopy, T.V. Basova, V.G. Kiselev, L.A. Sheludyakova, I.V. Yushina, *Thin Solid Films* **2013**, *548*, 650–656.

[35] Organic chemistry, J. Clayden, N. Greeves, S.G. Warren, *Organic Chemistry*, Oxford University Press, New YorK, **2012**.

[36] NMR chemical shifts of common laboratory solvents as trace impurities, H.E. Gottlieb, V. Kotlyar, A. Nudelman, *J. Org. Chem.* **1997**, *62*, 7512–7515.

[37] Hexadecafluorinated zinc phthalocyanine: photodynamic properties against the EMT-6 tumour in mice and pharmacokinetics using 65Zn as a radiotracer, R.W. Boyle, J. Rousseau, S.V. Kudrevich, M. Obochi, J.E. van Lier, *Br. J. Cancer* **1996**, *73*, 49–53.

[38] Polyfluoroarenes. Part XIV. Synthesis of halogenophthalocyanines, J. M. Birchall, R. N. Haszeldine, J. O. Morley, *J. Chem. Soc. C Org.* **1970**, *0*, 2667–2672

Appendix - The supporting information for Chapter 3

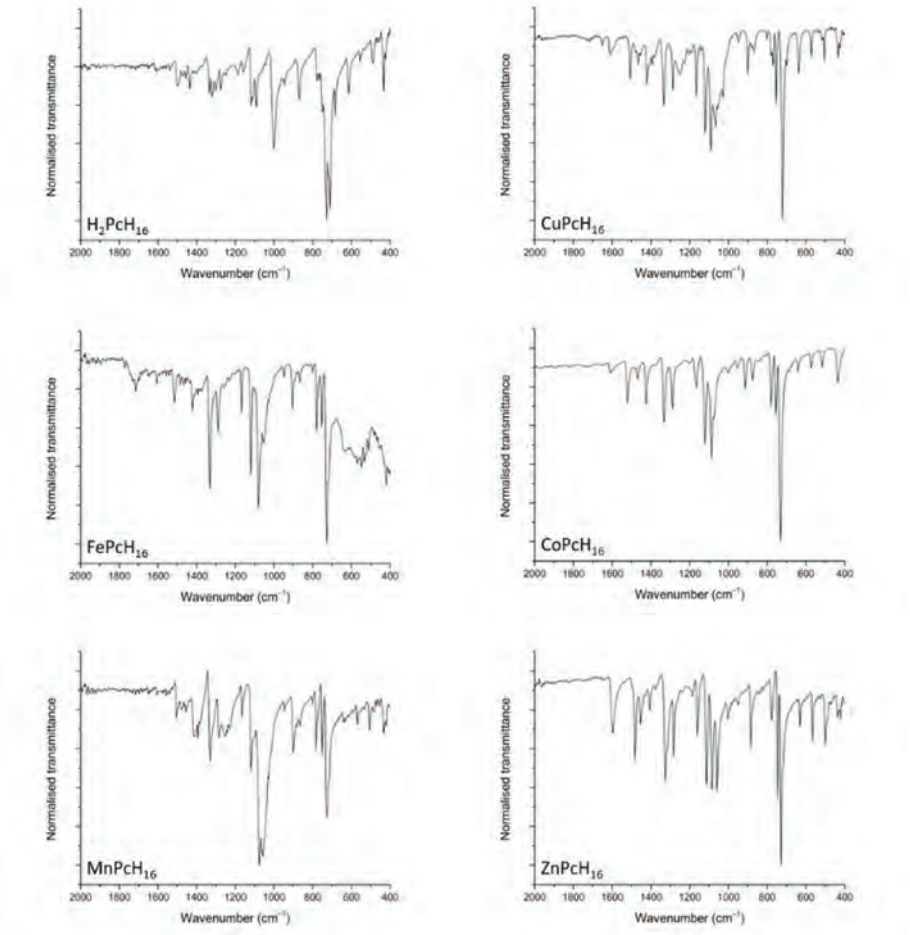

Figure S1: FTIR spectra of the metal-free H_2PcH_{16} ligand and the corresponding $MPcH_{16}$ complexes.

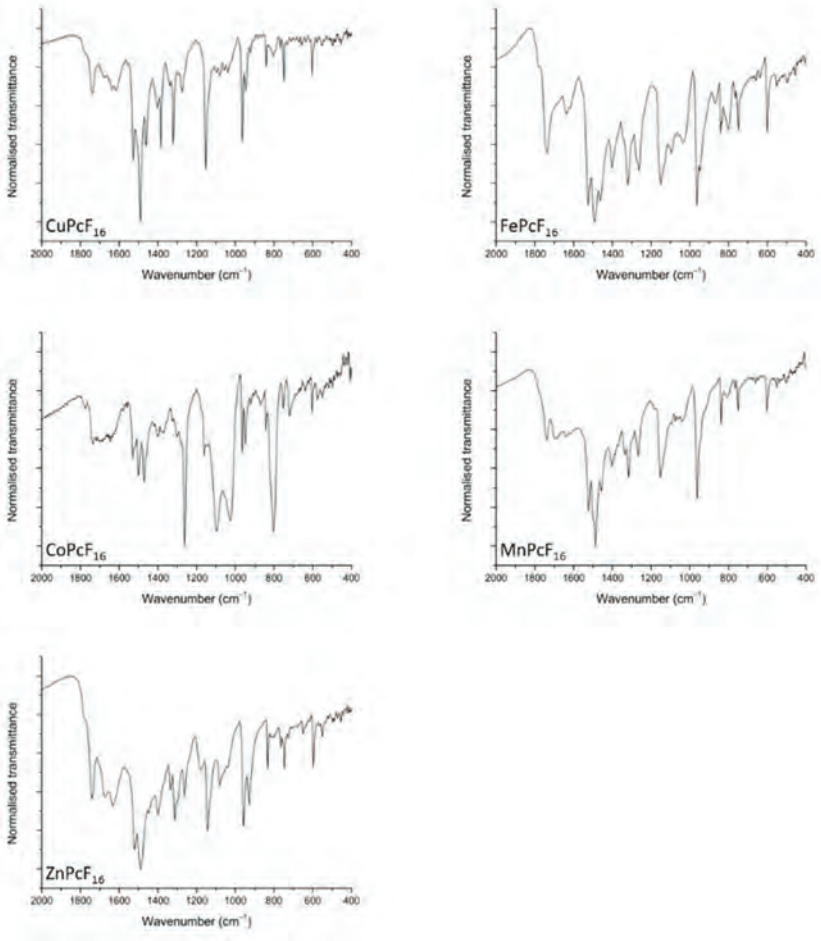

Figure S2: The FTIR spectra of the $MPcF_{16}$ complexes.

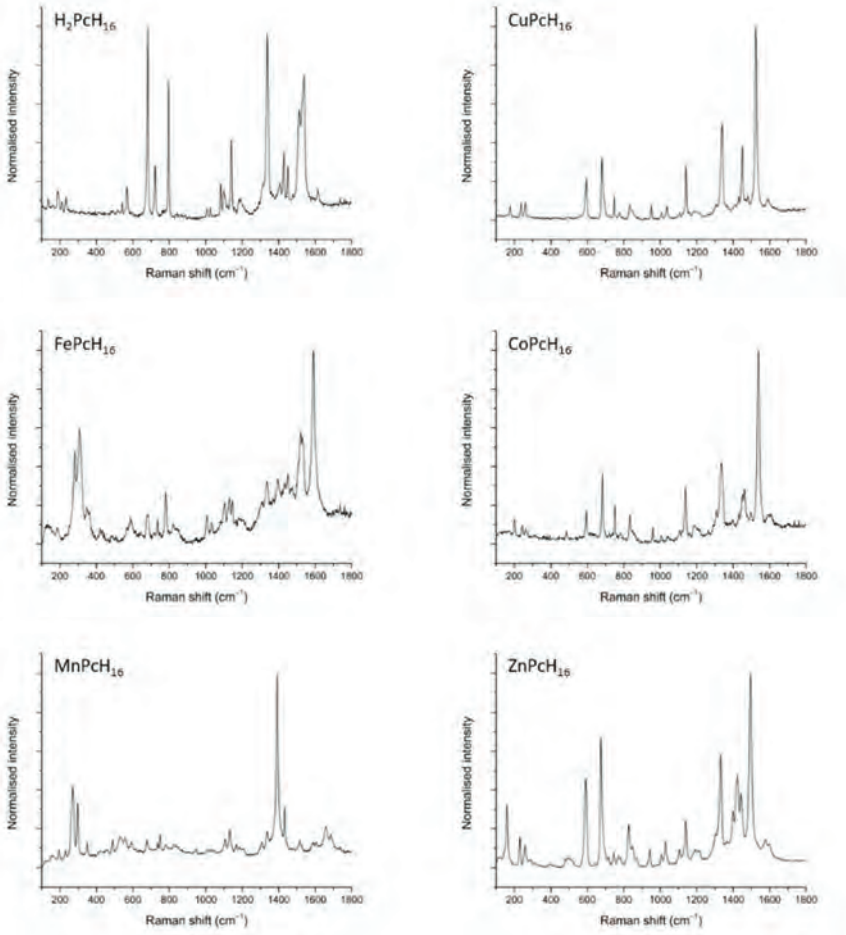

Figure S3: The Raman spectra of the metal-free H_2PcH_{16} ligand and the corresponding $MPcH_{16}$ complexes.

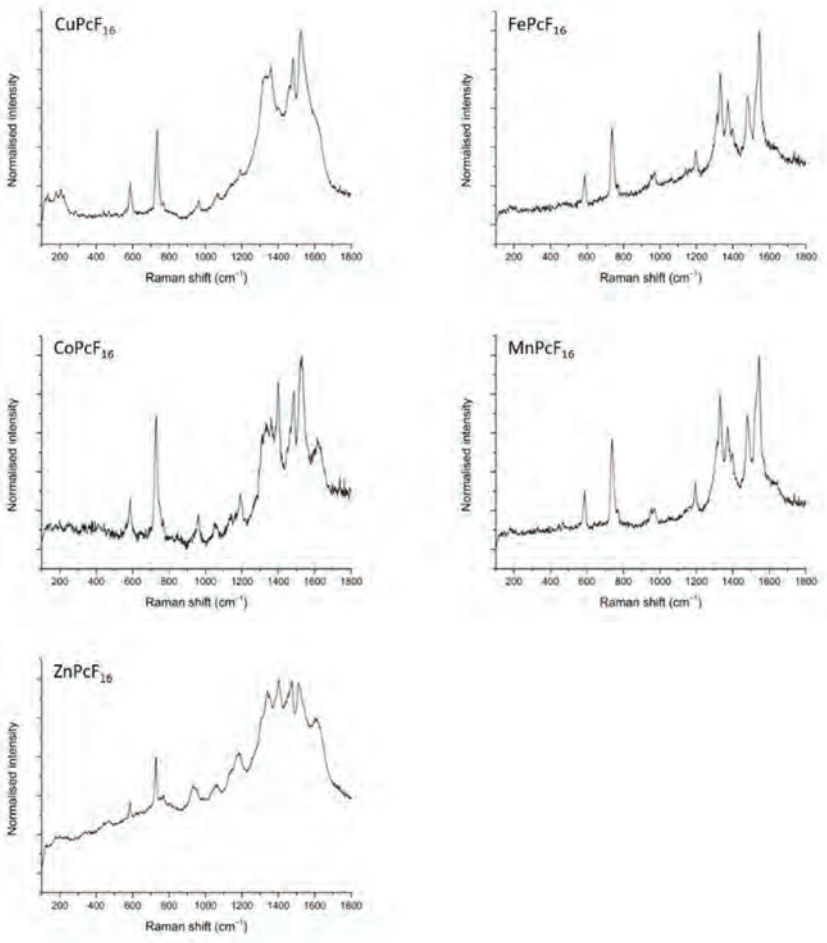

Figure S4: The Raman spectra of the $MPcF_{16}$ complexes.

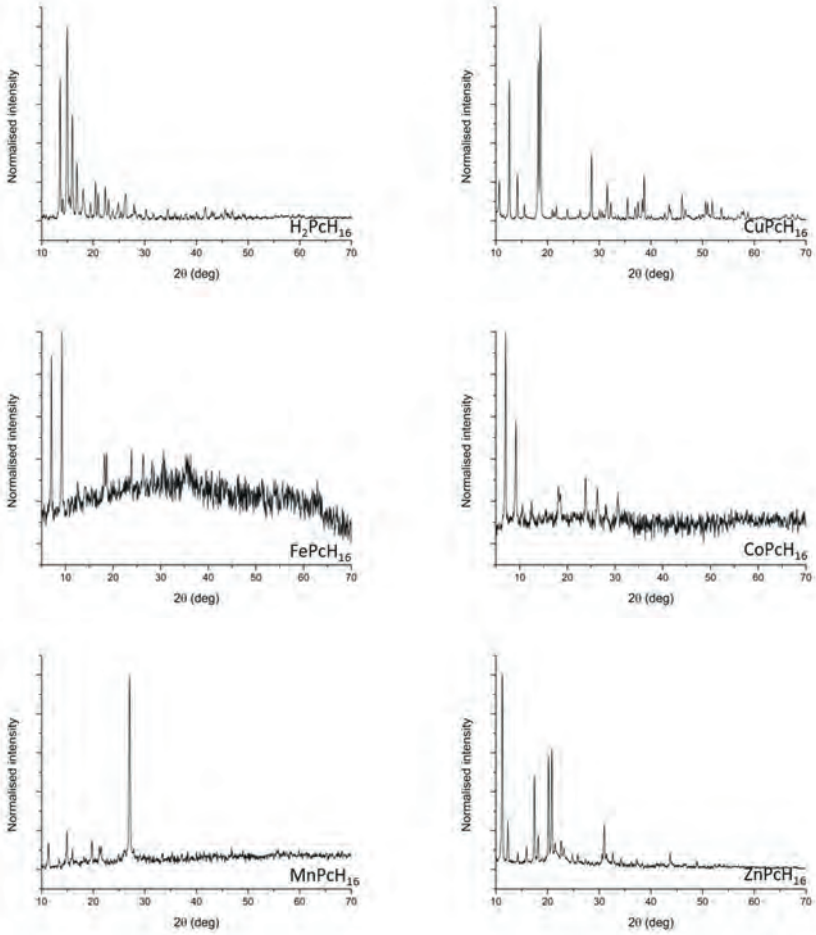

Figure S5: The powder XRD patterns of the corresponding complexes.

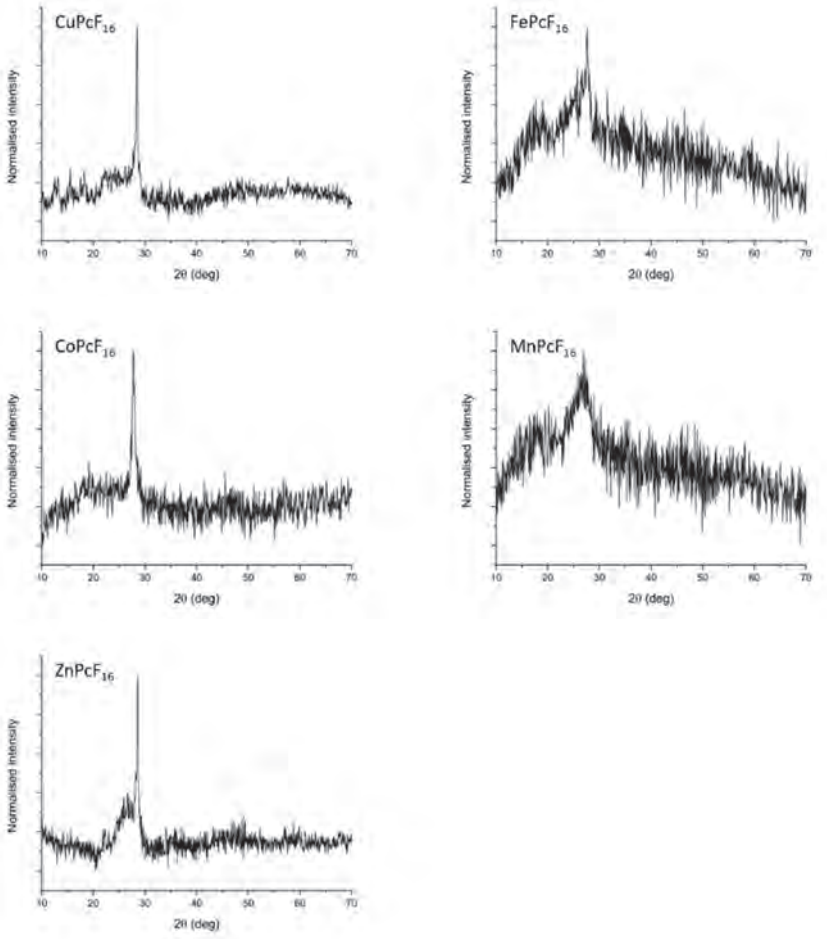

Figure S6: The powder XRD patterns of the MPcF16 complexes.

Designing catalytic polymers with controllable spatial and chemical properties

Chapter 4

Abstract

We report a simple and scalable concept for designing a family of covalently-bound materials wherein single-atom metal sites are dispersed with a high degree of spatial and chemical control. Our method is based on a "ring and linker" building block combination, with highly stable phthalocyanine macrocycles connected by a variety of linkers using amide bonds. This approach enables the design of solid materials with precise distances between the single-atom sites. It is also versatile, allowing for diverse combinations via "mix & match" options. We demonstrate the concept in the synthesis of nine different copper- or cobalt-containing polymers, as well as their application in the selective oxygen reduction reaction. Our results show a clear relation between linker length and activity, demonstrating the power of this simple synthetic approach.

Part of this work has been published as "Covalent structured catalytic materials containing single-atom metal sites with controllable spatial and chemical properties: concept and application", I.M. Denekamp, C. Deacon-Price, Z. Zhang, G. Rothenberg, *Catal. Sci. Technol.,* **2020**, 10, 6694 – 6700.

4.1 Introduction

Designing catalysts for specific applications requires spatial and chemical control. We see this in natural systems, where enzymes catalyse reactions that we chemists can only dream of with envy.[1] Many of these enzymes rely on single-atom sites.[2] Some, such as methane monooxygenase, go further, and combine two metal atoms in a bifunctional site.[3] The superb spatial and chemical control enables these enzymes to carry out selective transformations under very mild conditions – something that we cannot do in vitro. Yet even if we cannot exactly mimic the enzymatic conditions, we can still adapt concepts and pieces of the natural puzzle for designing new active materials.[4–6] Moreover, chemistry allows us to "mix & match" these concepts and properties, creating solid materials that can function under harsh industrial conditions: high temperatures, pressures, and corrosive environments. In this way, we can adapt nature's concepts to our needs.[7]

This is especially true for oxygen activation[8,9] and for oxidative transformations,[10] where selectivity and stability are a must. Here, nature typically uses the haem function, comprising a porphyrin macrocycle ligand with nitrogen atoms surrounding a single central metal atom. The active site is extremely well-defined, but the system is delicate, requiring a cumbersome protective protein shell. Ideally, we want to combine the specificity of the haem complex with the stability and functional flexibility of modern-day industrial materials. We want a stable material that can activate oxygen under a range of conditions, with highly defined monoatomic or diatomic sites.[11,12] Even more importantly, we want a flexible solution, where we can easily change the type of metal site, the distance between sites, and the properties of the surrounding environment. Last, but not least, the material must be scalable and affordable, so that it can be used in real-life applications. [13,14]

In this chapter, we present the concept and application of such designable materials, using a covalent building-block and linker approach. We use functionalised

phthalocyanines (Pcs) as stable synthetic porphyrin mimics, connecting these with a series of linkers into a solid network of well-defined single-atom sites. This approach is highly effective, giving full spatial and chemical control. By using phthalocyanines instead of porphyrins, we create materials with high thermal, chemical and mechanical stability.[15] Moreover, by "mixing" the phthalocyanine metal centres and linker lengths and types, we control both the distance between the metal sites and their surrounding environment. The effects of this control are demonstrated using the oxygen reduction reaction (ORR) as a case study.

Single atom sites are excellent catalysts.[16–21] In the case of ORR, single metal–N_x sites (where N_x denotes a complex with x nitrogen atoms ligating to the metal) achieve high activities.[22–24] We chose to focus on metal-phthalocyanine (MPc, N_4 site) as active sites in ORR, since these give excellent activity.[25,26] Our hypothesis was that by carefully controlling the distances between the active sites we can influence the ORR activity, e.g. through confinement effects.[27–29]

4.2 Results and Discussion

Our concept is based on MPc complex building blocks, the rings of which are modified with connecting groups. These are linked to each other, either directly or using various organic linkers. The result is a solid material with well-defined single-atom sites connected by strong covalent bonds. Our synthetic approach combines the advantages of the phthalocyanine macrocycles as ligands with simple solid catalyst separation by filtration, while at the same time avoiding the problem of π-stacking.

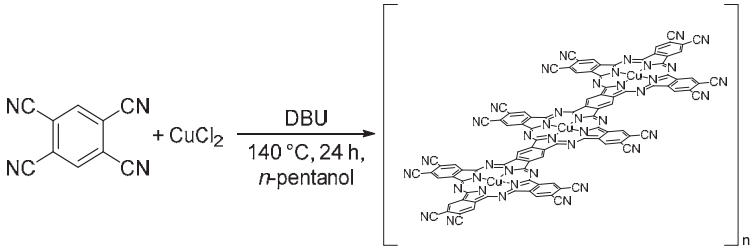

Scheme 1: The synthesis of the directly linked $CuPcC_0$ starting from 1,2,4,5-tetracyanobenzene and copper chloride.

We started by examining the possibility of linking the MPcs directly to each other. This can be done by polymerising the "double phthalonitrile" 1,2,4,5-tetracyanobenzene (**Scheme 1**). Building on the classic procedure, [30,31] we optimised the protocol using *n*-pentanol as solvent, with copper(II) chloride and a strong base, 1,8-diazabicyclo[5.4.0]undec-7-ene (DBU).[32] The resulting dark green powder was characterised by Fourier-transform infrared spectroscopy (FTIR) and MALDI-TOF (characterisation details for all materials are included in the experimental section). However, this route still has two major drawbacks. First, it gives a high degree of polydispersity, due to multiple points of initiation. This also increases branching, resulting in an unpredictable polymer structure. Second, the batch reproducibility is poor, because the polymerisation depends strongly on local conditions. Thus, this direct route is inherently unsuitable for making designed materials.

To overcome these issues, we turned to a sequential approach. In this step-by-step synthesis we first add the substituted Pc building block to the linker in a 1 : 4 ratio (see **Figure 1**). The building blocks react with the linkers via the coupling of acyl chlorides and amines, forming a nylon-type bond. This reaction is quick and efficient, giving near-quantitative yields under ambient atmosphere and 50 °C. After the Pc-linker node forms, four more equivalents of Pc are added, followed by 12 equivalents of linker, and so on. In this way, we grow the polymer as an expanding flat structure.

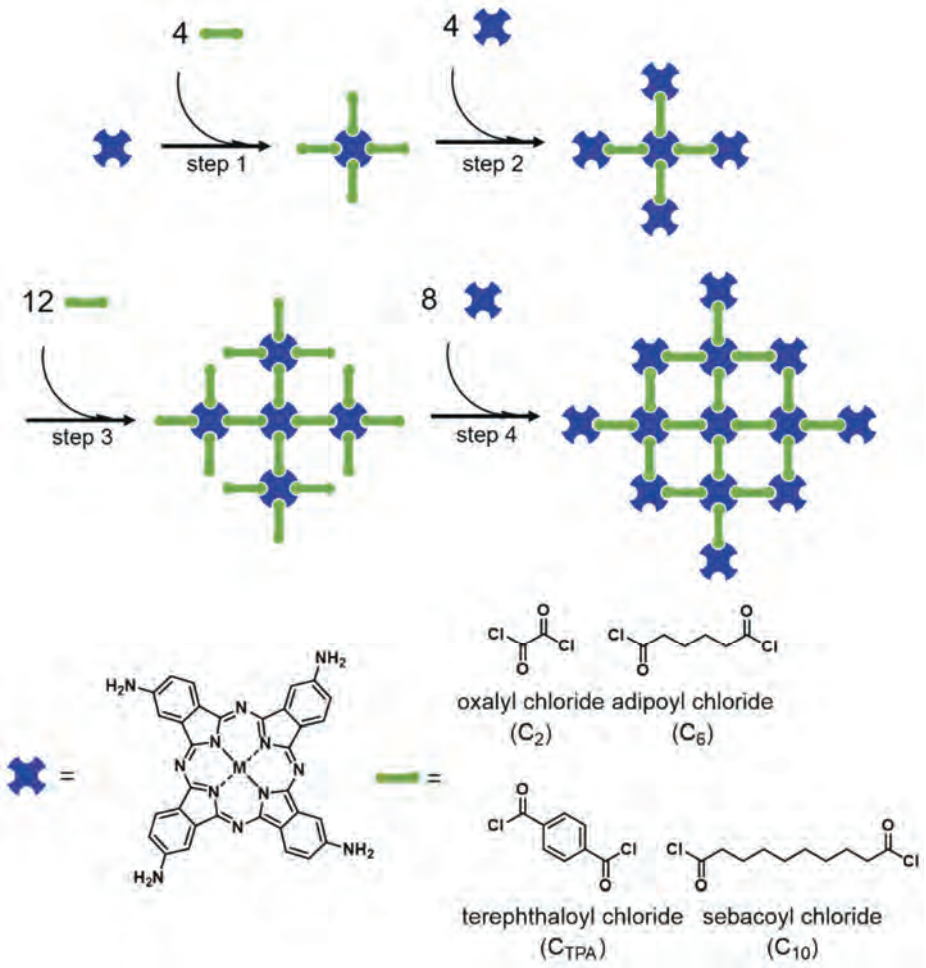

Figure 1: The synthesis of the polymers. Blue building blocks represent the $MPc(NH_2)_4$ and green linkers denote oxalyl chloride (C_2), adipoyl chloride (C_6), terephthaloyl chloride (C_{TPA}) and sebacoyl chloride (C_{10}). All polymers in this chapter were prepared by this four-step synthesis, with the exception of the $CuPcC_0$ which was made following the route shown in Scheme 1.

This step-by-step addition gives a polymer of known size and weight. It also allows the design of specific polymers, by varying the metals used in the Pc, the linker size, or the linker type. This feature is extremely important, because it holds the key to spatial and chemical control. You can create well-defined, complex polymers where you choose the metals in the different rings, as well as the flexibility and distance between the rings (because you can use different linkers in different steps). Here we used four different linkers (**Figure 1**): oxalyl chloride (C_2), adipoyl chloride (C_6), terephthaloyl chloride (C_{TPA}) and sebacoyl chloride (C_{10}).

Oxalyl chloride (C_2) is the shortest linker, containing only two carbon atoms. Once linked, it is essentially two connected and conjugated amide bonds, with an inter-metal distance of approximately 18 Å, and a linker distance of 6 Å. This may allow for easier electron transfer across the metal sites. Adipoyl chloride (C_6) is longer, approximately 10 Å, which increases the inter-metal distance to 23 Å. This linker is unconjugated and flexible. Its counterpart, terephthaloyl chloride (C_{TPA}), features the same linker and inter-metal distances, yet is conjugated and rigid. Comparing C_6 and C_{TPA} can help us quantify the effects of conjugation on the catalytic performance. Finally, sebacoyl chloride (C_{10}) is even longer, with a linker size of 15 Å, and a nominal inter-metal distance of 27 Å. In practice, the distances may be smaller, as such large flexible linkers may promote folding and stacking. By choosing these four different linkers, we can compare the effects of length and flexibility on the materials' performance.

First, we synthesised the monomer building block, $MPc(NH_2)_4$ (where M is either void, Co or Cu), by tetramerization of 4-aminophthalonitrile.[32] In the absence of metal (M = void) this gives the 2,9,16,23-tetra(amino) phthalocyanine, $H_2Pc(NH_2)_4$. The same procedure can be used for making $CuPc(NH_2)_4$ or $CoPc(NH_2)_4$, by adding a copper or cobalt salt, respectively. These new compounds were characterised by high-resolution mass spectrometry (HRMS) and FTIR. **Figure 2** shows one peak at ca. 426 cm^{-1}, attributed to the in-plane C–C–H bend, another at ca. 735cm^{-1} pertaining to the N–C–N inner ring "breathing". Further, we see the C–H in-plane bend at ca. 1095

cm^{-1} (1106 cm^{-1} for $H_2Pc(NH_2)_4$), the C–N stretch at ca. 1500 cm^{-1} and the C=C macrocycle ring deformation at ca. 1593 cm^{-1}. Additional characterisation details are included in the appendix.

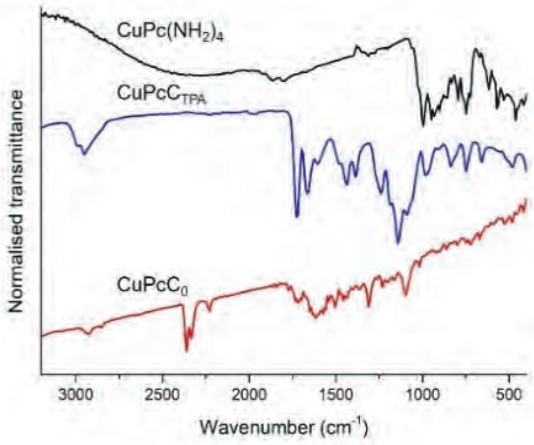

Figure 2: FTIR of $CuPc(NH_2)_4$ (black) $CuPcC_{TPA}$ (blue) and $CuPcC_0$ (red).

With the monomer and linkers at hand, we synthesised nine different copper-containing and cobalt-containing polymers. **Table 1** gives the designation codes and the key synthesis and structure parameters for each polymer. For example, in entry 3, $CuPcC_6$, Cu is the metal atom; Pc indicates phthalocyanine and C_6 denotes the linker (in this case, adipoyl chloride). Except for the linker-free direct-coupled sample, all of the polymers are based on three node rings connected by two sets of linkers (see **Figure 1**, right-hand structure).

Table 1. Designation and parameters of the Pc polymers.

Entry	Polymer	Linker		Diameter (Å) [a]	mw (KDa) [b]
		Length (Å)	Conjugation		
1	$CuPcC_0$	-	-	unknown	unknown
2	$CuPcC_2$	6	ü	84	9.1
3	$CuPcC_6$	10	x	104	10.0
4	$CuPcC_{TPA}$	10	ü	104	10.4
5	$CuPcC_{10}$	15	x	120	10.9
6	$CoPcC_2$	6	ü	84	9.1
7	$CoPcC_6$	10	x	104	10.0
8	$CoPcC_{TPA}$	10	ü	104	10.3
9	$CoPcC_{10}$	15	x	120	10.9

[a] *Nominal diameter based on a flat symmetric structure.* [b] *Theoretical mw of the polymer based on three node rings connected by two sets of linkers.*

The disadvantage of such highly stable high-molecular weight covalent polymers is that their analysis is extremely challenging. They are practically insoluble, regardless of solvent and conditions, precluding SEC and HRMS analysis (we did succeed in HRMS analysis of the smallest structure). For the $CuPcC_0$ we saw at least three MPcs connected to each other, after which the data becomes too noisy. They are also amorphous, ruling out X-ray diffraction. Moreover, as carbonaceous molecular species, they are too small and too transparent for microscopy analysis (we ran detailed SPM, SEM and TEM studies with no results). Three methods, however, are possible: elemental analysis, vibrational spectroscopy (FTIR) and X-ray absorption spectroscopy (XAS).

Elemental analysis is the most reliable quantitative method for determining the composition of samples. Analysis of $CuPcC_2$ and $CuPcC_{10}$ showed that each polymer containing 13 rings and 16 linkers (right-hand structure in **Figure 1**), showed that their elemental compositions fit well with the calculated values (calcd. for $CuPcC_2$: C: 58.9, H: 2.5, N: 23.9, Cu: 9.1 wt%; found: C: 58.9, H: 3.4, N: 22.8, Cu: 9.2 wt%; calcd. for $CuPcC_{10}$: C: 63.3, H: 4.5, N: 20.0, Cu: 7.6; found: C: 61.9, H: 5.9, N: 19.7, Cu: 7.6;).

Both samples contained <0.1 wt% of Cl, confirming that the reaction of the linkers was near-quantitative.

The FTIR spectra of $CuPcC_{TPA}$ and $CuPcC_0$ in **Figure 2** show that the overall profiles of the polymers are very similar. The strong peak at 1650 cm^{-1} indicates a C=O stretch vibration of the secondary amide. This peak confirms the polymerisation (cf. the spectrum of the pristine monomer building block). The same conclusion can be drawn from the peak at 2920 cm^{-1}, showing the alkane C–H stretch. All of the other C–H bonds are aromatic, pertaining to the Pc rings.

The X-ray absorption spectra (XAS) of $CuPc(NH_2)_4$ and $CuPcC_{TPA}$ are highly similar (**Figure 3**), suggesting that the copper centres in both materials are identical. CuPc has a Cu^{2+} metal centre, indicated by the pre-edge feature and the absorption edge positions.[33,34] The radial distribution indicates that the distance from Cu to its nearest neighbour is 1.5 Å (see details in the appendix), confirming the C–N dative bond.[33] The large distance (>20 Å) between the copper atoms even in the smallest CuPc polymer precludes the detection of any Cu–Cu interaction in the EXAFS region. The inset in **Figure 3** shows the residuals plot of the EXAFS data. The data itself is smoothed, but all the removed data is shown in the residuals plot. This plot shows a random scatter, confirming that no meaningful information was lost in the smoothing process.

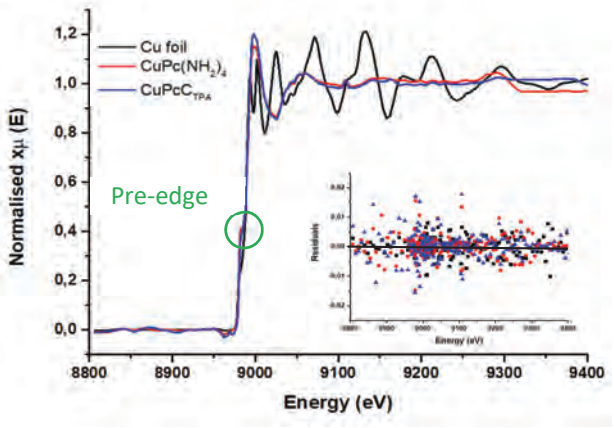

Figure 3: EXAFS data at the Cu K edge for Cu foil (black) , $CuPc(NH_2)_4$ (red) and $CuPcC_{TPA}$ (blue). The green circle shows the pre-edge position. The inset shows the residuals plot, which is unstructured.

Another experimental technique that combines analysis and performance studies is ORR. Here we follow the reduction of oxygen to water, typically via the four-electron route (**Scheme 2**). This reaction can happen in three ways: the first is the reduction of oxygen to hydrogen peroxide which is adsorbed on the surface, after which it is further reduced to water (or, in our basic environment, to OH^-).[35] The second pathway begins similarly with the reduction of oxygen to hydrogen peroxide, which then desorbs from the surface and is ultimately reduced to OH^- in the bulk solution.[36,37] Finally, there is also the (undesired) two electron reduction of oxygen to hydrogen peroxide as final product.

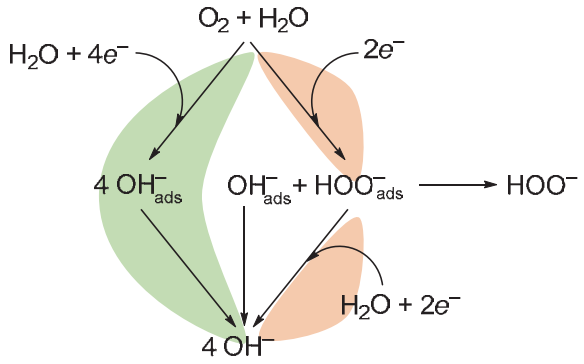

Scheme 2: The oxygen reduction reaction can proceed via either the direct four-electron route (green) or the indirect 2+2 electron route (orange). In the latter case, the reaction can also stop after the first step, giving one hydroxyl ion and one hydroperoxyl ion.

The mechanism of ORR on Pcs was studied by Chen *et al.*[38] and by Nørskov and co-workers.[39] In brief, oxygen binds with one oxygen atom to the metal and the other oxygen will position itself between two nitrogen atoms of the Pc.[38] Oxygen adsorption is the key step in controlling the ORR onset potential in a basic environment. After the adsorption of O_2, it can react in two ways. It can react with one proton and electron from the surrounding water to from the active OOH^-, or dissociate; leaving the surface as an unreacted molecule. After a proton transfer, the OH^- in the surrounding O_2, dissociation becomes more facile, since water at the surface is a stronger proton donor than OH^-.[36,39] Clustering of the copper atom centres is unlikely, since Pcs are stable at high pressure and temperature. Moreover, were clustering to occur, all the LSV curves would be the same, because the metal distance is the only difference between the polymers. This is not the case, hence the copper atoms do not cluster.

Prior to reaction, we supported the Pc and polymerised Pc samples on activated carbon to increase their conductivity and adhesion to the electrode surface. The ORR

activity was measured with linear sweep voltammetry (LSV) in a 0.1 M KOH electrolyte, degassed with O_2 and using a scan rate of 10 mV s^{-1}. Control experiments confirmed that unsupported monomer samples and metal-free monomers have little or no activity (**Figure 4**). Of the two supported monomers, the $CoPcH_{16}$ outperformed its copper counterpart, giving a lower onset potential. However, in the following example we present the copper-containing samples, as the differences between the different linker combinations are easier to see and analyse (the full data for the cobalt-containing samples is included in the appendix). Both $CoPcH_{16}$ and $CuPcH_{16}$ are stable under these oxidative conditions, as shown also elsewhere.[40]

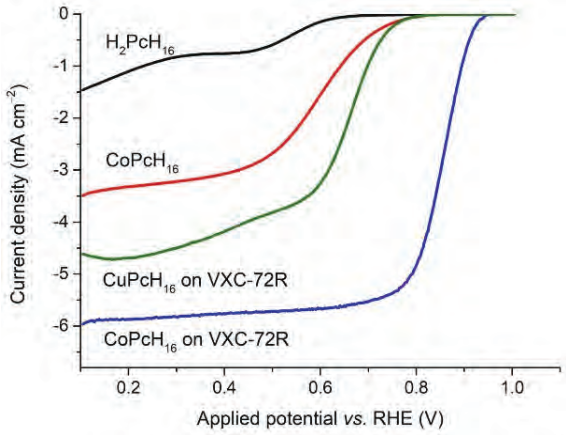

Figure 4: LSV curve of different monomer Pcs obtained in 0.1 M KOH, degassed with O_2, a scan rate of 10 mVs^{-1} and a rotation speed of 1600 rpm. Shown is H_2PcH_{16} (black), $CoPcH_{16}$ (red) $CuPcH_{16}$ supported on VXC-72R (green) and $CoPcH_{16}$ supported on VXC-72R (blue).

Figure 5 shows the linear sweep voltammetry curves of the polymer CuPc set. Shorter linkers give lower onset potentials. This may reflect the effect of the inter-metal distance. When the metal ions are closer to each other, the ORR activity increases. This effect is observed both for cobalt and copper. The monomer CuPc (dashed curve in **Figure 5**) shows an onset potential similar to that of the polymers with intermediate linker sizes. However, the factors affecting the performance of the monomer catalysts are more complex. The MPc monomers can stack on the surface, resulting in many possible interactions between them.

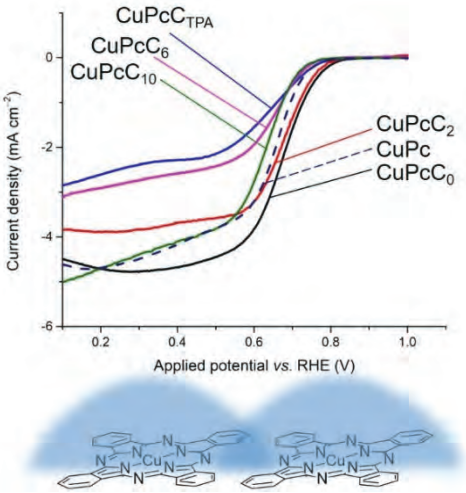

Figure 5: Top: LSV curves of CuPcC$_0$ (black), CuPcC$_2$ (red) CuPcC$_6$ (pink), CuPcC$_{TPA}$ (blue), CuPcC$_{10}$ (green) and monomer CuPc (dashed blue) obtained in 0.1 M KOH, degassed with O$_2$, a scan rate of 10 mVs^{-1} and a rotation speed of 1600 rpm. Bottom: Illustration of two adjacent CuPcs with overlapping solvation shells.

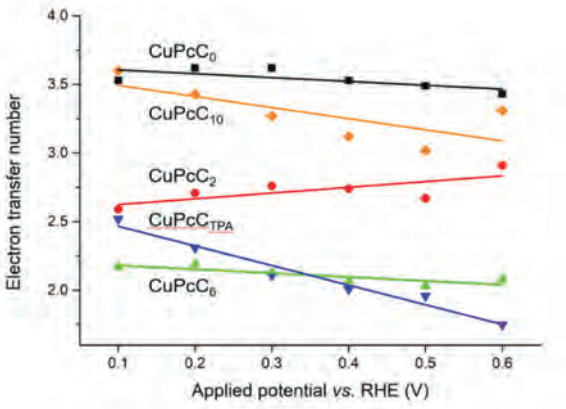

Figure 6: Data obtained from the Koutecký-Levich analysis, showing the electron transfer number of each polymer at a certain potential. Shown is CuPcC$_0$ (black), CuPcC$_2$ (red) CuPcC$_6$ (green), CuPcC$_{TPA}$ (blue), CuPcC$_{10}$ (orange).

We can explain the influence of the inter-metal distance on the ORR performance if we consider the solvation shell. The metal ions can polarise the water molecules to accommodate charges on the surface.[41] This creates a different environment in the immediate vicinity of the copper(or cobalt) Pcs. The "thickness" of this shell is typically 2–3 molecular layers (4–5 Å). When two Pcs are within the distance of influence, their solvation shells will partially overlap (see **Figure 5**, bottom), increasing the likelihood of the four-electron route. This holds true for the C_0 and C_2 linkers, but doesn't apply to the longer ones, explaining the difference in ORR activity.

Table 2. Onset Potentials of Pc polymers and related benchmarks.

Entry	Material	Onset Potential (V *vs.* RHE)	Entry	Material	Onset Potential (V *vs.* RHE)
1	Pt/C	0.94	5	$CuPcC_0$	0.81
2	CuO/C	0.77	6	$CuPcC_2$	0.80
3	$CuPcH_{16}/C$	0.73	7	$CuPcC_6$	0.76
4	Yasuda et al.[25]	0.97	8	$CuPcC_{TPA}$	0.77
5	Liu et al.[26]	0.99	9	$CuPcC_{10}$	0.75

The onset potential is shown at a current density of 100 μA/cm². All materials are supported on carbon VXC-72R (C). The Pt loading is 20 wt%.

Table 2 compares the onset potentials (V vs. RHE) of our five polymer Pcs to those of Pt/C, CuO/C and CuPc benchmark materials, as well as analogous polymers. The ORR performance of our polymers is good, but not exceptional. However, we are not screening here for an optimised ORR catalyst. Rather, we are showing that this synthesis method gives easy access to covalent materials with good spatial and chemical control. The ORR activity strongly depends on the inter-metal distance, yet the product selectivity shows a different trend. Koutecký–Levich analysis (**Figure 6**) shows that the middle-sized linkers give the hydrogen peroxide product (top section of the orange route in **Scheme 2** above). Conversely, catalysts with no linker (C_0) or with long linkers (C_{10}) are selective towards the OH^- product (green route in **Scheme 2**). A detailed mechanistic study using rotating ring-disk electrode (RRDE) is out of

the scope of this chapter,[42–44] but it is likely that the two extreme cases (short vs. long linkers) are influenced by different factors (*cf.* the mass-transfer barrier observed for the polymer with the C_{10} linker in **Figure 5**, which is not observed for the short linkers).

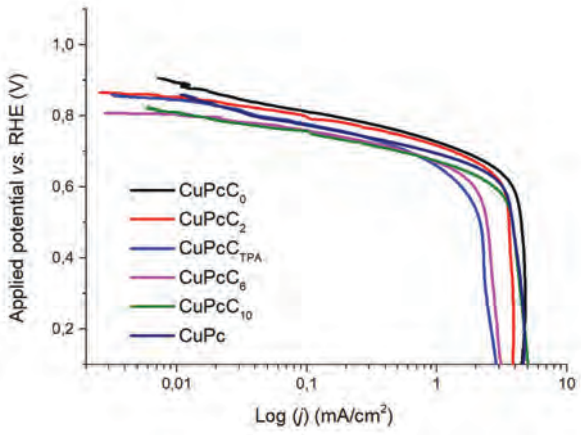

Figure 7: Tafel plot of the $CuPcC_0$ (black), $CuPcC_2$ (red), $CuPcC_{TPA}$ (blue), $CuPcC_6$ (pink), $CuPcC_{10}$ (green) and $CuPcH_{16}$ (navy) obtained in 0.1 M KOH, degassed with O_2, at a scan rate of 10 mVs^{-1} and a rotation speed of 1600 rpm.

The slope of the Tafel plot (**Figure 7**) gives information about the rate-determining step (RDS). If this slope is around 120 mV dec^{-1}, the RDS is an electron transfer. If not, it is an adsorption or desorption of species, such as the adsorption of oxygen or the desorption of OH^- or OOH^-.[45,46] The RDS scan change according to the applied current or potential. Thus, we studied both the low current density (LCD) and high current density (HCD) to monitor these changes in the RDS. In our case, the LCD shows a slope between 60 and 70 mV dec^{-1}, indicating an adsorption or desorption in the RDS. In the HCD the slope is between 100 and 120 mV dec^{-1}, indicating partly adsorption or desorption, and an electron transfer as RDS (see appendix for the exact numbers). This could be an adsorbed OH^- species that desorbs to give OH^- in solution or absorbed O_2 undergoes an electron transfer and becomes adsorbed OOH^-, which is the first step of ORR.

4.3 Conclusions

The "ring and linker" method presented here is a scalable and structured approach for preparing covalently-bound macrocyclic polymer solids with well-defined single-atom sites. This method allows for excellent spatial and chemical control, while benefitting from the strength and stability of covalent bonding. The resulting polymers are good ORR catalysts. Moreover, the generality of our method opens opportunities for designing new types of catalysts and performance materials.

4.4 Experimental Section

Materials and Instrumentation Unless otherwise noted, all chemicals were purchased from either VWR chemicals, Fluorochem or Merck and used without further purification. Solvents were dried prior to reaction over 3 Å molecular sieves. Carbon Black - Vulcan XC-72R was purchased from Dols International BV. All experiments were performed under nitrogen atmosphere, unless stated otherwise. FTIR spectra (4000–400 cm^{-1}, resol. 0.5 cm^{-1}) were recorded on a Varian 660 FTIR spectrometer using ATR and the transmission technique. X-Ray diffraction (XRD) patterns were obtained with a MiniFlex II diffractometer using Ni-filtered CuKα radiation. The X-ray tube was operated at 30 kV and 15 mA, with a 0.01° step and 1s dwell time. Raman spectra were recorded using a Renishaw InVia system (532 and 632.8 nm) and a Kaiser Optical Systems RXN-4 system (785 nm) coupled with fibre optics to an immersion probe with a short focal length. ICP analysis was performed by Kolbe GmbH (Germany). The experimental values obtained were corrected for the presence of oxygen. Mass spectra were collected on two instruments: (A) AccuTOF LC, JMS-T100LP Mass spectrometer (JEOL, Japan). ESI source, positive-ion mode; needle voltage 2500V, orifice 1 voltage 120V, orifice 2 voltage 9V; ring Lens voltage 22V; orifice 1 80 °C, desolvating chamber 250 °C. The samples were measured using flow injection with a flow rate of 0.01 mL/min, and the spectra were recorded with an average duration of 0.5 min. (B) MALDI-TOF- Instrument, UltraFlextreme Company Bruker Daltonik, Bremen, Germany was used for the measurements. Matrix solution was α-cyanno-4-hydroxycinnamic-acid in 50% (0.1% TFA) and 50% MeOH (10 mgHCCA/mL). (For DHB matrix: 20 mgDHB/mL) The matrix solution was applied by pipet at the ratio of 1:1 analyte/matrix (1 μL each). The crystallisation occurred at room temperature, for a few minutes. In one spot, a standard peptide mix (Bruker) was used for the calibration of the instrument. The laser power with which the measurements were performed was adjusted per experiment, with acquisitions of 1000 or 1500 laser shots per sample. X-ray absorption spectra were collected at the beamline

1W1B of the Beijing Synchrotron Radiation Facility (BSRF, Beijing, China) using a transmission mode. The XAS spectra and EXAFS interference functions were extracted from the raw experimental data using Athena software.[47] The radial distributions are calculated from the magnitude of the k^2-weighted interference function $X(k)$ using a Hanning window over a k range of 3.0–12.8 $Å^{-1}$.

Electrochemical Procedures. Electrodes were prepared using a 1 wt% metal ratio on Vulcan XC-72R carbon powder. In a typical preparation, the catalyst (10–16 mg) was mixed with Vulcan XC-72R carbon powder (100 mg). THF (5 mL) was then added, and the mixture was placed in an ultrasonic bath for > 24 h. After evaporation, the impregnated polymer is isolated. The preparation of the metal oxides on Vulcan XC-72R differs from this method. Vulcan XC-72R was prepared by heating to 150 °C in a sand bath under vacuum overnight. 0.1 mL of a 1 wt% metal ratio of metal nitrate was deposited dropwise on to the Vulcan XC-72R while stirring. The catalysts were then dried overnight at 70 °C in an oven. The catalysts were then oxidised in a tubular furnace at 400 °C for 1 h.

Inks of the catalytic powders were prepared according to the following proportions: 1.0 mL EtOH, 10 µL Nafion® (D-521 dispersion 5% wt in water/isopropanol, Alfa Aesar 42117), and 1 mg catalyst powder. The inks were placed in an ultrasonic bath and stirred for several hours. The working electrode substrate was a Φ = 5 mm (A = 0.196 cm^2) glassy carbon electrode (Gamry, USA), which was polished by diamond polishing films with 1 and 0.1 µm particles (Allied High Tech Products, USA), and rinsed well. Inks were deposited by drop-casting 5 µL portions x 6, with air drying between each drop. The total catalyst loading was 30 µg, or 153 µg/cm^2.

Electrochemical experiments were performed in a 3-electrode home-made glass cell, filled with KOH (0.1 M, 150 mL), stabilized at 25.0 ± 0.1 °C in a water bath. A Gamry Reference 600 potentiostat was employed, together with a Gamry RDE710 Rotating Electrode setup. Saturated calomel electrode (SCE, Gamry, USA) separated from the solution by a 10 cm bridge was used as a reference electrode, and a graphite rod

(Gamry, USA) as a counter electrode. Potentials are reported *vs.* reversible hydrogen electrode (RHE) by adding 1.011 for pH 13. Nitrogen (99.999%) or oxygen (99.999%) were bubbled for 30 min to saturate the solution, and were flowed above the solution (so-called 'gas blanket') during the experiments. Linear scan voltammograms were measured from 0.1 to 1.0 V vs. RHE with a scan rate of 10 mV/s at rotating speeds of 400, 600, 900, 1200, 1600, 2000 and rpm. Cyclic voltammetry was measured from -0.2 to 0.2 V with a scan rate of 200 mV/s for 50 cycles, from -0.2 to 0.2 V with a scan rate of 20 mV/s with 5 cycles, and then from 0 to -0.9 V with a scan rate of 10 mV/s for 3 cycles. All cyclic voltammetry was performed without rotation.

General procedure for synthesising metal-containing tetra-amino phthalocyanines ($MPc(NH_2)_4$). This is a modification of a published, analogous procedure.[32] 4-aminophthalonitrile and the corresponding metal salt were dissolved in *n*-pentanol. 1,8-diazabicyclo[5.4.0]undec-7-ene (DBU) was added and the mixture was heated for 2 h at 140 °C, forming a black coloured solution. The mixture was cooled down to ambient temperature, after which it was vacuum filtered and washed with water (5 × 10 mL) and then with EtOH (5 × 10 mL). The residue was dried under air.

> **Example: $CoPc(NH_2)_4$** : 4-aminophthalonitrile (286 mg, 2.0 mmol) and cobalt(II) chloride hexahydrate (0.119 g, 0.5 mmol) were dissolved in n-pentanol (2 mL) together with DBU (0.1 mL, 0.7 mmol). The mixture was heated at 140 °C for 2 h after which a black solution was formed. The mixture was allowed to cool down to room temperature, after which the product was obtained by vacuum filtration. The product was washed with water (5 × 10 mL) and EtOH (5 × 10 mL). The black powder was dried in air overnight. This gave $CoPc(NH_2)_4$, as a black powder, 0.14 g (45 mol% yield based on 4-aminophthalonitrile). HRMS (ESI+) m/z calculated $C_{32}H_{20}CoN_{12}$, 631.127, found, 631.124. FTIR (cm^{-1}): 1607, 1493, 1385, 1316, 1256, 1201, 1093, 836, 738, 426.

The synthesis of $CuPc(NH_2)_4$ was similarly performed, using $CuCl_2$ (68 mg, 0.5 mmol, 68 mol% yield based on 4-aminophthalonitrile) instead of the cobalt salt.

Procedure for the synthesis of $CuPcC_0$.1,2,4,5-tetracyanobenzene (100 mg, 0.6 mmol) and copper(II)chloride (75 mg, 0.6 mmol) were dissolved in *n*-pentanol (2 mL). DBU (0.1 mL, 0.7 mmol) was added and the mixture was heated for 24 h at 140 °C, forming a green solution. The reaction was cooled down to ambient temperature, filtered and washed with water (5 × 10 mL) followed by EtOH (2 × 10 mL) and finally with acetone (1 × 10 mL). The dark green precipitate was dried under a N_2 flow. This gave $CuPcC_0$, as a dark green product, 75.2 mg. FTIR (cm^{-1}): 3333, 2930, 2230, 1574, 1308, 1092, 748. HRMS (FD+) m/z calc.for three connected CuPcs: 1374.292 Da, found: 1374.105 Da.

General procedure of $PMPcC_x$ (M = Cu/Co. X= 2,6,10, TPA (teraphthaloyl chloride)). Stock solutions of $MPc(NH_2)_4$ and the corresponding linker were made in dimethylformamide after which the linker and $MPc(NH_2)_4$ and K_2CO_3 were combined at 50 °C. After 4 h, $MPc(NH_2)_4$ and K_2CO_3 were added to the solution and left for 16 h. To this mixture, more linker and K_2CO_3 was added and after 4 h. More $MPc(NH_2)_4$ and K_2CO_3 was added and allowed to react for 16 h. The mixture was cooled down, gravity filtrate and washed with water (5 × 10 mL), EtOH (5 × 10 mL) and dimethylformamide (2 × 10 mL). The residue was dried under air.

Example: $PolyCoPcC_{TPA}$: Stock solutions of 10 mg/mL of tetra-amino cobalt phthalocyanine and terephthaloyl chloride were made in dimethylformamide. Tetra-amino cobalt phthalocyanine (415 µL, 6.6 µmol) and potassium carbonate (16 mg, 1.1 mmol) were added together and heated to 50 °C. Terephthaloyl chloride (540 µL, $2.6x10^{-2}$ mmol) was then added, and the reaction mixture was stirred at 50 °C for 4 h. Tetra-amino cobalt phthalocyanine (1.66 mL, $2.6x10^{-2}$ mmol) and potassium carbonate (16 mg, 1.1 mmol) were added to the reaction mixture, and it was allowed to stir for 16 h. Terephthaloyl chloride (1.61 mL, $7.9x10^{-2}$ mmol) and potassium

carbonate (48 mg, 3.3 mmol) were then added, and the reaction mixture was stirred at 50 °C for 4 h. Tetra-amino cobalt phthalocyanine (5.0 mL, $7.9x10^{-2}$ mmol) and potassium carbonate (48 mg, 3.3 mmol) were added to the reaction mixture, and it was allowed to stir for 16 h. The crude reaction mixture was then filtered and washed with water (5 × 10 mL), giving at green filtrate and black residue, followed by ethanol (5 × 10 mL), giving at green filtrate and black residue, and then dimethylformamide (2 × 10 mL), giving a dark green filtrate and black residue. This dark green filtrate was then evaporated, yielding a very dark green residue. This gave the product, yielding 0.0374 g of dark green solid. ATR-FTIR: $\mu(cm^{-1})$ = 1658, 1606, 1522, 1495, 1471, 1437, 1408, 1385, 1352, 1319, 1259, 1192, 1132, 1097, 1061, 891, 833.

4.5 References

[1] Bio-inspired Murray materials for mass transfer and activity, X. Zheng, G. Shen, C. Wang, Y. Li, D. Dunphy, T. Hasan, C.J. Brinker, B.-L. Su, *Nat. Commun.* **2017**, *8*, 1–9.

[2] A stable single-site palladium catalyst for hydrogenations, G. Vilé, D. Albani, M. Nachtegaal, Z. Chen, D. Dontsova, M. Antonietti, N. López, J. Pérez-Ramírez, *Angew. Chem. Int. Ed.* **2015**, *54*, 11265–11269.

[3] Dioxygen activation and methane hydroxylation by soluble methane monooxygenase: A tale of two irons and three proteins, M. Merkx, D.A. Kopp, M.H. Sazinsky, J.L. Blazyk, J. Müller, S.J. Lippard, *Angew. Chem. Int. Ed.* **2001**, *40*, 2782–2807.

[4] Superhydrophobic surfaces: From natural to biomimetic to functional, Z. Guo, W. Liu, B.-L. Su, *J. Colloid Interface Sci.* **2011**, *353*, 335–355.

[5] A biocompatible bottom-up route for the preparation of hierarchical biohybrid materials, M.C. Gutiérrez, M. Jobbágy, N. Rapún, M.L. Ferrer, F. del Monte, *Adv. Mater.* **2006**, *18*, 1137–1140.

[6] A novel approach for preparation of thermoresponsive polymer magnetic microspheres with core–shell structure, Y.H. Deng, W.L. Yang, C.C. Wang, S.K. Fu, *Adv. Mater.* **2003**, *15*, 1729–1732.

[7] Significant enhancement of thermal conductivity in bioinspired freestanding boron nitride papers filled with graphene oxide, Y. Yao, X. Zeng, F. Wang, R. Sun, J. Xu, C.-P. Wong, *Chem. Mater.* **2016**, *28*, 1049–1057.

[8] Activation of O_2 by organosilicon reagents yields quantitative amounts of H_2O_2 or $(Me_3Si)_2O_2$ for efficient O-transfer reactions, K. Yamamoto, S. Tanaka, H. Hosoya, H. Tsurugi, K. Mashima, C. Copéret, *Helv. Chim. Acta* **2018**, *101*, e1800156.

[9] Oxidation of alcohols to carbonyl compounds catalyzed by oxo-bridged dinuclear cerium complexes with pentadentate Schiff-Base ligands under a dioxygen atmosphere, S. Shirase, K. Shinohara, H. Tsurugi, K. Mashima, *ACS Catal.* **2018**, *8*, 6939–6947.

[10] Catalyst parameters determining activity and selectivity of supported gold nanoparticles for the aerobic oxidation of alcohols: The molecular reaction mechanism, A. Abad, A. Corma, H. García, *Chem. – Eur. J.* **2008**, *14*, 212–222.

[11] Selective hydrogenation of 1,3-butadiene on platinum–copper alloys at the single-atom limit, F.R. Lucci, J. Liu, M.D. Marcinkowski, M. Yang, L.F. Allard, M. Flytzani-Stephanopoulos, E.C.H. Sykes, *Nat. Commun.* **2015**, *6*, 1–8.

[12] Design principle of Fe–N–C electrocatalysts: How to optimize multimodal porous structures?, S.H. Lee, J. Kim, D.Y. Chung, J.M. Yoo, H.S. Lee, M.J. Kim, B.S. Mun, S.G. Kwon, Y.E. Sung, T. Hyeon, *J. Am. Chem. Soc.* **2019**, *141*, 2035–2045.

[13] Investigation of the oxygen storage capacity behaviour of three way catalysts using spatio-temporal analysis, C. Coney, C. Hardacre, K. Morgan, N. Artioli, A.P.E. York, P. Millington, A. Kolpin, A. Goguet, *Appl. Catal. B Environ.* **2019**, *258*, 117918.

[14] Oxygen reduction reactions in ionic liquids and the formulation of a general ORR mechanism for Li–air batteries, C.J. Allen, J. Hwang, R. Kautz, S. Mukerjee, E.J. Plichta, M.A. Hendrickson, K.M. Abraham, *J. Phys. Chem. C* **2012**, *116*, 20755–20764.

[15] Porphyrins and phthalocyanines: photosensitizers and photocatalysts, R.M. Ion, *Phthalocyanines Some Curr. Appl.* **2017**, DOI 10.5772/intechopen.68654.

[16] Direct transformation of bulk copper into copper single sites via emitting and trapping of atoms, Y. Qu, Z. Li, W. Chen, Y. Lin, T. Yuan, Z. Yang, C. Zhao, J. Wang, C. Zhao, X. Wang, et al., *Nat. Catal.* **2018**, *1*, 781–786.

[17] Recent progresses in the research of single-atom catalysts, J. Li, Y. Li, T. Zhang, *Sci. China Mater.* **2020**, *63*, 889–891.

[18] Control of solid catalysts down to the atomic scale: Where is the limit?, F. Schüth, *Angew. Chem. Int. Ed.* **2014**, *53*, 8599–8604.

[19] The power of single-atom catalysis, S. Liang, C. Hao, Y. Shi, *ChemCatChem* **2015**, *7*, 2559–2567.

[20] Single-site heterogeneous catalysts, J.M. Thomas, R. Raja, D.W. Lewis, *Angew. Chem. Int. Ed.* **2005**, *44*, 6456–6482.

[21] Local platinum environments in a solid analogue of the molecular periana catalyst, M. Soorholtz, L.C. Jones, D. Samuelis, C. Weidenthaler, R.J. White, M.M. Titirici, D.A. Cullen, T. Zimmermann, M. Antonietti, J. Maier, et al., *ACS Catal.* **2016**, *6*, 2332–2340.

[22] Single cobalt atoms with precise N-coordination as superior oxygen reduction reaction catalysts, P. Yin, T. Yao, Y. Wu, L. Zheng, Y. Lin, W. Liu, H. Ju, J. Zhu, X. Hong, Z. Deng, et al., *Angew. Chem.* **2016**, *128*, 10958–10963.

[23] Stabilization of single metal atoms on graphitic carbon nitride, Z. Chen, S. Mitchell, E. Vorobyeva, R.K. Leary, R. Hauert, T. Furnival, Q.M. Ramasse, J.M. Thomas, P.A. Midgley, D. Dontsova, et al., *Adv. Funct. Mater.* **2017**, *27*, 1605785.

[24] A pyrolysis-free path toward superiorly catalytic nitrogen-coordinated single atom, P. Peng, L. Shi, F. Huo, C. Mi, X. Wu, S. Zhang, Z. Xiang, *Sci. Adv.* **2019**, *5*, eaaw2322.

[25] Iron–nitrogen-doped vertically aligned carbon nanotube electrocatalyst for the oxygen reduction reaction, S. Yasuda, A. Furuya, Y. Uchibori, J. Kim, K. Murakoshi, *Adv. Funct. Mater.* **2016**, *26*, 738–744.

[26] Iron(II) phthalocyanine covalently functionalized graphene as a highly efficient non-precious-metal catalyst for the oxygen reduction reaction in alkaline media, Y. Liu, Y.Y. Wu, G.J. Lv, T. Pu, X. Q. He, L.L. Cui, *Electrochimica Acta* **2013**, *112*, 269–278.

[27] Selective catalytic oxidation of cyclohexene with molecular oxygen: Radical versus nonradical pathways, I.M. Denekamp, M. Antens, T.K. Slot, G. Rothenberg, *ChemCatChem* **2018**, *10*, 1035–1041.

[28] Unraveling the synergy between gold nanoparticles and chromium-hydrotalcites in aerobic oxidation of alcohols, P. Liu, V. Degirmenci, E.J.M. Hensen, *J. Catal.* **2014**, *313*, 80–91.

[29] Cooperative surface-particle catalysis: The role of the "active doughnut" in catalytic oxidation, T.K. Slot, D. Eisenberg, G. Rothenberg, *ChemCatChem* **2018**, *10*, 2119–2124.

[30] Polybenzimidazoles, new thermally stable polymers, H. Vogel, C.S. Marvel, *J. Polym. Sci.* **1961**, *50*, 511–539.

[31] Polymers from aromatic nitriles and amines: Polybenzimidazoles and related polymers, D.I. Packham, J.D. Davies, H.M. Paisley, *Polymer* **1969**, *10*, 923–931.

[32] A simple synthesis of symmetric phthalocyanines and their respective perfluoro and transition-metal complexes, I.M. Denekamp, F.L.P. Veenstra, P. Jungbacker, G. Rothenberg, *Appl. Organomet. Chem.* **2019**, *33*, e4872.

[33] Local environment of metal ions in phthalocyanines: K-edge X-ray absorption spectra, G. Rossi, F. d'Acapito, L. Amidani, F. Boscherini, M. Pedio, *Phys. Chem. Chem. Phys.* **2016**, *18*, 23686–23694.

[34] *Ab initio* x-ray absorption study of copper K -edge XANES spectra in Cu(II) compounds, J. Chaboy, A. Muñoz-Páez, F. Carrera, P. Merkling, E.S. Marcos, *Phys. Rev. B* **2005**, *71*, DOI 10.1103/PhysRevB.71.134208.

[35] Atomically dispersed Fe-N-P-C complex electrocatalysts for superior oxygen reduction, Y. Li, B. Chen, X. Duan, S. Chen, D. Liu, K. Zang, R. Si, F. Lou, X. Wang, M. Rønning, et al., *Appl. Catal. B Environ.* **2019**, *249*, 306–315.

[36] Oxygen reduction reaction mechanism on nitrogen-doped graphene: A density functional theory study, L. Yu, X. Pan, X. Cao, P. Hu, X. Bao, *J. Catal.* **2011**, *282*, 183–190.

[37] Oxygen reduction reaction kinetics and mechanism on platinum nanoparticles inside Nafion®, O. Antoine, Y. Bultel, R. Durand, *J. Electroanal. Chem.* **2001**, *499*, 85–94.

[38] Unraveling oxygen reduction reaction mechanisms on carbon-supported Fe-phthalocyanine and Co-phthalocyanine catalysts in alkaline solutions, R. Chen, H. Li, D. Chu, G. Wang, *J. Phys. Chem. C* **2009**, *113*, 20689–20697.

[39] The oxygen reduction reaction mechanism on Pt(111) from density functional theory calculations, V. Tripković, E. Skúlason, S. Siahrostami, J.K. Nørskov, J. Rossmeisl, *Electrochimica Acta* **2010**, *55*, 7975–7981.

[40] A copper single-atom catalyst towards efficient and durable oxygen reduction for fuel cells, L. Cui, L. Cui, Z. Li, J. Zhang, H. Wang, S. Lu, Y. Xiang, *J. Mater. Chem. A* **2019**, *7*, 16690–16695.

[41] Dynamics of water molecules in aqueous solvation shells, M.F. Kropman, H.J. Bakker, *Science* **2001**, *291*, 2118–2120.

[42] Polyoxometalates covalently combined with graphitic carbon nitride for photocatalytic hydrogen peroxide production, S. Zhao, X. Zhao, S. Ouyang, Y. Zhu, *Catal. Sci. Technol.* **2018**, *8*, 1686–1695.

[43] N-doped hierarchical porous metal-free catalysts derived from covalent triazine frameworks for the efficient oxygen reduction reaction, Y. Cao, Y. Zhu, X. Chen, B.S. Abraha, W. Peng, Y. Li, G. Zhang, F. Zhang, X. Fan, *Catal. Sci. Technol.* **2019**, *9*, 6606–6612.

[44] Microwave-assisted synthesis of porous Mn_2O_3 nanoballs as bifunctional electrocatalyst for oxygen reduction and evolution reaction, S. Ghosh, P. Kar, N. Bhandary, S. Basu, S. Sardar, T. Maiyalagan, D. Majumdar, S.K. Bhattacharya, A. Bhaumik, P. Lemmens, et al., *Catal. Sci. Technol.* **2016**, *6*, 1417–1429.

[45] Insight on Tafel slopes from a microkinetic analysis of aqueous electrocatalysis for energy conversion, T. Shinagawa, A.T. Garcia-Esparza, K. Takanabe, *Sci. Rep.* **2015**, *5*, 13801.

[46] Tafel kinetics of electrocatalytic reactions: From experiment to first-principles, Y.H. Fang, Z.P. Liu, *ACS Catal.* **2014**, *4*, 4364–4376.

[47] ATHENA, ARTEMIS, HEPHAESTUS: data analysis for X-ray absorption spectroscopy using IFEFFIT, B. Ravel, M. Newville, *J. Synchrotron Radiat.* **2005**, *12*, 537–541.

Appendix - The supporting information for Chapter 4

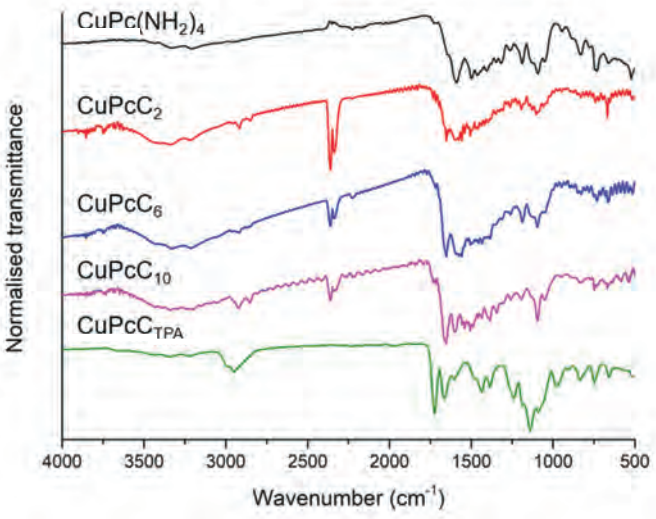

Figure S1: FTIR spectra of the $CuPc(NH_2)_4$ (black), $CuPcC_2$ (red), $CuPcC_6$ (blue), $CuPcC_{10}$(purple) and $CuPcC_{TPA}$ (green).

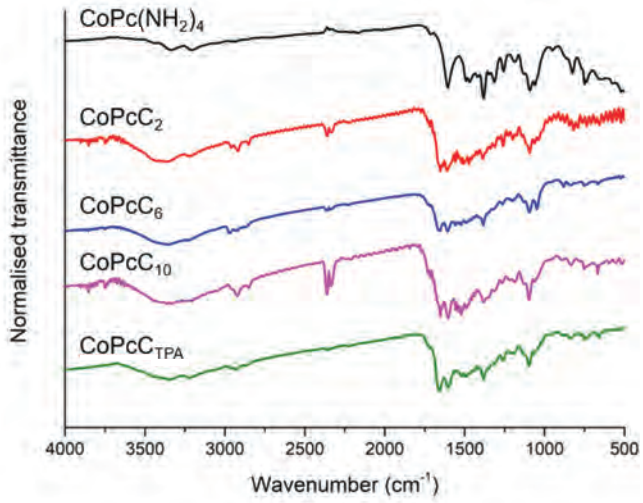

Figure S2: FTIR spectra of the $CoPc(NH_2)_4$ (black), $CoPcC_2$ (red), $CoPcC_6$ (blue), $CoPcC_{10}$(purple) and $CoPcC_{TPA}$ (green).

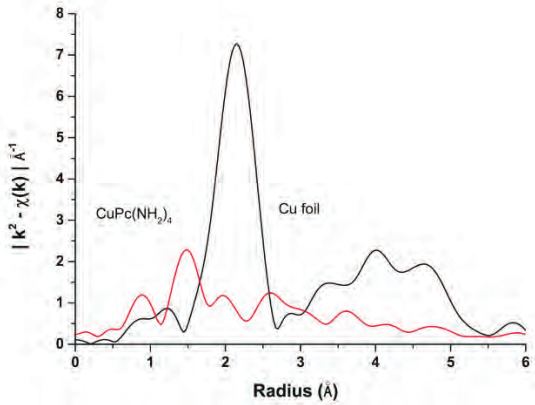

Figure S3: k^2-weighted $\chi(k)$ EXAFS data for Cu foil (black) and $CuPc(NH_2)_4$ (red) processed with data from a k range of 3–13 $Å^{-1}$.

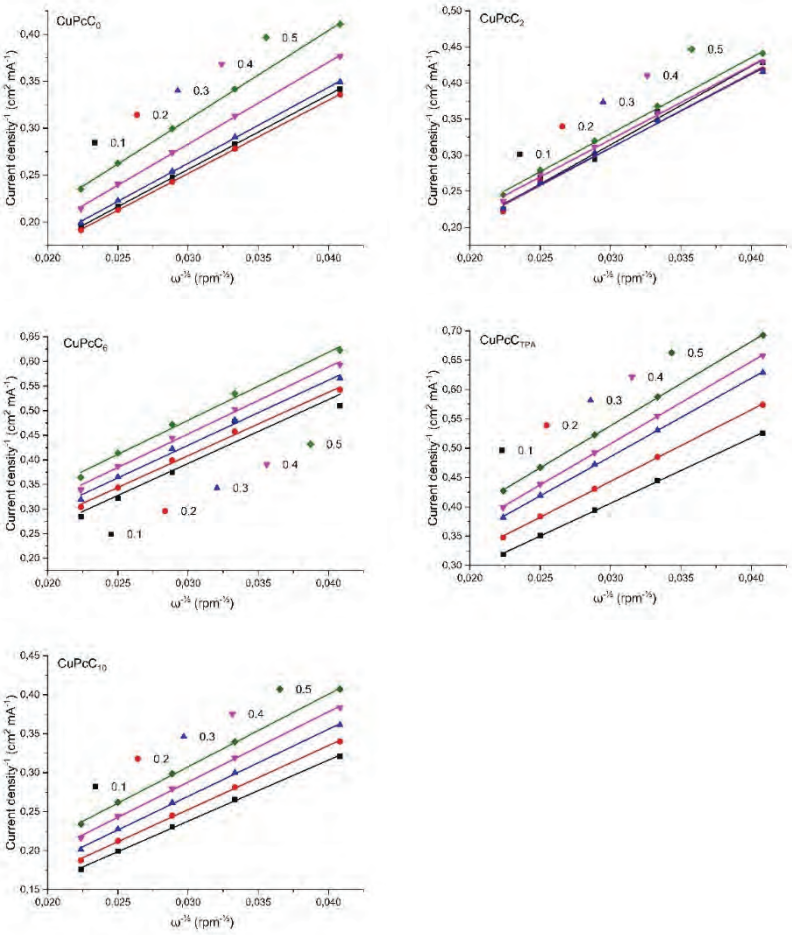

Figure S4: Koutecký–Levich plots of $CuPcC_0$, $CuPcC_2$, $CuPcC_6$, $CuPcC_{10}$, and $CuPcC_{TPA}$.

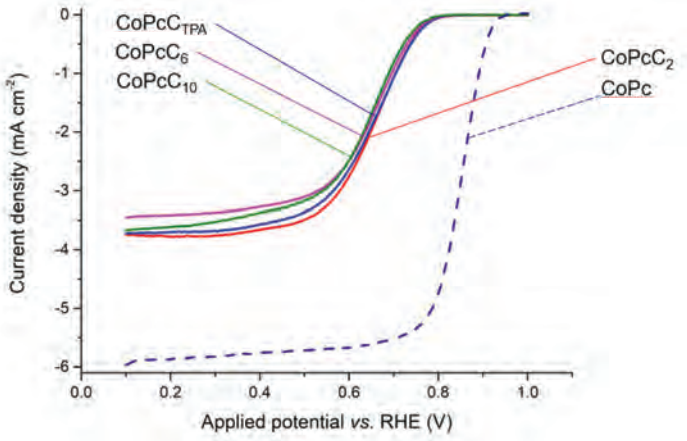

Figure S5: LSV curve of the CoPc(NH$_2$)$_4$ (dotted curve), CoPcC$_2$ (red), CoPcC$_6$ (purple), CoPcC$_{10}$(green) and CoPcC$_{TPA}$ (blue) obtained in 0.1 M KOH, degassed with O$_2$, a scan rate of 10 mVs^{-1} and a rotation speed of 1600 rpm.

Table S1. Tafel plot slope values calculated between the low current density (LCD) and the high current density (HCD).

Entry	Polymer	LCD ($mVdec^{-1}$)	HCD ($mVdec^{-1}$)
1	$CuPcC_0$	64	125
2	$CuPcC_2$	65	112
3	$CuPcC_6$	62	105
4	$CuPcC_{TPA}$	70	120
5	$CuPcC_{10}$	64	101
6	$CuPcH_{16}$	66	110

References:

[1] ATHENA, ARTEMIS, HEPHAESTUS: data analysis for X-ray absorption spectroscopy using IFEFFIT, B. Ravel, M. Newville, *J. Synchrotron Radiat.* **2005**, *12*, 537–541.

[2] A simple synthesis of symmetric phthalocyanines and their respective perfluoro and transition-metal complexes, I.M. Denekamp, F.L.P. Veenstra, P. Jungbacker, G. Rothenberg, *Appl. Organomet. Chem.* **2019**, *33*, e4872.

Towards rational design of zeolites

Chapter 5

Abstract

In this chapter we set the stage for designing new zeolite catalyst, by gaining insight into their multi-stage synthesis. We approach this from two directions: collecting information by analysing a generic database of known zeolites, and running a parameter-driven research on a specific zeolite example. The generic database, consisting of 76 zeolites, each of which is described by 40 descriptors, shows us important values into the first stages of the synthesis: monomer/dimer reactions and colloid formation. The specific set looks at the synthesis of Linde Type A (LTA), a robust and simplistic zeolite, and highlights the importance of parameters that can change selectivity between two different zeolite products. Our results show that such combined computational + experimental descriptor studies can move us forward towards the design of new zeolites.

5.1 Introduction

Zeolites are porous crystalline aluminosilicates that are used as adsorbents and as industrial catalysts.[1–4] They are composed of TO_4 tetrahedral units, where T is most commonly Si or Al (other T atoms are also possible). Zeolites have regularly sized pores, channels and cages, and can be modified by changing their acidity, composition, active sites as well as cage and pore sizes.[5,6]

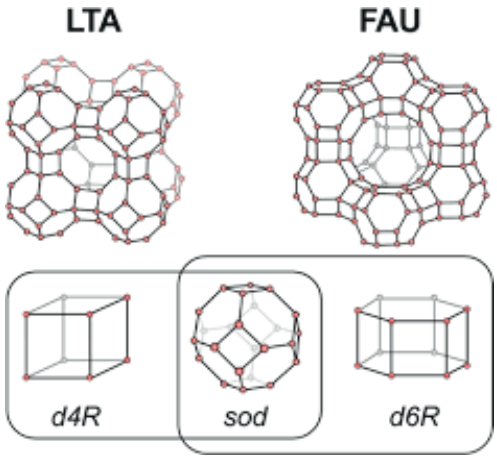

Figure 1. Illustrations of LTA and FAU crystal structures. Reprinted from ref. [7] with permission from Chem. Mater.

Looking at the structure, we see that the T atoms connect to form secondary building blocks (SBUs) which construct the final framework. An example of this can be seen in **Figure 1**.[7] Here, the SBUs *d4R* and *sod* make up LTA, whereas *sod* and *d6R* make FAU. In theory we can make up any type of zeolite, with different T atoms and SBUs. This is a challenge for industry, where in theory a zeolite can be designed for any type of catalytic reaction.

As part of a collaboration project, we were asked by our industrial partner whether we could use our previously designed tools for making zeolite confined spaces. In chapter

3 we introduced a "ring and linker" building block combination, where phthalocyanine (Pc) macrocycles were connected using linkers to form a designed polymer. We could change many aspects of this polymer, such as metal type, metal distance and chemical environmental, effectively changing its confined space. There is a resemblance between the Pc and the SBU. Just like we design our Pcs, we can tailor the SBUs to fit industrial needs. However, there are material challenges in designing zeolites. To date, less than 300 zeolites have been synthesised, and not for lack of effort.[8,9] And while there are similarities between Pcs and SBUs, there are also differences. Pc building blocks are preformed, whereas SBUs have to be formed in solution in an equilibrium. This difference means that we cannot use the same synthetic approach. To design zeolites, we have to first understand how they are made.

The synthesis of a zeolite goes through four stages, shown in **Figure 2**. These different stages all individually influence the final zeolite. To examine every single stage, we used two different data sets, one a general set with information of multiple known zeolites, and the other a specific set where the zeolite synthesis is examined in detail.

Our general set comprises 76 known zeolites (see appendix for details), the parameters of which were calculated based on proven synthesis and characterisation data. We used predictive modelling to obtain insight into the colloid stage, where the gel is formed. For the specific set, we chose the synthesis of Linde Type A (LTA). This is a robust zeolite, with a relatively simple synthesis protocol, starting from a base, silica and alumina precursors. This set gave us insight into the first synthesis stage, where molecular precursors form the very first building blocks. Combining the knowledge of both data sets gave us the first insights to designed zeolite oxidation catalysts.

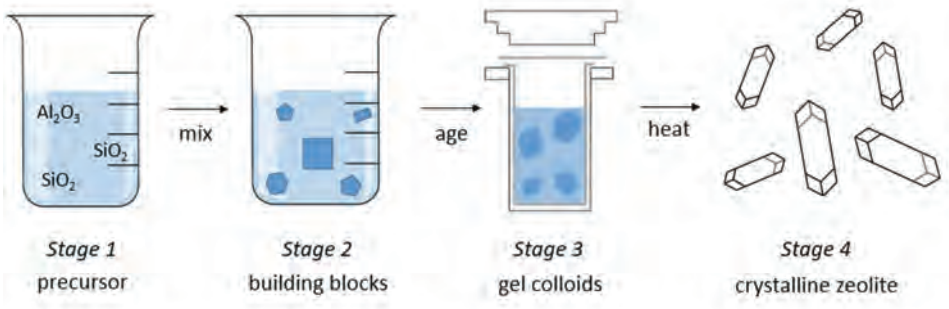

Figure 2. Overview of steps during zeolite synthesis.

5.2 Results and Discussion

Dataset assembly and descriptor selection. The synthesis descriptors were collected from "*verified syntheses of zeolitic materials*" published by Robson and Lillerud on behalf of the Synthesis Commission of the International Zeolite Association.[10] Synthesis descriptors included in the database are: batch composition (number of T atoms in the framework, structure-directing agent (SDA), solvent), crystallization time (h), crystallization temperature (°C), agitation during crystallization (rpm) and gel ageing/incubation (h). These were chosen because most of the synthesis descriptions included these parameters. Some parameters, such as stirring before gel formation are not described in the database and are therefore not in our synthesis descriptors. The database consists of 76 zeolites and 40 variables in total and can be found in the appendix. These zeolites were chosen since their parameters were possible to translate to descriptors and did not have certain parameters that were unique to them. We analysed the data using principal component analysis (PCA) and Pearson's correlation. Pearson's correlation coefficient measures the statistical relationship between variables. The correlation is a number between –1 and +1 and indicates if two variables are linearly related and to which order. [11,12]

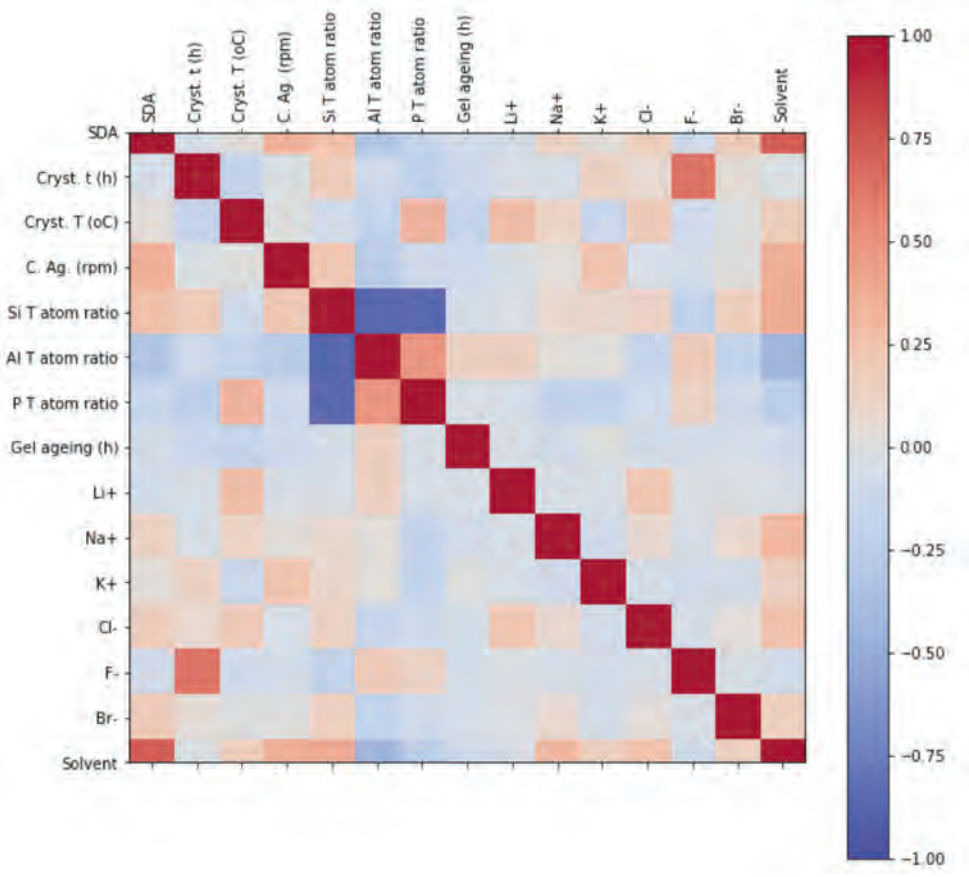

Figure 3. Pearson correlation diagram for the zeolite synthesis descriptors. Strong positive correlations in red, strong negative correlations in blue. To simplify the system, we only note the amount of SDA used, without specific SDA descriptors. When specific SDA descriptors were used, no significant correlation was observed between these and the synthesis descriptors.

The Pearson correlation in **Figure 3** shows all the descriptors used in synthesis and their respective correlations. There are strong negative correlations between Si and Al, and P atoms. Since silicon is the main T-atom in the framework, any replacement by aluminum and phosphorus will mean a decrease in silica, therefore having a strong negative correlation. The positive correlation of P and Al atoms is explained by AlPO and SAPO zeolites in the database, both having alternating phosphorus and alumina corners. Solvent and the amount of SDA are strongly correlated due to the solubility of the SDA in water. Increasing the SDA amount means having to increase the solvent, since undissolved material prevents proper gel formation. Another explanation is the interaction between water and the SDA, where water can order around the SDA. This is however depended on the hydrophilicity or hydrophobicity of the SDA (note that although fluoride anions show a strong correlation with the crystallization time, this result is not statistically significant as fluoride anions are rare in zeolites, especially in the dataset we used).

This generic dataset gives information about the colloid stage, where the first building units assemble. The amount of water and T atoms determine if the colloidal gel can be formed, and thus the necessary SBUs. To gain insight into the synthesis stage, Extratrees, a classification method,[13] was applied to the variables. In this way we could rank the variables by importance.

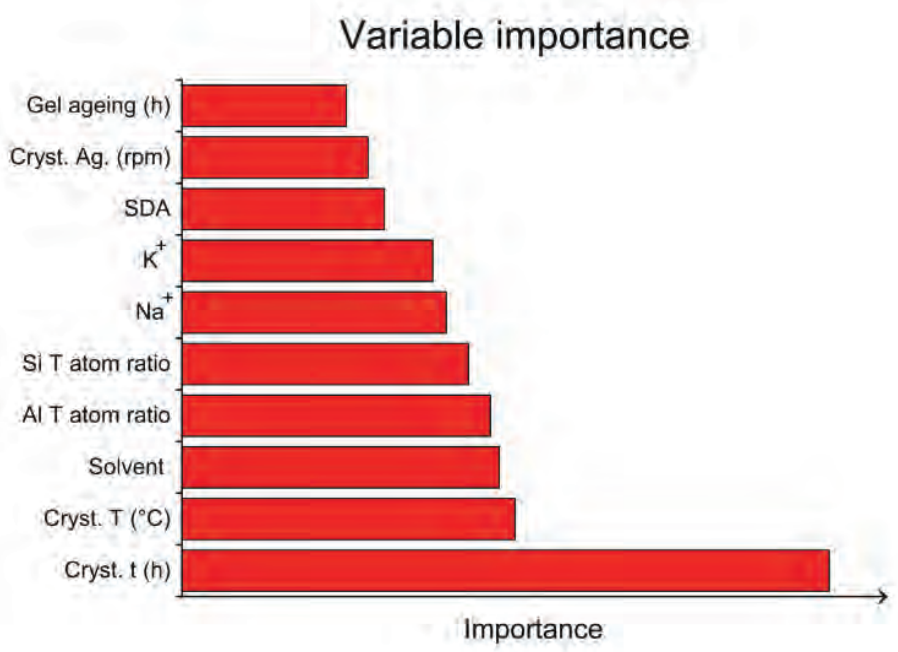

Figure 4. Variable importance extracted from Extratrees, ordered by increasing importance in classification.

Figure 4 shows that the most influential variables are the crystallisation time and temperature. Since most zeolites are kinetically controlled products, crystallisation time and temperature are of the highest importance. In the Pearson correlation these two factors showed no correlation, indicating that they work independently from each other. The amount of solvent is the third most important variable, which could be due to solubility of precursors, or pH of the solution. Gel ageing and agitation do not impact the different outcome between zeolite syntheses, but these are mainly used to decrease the crystallization time or decrease the number of competing phases in the final product.[14]

The total general set of zeolites gives insight into the colloidal ***and*** the synthesis step, which is between the colloid stage and the final zeolite. To understand the first step in the synthesis, we studied the preparation of LTA. We chose LTA because it is a very robust zeolite, having a fairly easy synthesis protocol with minimal reactants, and because it is of industrial relevance (LTA is ideal for ion-exchange and is therefore used in laundry detergents).[15] Its synthesis only requires silica, alumina, base and water as solvent. By having fewer precursors, we limit the number of factors influencing the synthesis. Also, most zeolites consist of silica, a base and a solvent, so the conclusion we drew from this specific set also applies across the board. We synthesised LTA and changed the synthesis parameters to determine the effects on the resulting product. This could be amorphous material, competing phases (GIS or SOD), lack of solid product or a different crystalline product.[16,17] The synthesis parameters and their respective ranges are shown in **Table 1**.

Table 1. Parameters and ranges applied to the synthesis of LTA.

Entry	Parameter	Range
1	OH^-	0 – 90 mmol
2	Si concentration	0 – 35 mmol
3	Al concentration	0 – 20 mmol
4	Gel stirring time	0 – 10 mmol
5	Aging time	0 – 7 days
6	Synthesis temperature	90 – 175 °C
7	Synthesis time	0 – 16 h
8	Synthesis agitation	0 – 16 rpm

Figure 5 shows the powder x-ray diffraction (XRD) patterns of LTA (red) and SOD (blue). We found that manual stirring of the gel phase for 5 minutes to maintain a homogeneous mixture was the main parameter correlated with the formation of pure crystalline LTA. This is the precursors stage, where stirring resulted in LTA (red), and

no stirring resulting in both LTA and SOD (a competing phase, shown in blue). These results suggest that homogeneity of the starting mixture ensures proper distribution of aluminosilicates where different SBUs can form and thus results in competing zeolite phases.

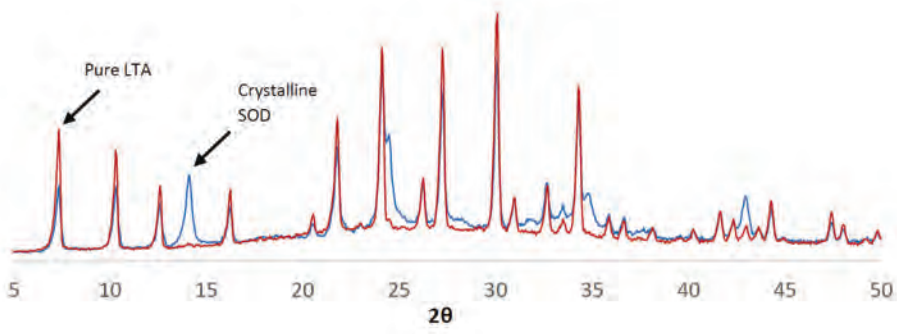

Figure 5. XRD patterns showing how stirring of the gel phase resulting in LTA (red), and no stirring resulting in SOD (blue) gel phase ensures no SOD formation.

As mentioned before, zeolites are kinetically controlled products. Once LTA is formed, a continuation of the synthesis conditions will result in SOD, a more thermodynamically stable phase, ultimately leading to the most stable phases: SiO_2 and Al_2O_3. Because of this temperature and time highly influences the reaction, with higher temperatures overcoming larger energy barriers and giving different zeolite phases. Without gel aging, successful synthesis of LTA was possible within 4 h over a range of temperatures. However, 120–150 °C were optimal temperatures for the LTA product. Higher temperatures resulted in the zeolite ANA.[18] Below 120 °C a mixture between SOD and LTA was obtained (below 80 °C the result was an amorphous material). This shows what our general set already predicted, namely that synthesis time and temperature are the most important criteria that influence different zeolite outcomes. Rotation or agitation of the synthesis vessels resulted in formation of the

competing phase SOD. Gel aging had an effect after 7 days, lowering the reaction time to 1 h, forming LTA.

The formation of the different clusters depends on the concentrations of sodium silicate and sodium aluminate, as this will affect the final zeolite. Lower concentrations of sodium silicate (0.3 eq) resulted in the SOD, whereas mildly lower concentrations (0.6–0.8 eq) resulted in mixtures of LTA and SOD. Lowering the concentration of sodium aluminate yielded a mixture of the competing phases SOD and GIS. This was also predicted from our general set, where silica and alumina atoms highly influence each other. Changing the values of these parameters will give different zeolites.

A lower pH will affect the solubility of the starting materials. Lowering the OH^- concentration resulted in predominantly crystalline LTA with trace amounts of SOD. However, dissolving sodium aluminate in the low basic concentration required a longer stirring time.

5.3 Conclusion

Translating our previous experiences and knowledge into a new challenge like the synthesis of zeolites is not as simple as it seems. Where zeolites and Pcs are both made up out of SBUs, the SBUs of zeolites are made in solution, unlike for Pcs, where they are pre-assembled. Because the Pc SBUs are pre-assembled, it gives us the opportunity to make small changes, designing them to our needs and then make them into their final polymers. However, the SBUs of zeolites form *in situ* in solution. This creates a double challenge: build the right SBUs for the zeolite *and* implement these small designs, simultaneously. Making the correct SBUs is critical for zeolites, as a small difference in SBU can result in a completely different zeolite. Thus, we altered our approach for making zeolites, to first gain understanding in their different zeolite stages. What we found is that each stage influences the final product. To find the crucial factors in each stage, two sets were used, a generic set and a specific set.

The generic set shows us the influences in the colloidal stage. Here, SDA and water show a correlation due to solubility. The number of T atoms Al, Si and P show correlation, unsurprisingly since these are of importance in multiple stages of a zeolite synthesis. In the precursor stage the number of T atoms influence if a gel can be formed, and in the building block stage the T atoms form the SBUs. Since the T atoms influence two stages, they will show key importance within the synthesis, shown by our Pearson correlation. Besides the colloidal stage, we gain insight into the synthesis stage, where temperature and the duration of synthesis are the most influential factors. The specific set for LTA, however, indicates that the very first stage is influenced by the mixing to ensure a homogeneous mixture.

In general, both sets give us insight into the different steps in a zeolite synthesis, but overall, we conclude that a zeolite synthesis is not determined by one specific stage. If the SBUs in the first stages are wrong, no matter what you try, you can't end up with

a desired zeolite. And with the right building blocks, one can still synthesise a different zeolite. There is little correlation to see in the Pearson diagram, mainly because there are so many factors of influence. The synthesis of a zeolite is very complex. However, steps can be made to gain insight, especially when a bigger database can be made. This larger database would have more types of zeolites, but also zeolites that have certain stages in common to gain insight into formation mechanisms. This would answer many open questions and could possibly give clues to a new zeolite. This chapter is finished, but the work in this field has only begun.

5.4 Experimental Section

Materials and Instrumentation All chemicals used were obtained from Merck and Euro Support and used as received, unless stated otherwise. Autoclaves used were 25 mL stainless steel autoclaves containing Teflon liners. All synthesis methods were obtained from Verified Zeolite Syntheses.

Powder-X-Ray diffraction (XRD) measurements were done on a Rigaku Miniflex II Desktop X-ray Diffractometer using quartz measuring plates. The parameters used were 5-50° range, 0.05° steps at a rate of 5°/minute. All data was interpreted through Rigaku PDXL2 software. FTIR spectra were recorded on a Thermo Scientific Nicolet iS50 FTIR with measurements taken via KBr pellets between 4000-400 cm^{-1} under a resolution of 32 cm^{-1}. All data was collected using the Omnic software package. Scanning Electron Microscopy with energy dispersive X-ray analysis (SEM-EDX) were done on a Verios-640 HRSEM using an accelerating voltage of 5 kV in secondary electron mode. This was done with a working distance of 2-5 mm.

Quality of splits in Extratrees regression and classification were determined by Gini index. Prior to PCA the columns were standardized, no limit for the number of components was chosen. Pearson correlation, principal component analysis and extremely randomized trees regression/classification were all constructed using scikit-learn.

LTA (Linde Type A) synthesis NaOH (0.2892 g, 7.23 mmol, 1 eq.) was dissolved in H_2O (32 mL, 1.78 mol). Then the solution was split in two, and to the first half of this solution, NaO_2:Al_2O_3 (3.3032 g, 40.30 mmol, 5.57 eq.) was added and mixed until dissolved. This formed a clear, pale yellow solution. To the second half of the NaOH solution, Na_2SiO_3 (6.1920 g, 50.73 mmol, 7.02 eq.) was added. This was thoroughly mixed to form a clear solution. Both solutions were poured into the autoclave liner

simultaneously, immediately forming a liquid white gel. The solution was mixed thoroughly for 5 min using a spatula or mechanical stirrer. If aging was done, the final mixture was left at room temperature for a set time period. If no aging was done, the mixture was transferred to an autoclave and put in a preheated oven between 90–175 °C for the desired time (4–16 h). If stirring during hydrothermal synthesis was done, the autoclave was placed in a rotating oven at 16 rpm. All autoclaves were left to cool to room temperature before being filtered and washed with 100 mL H_2O. The product was dried at 110 °C for 16 h to ensure the dehydrated form of the zeolite. The final product was a fine, white powder (3.7909 g).

XRD (2θ°); 7.35, 10.30, 12.60, 16.20, 20.45, 24.15, 26.30, 27.25, 30.10, 30.90, 32.65, 34.30, 36.00, 36.60, 38.10, 40.20, 41.60, 42.25, 42.90, 43.60, 44.35, 47.35, 48.00, 49.95

5.5 References

[1] Sorptive and molecular-sieve properties of a new zeolitic mineral, R.M. Barrer, D.W. Riley, *J. Chem. Soc. Resumed* **1948**, 133–143.

[2] Molecular sieve adsorbents, R.M. Barrer, P.J. Denny, E.M. Flanigen, *Molecular Sieve Adsorbents*, **1967**, US3306922A.

[3] Application of zeolites in aquaculture industry: a review, Z. Ghasemi, I. Sourinejad, H. Kazemian, S. Rohani, *Rev. Aquac.* **2018**, *10*, 75–95.

[4] Phthalocyanines and some current applications, Y. Yilmaz, *Phthalocyanines and Some Current Applications*, BoD – Books On Demand, **2017**.

[5] Towards the rational design of efficient organic structure-directing agents for zeolite synthesis, M. Moliner, F. Rey, A. Corma, *Angew. Chem. Int. Ed.* **2013**, *52*, 13880–13889.

[6] Zeolite types and structures, R.W. Broach, in *Zeolites Ind. Sep. Catal.*, John Wiley & Sons, Ltd, **2010**, pp. 27–59.

[7] Nucleation of FAU and LTA zeolites from heterogeneous aluminosilicate precursors, M.D. Oleksiak, J.A. Soltis, M.T. Conato, R.L. Penn, J.D. Rimer, *Chem. Mater.* **2016**, *28*, 4906–4916.

[8] The zeolite conundrum: Why are there so many hypothetical zeolites and so few observed? A possible answer from the zeolite-type frameworks perceived as packings of tiles, V.A. Blatov, G.D. Ilyushin, D.M. Proserpio, *Chem. Mater.* **2013**, *25*, 412–424.

[9] Needs and trends in rational synthesis of zeolitic materials, Z. Wang, J. Yu, R. Xu, *Chem. Soc. Rev.* **2012**, *41*, 1729–1741.

[10] Verified syntheses of zeolitic materials, S. Mintova, A. Ristić, M. Rangus, N. Novak Tušar, *Verified Syntheses of Zeolitic Materials*, Synthesis Commission Of The International Zeolite Association, S. l., **2016**.

[11] Pearson correlation coefficient, J. Benesty, J. Chen, Y. Huang, I. Cohen, in *Noise Reduct. Speech Process.* (Eds.: I. Cohen, Y. Huang, J. Chen, J. Benesty), Springer, Berlin, Heidelberg, **2009**, pp. 1–4.

[12] Comparison of values of Pearson's and Spearman's correlation coefficients on the same sets of data, J. Hauke, T. Kossowski, *Quaest. Geogr.* **2011**, *30*, 87–93.

[13] Extremely randomized trees, P. Geurts, D. Ernst, L. Wehenkel, *Mach. Learn.* **2006**, *63*, 3–42.

[14] Effect of agitation on the synthesis of zeolite beta and its synthesis mechanism in absence of alkali cations, L. Ding, Y. Zheng, Z. Zhang, Z. Ring, J. Chen, *Microporous Mesoporous Mater.* **2006**, *94*, 1–8.

[15] LTA and ion-exchanged LTA zeolite membranes for dehydration of natural gas, S. Shirazian, S.N. Ashrafizadeh, *J. Ind. Eng. Chem.* **2015**, *22*, 132–137.

[16] Preparation and characterization of Na-LTA zeolite from Tunisian sand and aluminum scrap, H. Tounsi, S. Mseddi, S. Djemel, *Phys. Procedia* **2009**, *2*, 1065–1074.

[17] Zeolites upon heating: Factors governing their thermal stability and structural changes, G. Cruciani, *J. Phys. Chem. Solids* **2006**, *67*, 1973–1994.

[18] Linking synthesis and structure descriptors from a large collection of synthetic records of zeolite materials, K. Muraoka, Y. Sada, D. Miyazaki, W. Chaikittisilp, T. Okubo, *Nat. Commun.* **2019**, *10*, 4459.

Appendix - The supporting information for Chapter 5

Database

Table 2 shows the dataset used in this research. It states the name of the zeolite; crystallisation time in hours; crystallisation temperature in °C; crystallisation agitation in rounds per minute; gel aging time in hours; batch composition, indicating the ratios between the T atoms in the framework: SDA: solvent. The solvent is often water.

Table 2. Database of the zeolites

Zeolite	SDA	Cryst. t (h)	Cryst. T (°C)	Cryst. Ag. (rpm)	Si T atom ratio	Al T atom ratio	P T atom ratio	Gel ageing (h)	Li^+	Na^+	K^+	Cl^-	F^-	Br^-	Solvent
Li-ABW	0	72	250	0	50	50	0	0	4.3	1	0	4.3	0	0	154
AEI (AlPO4-18)	2	69	215	60	50	0	50	0	0	0	0	0	0	0	60
Nanosized AEI (AlPO4-18)	6.32	48	100	0	0	50	50	24	0	0	0	0	0	0	186
AEI (SAPO-18) DPEA	1.6	192	160	0	9	49	42	0	0	0	0	0	0	0	50
AEI (SAPO-18) TEA	2	120	215	60	2	48	50	0	0	0	0	0.015	0	0	70
AEL (AlPO4-11)	2.37	18	145	0	0	50	50	0	0	0	0	0	1.8	0	156
AET(AlPO4-8)	1	25	125	0	0	50	50	10	0	0	0	0	0	0	45
AFI (AlPO4-5)	1.6	6	180	0	0	50	50	0	0	0	0	0	1.3	0	425
AFI (SAPO-5)	0.15	3	200	0	16	49	35	1.5	0	0	0	0	0	0	13
AFI (SSZ-24)	15	168	150	0	100	0	0	0	0	0	10	0	0	0	4400
AFO (nanosized AlPO-41)	2.8	24	180	1	0	50	50	0	0	0	0	0	0	0	25
AFO (SAPO-41)	4	264	180	0	3	51	46	0	0	0	0	0	0	0	58.2
ANA (Analcime)	6.1	24	200	0	68	32	0	0	0	9	0	0	0	0	380
AST (AlPO4-16)	1	24	150	0	0	50	50	0	0	0	0	0	1	0	60
BEA (Beta)	25	20	135	60	93	7	0	0	0	3.94	2	2.9	0	0	750
CAN (cancrinite)	0	48	200	0	50	50	0	0	0	196	0	0	0	0	1386
CDO (CDS-1)	3.41	240	150	0	100	0	0	0	0	0	0.015	0	0	0	16.2
CHA (chabazite)	0	96	95	0	68	32	0	0	0	0.34	4	0	0	0	224
CHA (SSZ-13)	20	96	160	0	93	7	0	0	0	20	0	0	0	0	4400
CHA (SAPO-34)	2.09	24	200	0	21	47	32	0	0	0	0	0	0	0	66
CHA (SAPO-44)	1.9	48	190	0	18	48	34	0	0	0	0	0	0	0	63

Table 2. Database of the zeolites (cont.)

Zeolite	SDA	Cryst. t (h)	Cryst. T (°C)	Cryst. Ag. (rpm)	Si T atom ratio	Al T atom ratio	P T atom ratio	Gel ageing (h)	Li^+	Na^+	K^+	Cl^-	F^-	Br^-	Solvent
EAB (TMA-E)	10	336	80	1	74	26	0	0	0	6	0	0	0	0	500
EDI (Barrer K-F)	0	576	80	1	50	50	0	0	0	0	39.8	0	0	0	378
EDI (Linde type F)	0	96	95	1	50	50	0	0	0	0	10.52	0	0	0	94.5
EDI (nanosized Linde F)	4.74	72	100	0	60	40	0	72	0	0.1	0	0	0	0	244
EMT (EMC-2)	0.87	576	110	0	79	21	0	0	0	4.4	0	0	0	0	140
EMT (Nanosized Na-EMC-2)	0	36	30	0	53	47	0	0	0	4.4	0	0	0	0	222
ERI (Erionite)	0.2	288	100	0	75	25	0	0	0	30	10	0	0	0	350
FAU (Linde type X)	0	8	90	0	55	45	0	0	0	17	0	0	0	0	325
FAU (Silica type X)	0	2	100	0	50.5	49.5	0	0	0	2.75	3.3	0	0	0	122
FAU (Nanosized Linde type Na-X)	0	24	50	0	54	46	0	24	0	18	0	0	0	0	122
FAU (Nanosized Linde type TMA-Y)	11	48	100	0	63	37	0	24	0	0	0	0	0	0	570
FAU (High Si EMC-1)	0.5	192	110	0	79	21	0	0	0	4.2	0	0	0	0	100
FAU (SAPO-37)	2	13	200	0	17	47	36	0	0	0	0	0	0	0	50
FER (ZSM-35)	19.7	240	177	15	87	13	0	0	0	3.7	0	0	0	0	592
GIS (zeolite P)	0	1440	85	0	54	46	0	0	0	5.28	0	0	5.28	0	105.6
IMF (IM-5)	4.5	336	160	100	93	7	0	0	0	22	0	0	0	9	1200
KFI (ZK-5)	0	115	150	0	77	23	0	0	0	0	4.6	0	0	0	160

Table 2. Database of the zeolites (cont.)

Zeolite	SDA	Cryst. t (h)	Cryst. T (°C)	Cryst. Ag. (rpm)	Si T atom ratio	Al T atom ratio	P T atom ratio	Gel ageing (h)	Li^+	Na^+	K^+	Cl^-	F^-	Br^-	Solvent
KFI (High Si)	1	120	150	0	79	21	0	0	0	0	1.15	0	0	0	220
LTA (Linde type A)	0	4	99	0	50	50	0	0	0	6.33	0	0	0	0	128
LTA (nanosized linde type TMA-A)	26.8	168	40	175	50	50	0	0	0	16	0	0	0	0	721
LTA (ZK-4)	8.26	48	100	0	59	41	0	0	0	3.1	0	0	0	0	320
LTA (Zeolite Alpha)	4.74	30	90	0	75	25	0	0	0	2.14	0	0	0	0	120
LTF (LZ-135)	5	240	100	0	71	29	0	0	0	5.6	0	5	0	5	156
LTL (Linde type L)	0	48	175	0	76	24	0	0	0	0	4.7	0	0	0	160
LTL (nanosized Linde type L)	0	20	170	0	73	27	0	40	0	0	10	0	0	0	200
MEL (Nanosized TBA-silicalite-2)	0.3	68	90	0	100	0	0	0	0	0	0	0	0	0	17
MER (Linde W)	0	48	150	0	65	35	0	0	0	0.1	6	0	0	0	100
MFI (High Al-ZSM-5)	0	40	180	0	93	7	0	16	0	0	6.5	0	0	0	958
MFI (Nanosized TPA-silicalite-1)	9	30	90	0	100	0	0	0	0	0	0	0	0	0	480
MFI (template free ZSM-5)	0	35	150	200	96	4	0	0	0	20	0	0	0	0	2250
MFI (silicalite-1)	0.08	336	200	0	100	0	0	0	0	0	0	0	0.04	0.08	20
MFS (ZSM-57)	0	168	160	43	98	2	0	0	0	0.5	0	0	0	0	40
MOR (mordenite)	0	24	170	0	90	10	0	0	0	12	0	0	0	0	780

Table 2. Database of the zeolites (cont.)

Zeolite	SDA	Cryst. t (h)	Cryst. T (°C)	Cryst. Ag. (rpm)	Si T atom ratio	Al T atom ratio	P T atom ratio	Gel ageing (h)	Li^+	Na^+	K^+	Cl^-	F^-	Br^-	Solvent
MOZ (ZSM-10)	0.06	360	100	60	88	12	0	0	0	0	0.73	0	0	0	29.5
MSE (MCM-86)	0.1	384	160	0	88.6	11.4	0	0	0	0	0.375	0	0	0	30
MTN (ZSM-39)	16	336	200	0	100	0	0	0	0	30	0	16	0	0	3387
MTT (SSZ-32)	0.04	144	170	35	93.56	6.44	0	0	0	0	0.04	0	0	0	6.07
MTT (ZSM-23)	46.2	50	180	30	97	3	0	0	0	52	0	0	0	0	4610
MTW (ZSM-12)	20	144	140	0	97	3	0	0	0	20	0	0	0	20	2000
MWW (MCM-22)	15	168	150	60	94	6	0	0	0	5.4	0	0	0	0	1347
OFF (Linde type T)	0	168	140	0	78	22	0	24	0	8.32	2.5	0	0	0	175
OFF (offretite)	1.73	20	160	0	79	21	0	0	0	6	2	3.46	0	0	324
PAU (ECR-18)	2.8	384	100	0	76	24	0	0	0	1.2	1.4	0	0	0	140
PHI (Phillipsite)	0	8	100	168	72	28	0	0	0	13.9	7	0	0	0	325
PHI (High Al Phillipsite)	0	168	100	0	67	33	0	24	0	3.06	0.88	0	0	0	82.7
RHO (High silica Rho)	0.5	192	110	0	80	20	0	0	0	3.6	0	0	0	0	100
RSN (RUB-17)	0.08	240	180	0	78	0	0	0	0	0	0.5	0	0	0	44
SOD (NaBr sodalite)	0	24	95	0	50	50	0	0	0	20	0	0	0	0	144
STI (TNU-10)	4.5	168	160	100	88	12	0	0	0	30	0	0	0	0	1200
STT (SSZ-23)	0.51	264	150	60	100	0	0	0	0	0	0	0	0.51	0	0
TON (ZSM-22)	27.3	72	160	400	95	5	0	0	0	0	20.8	0	0	0	3588
TUN (TNU-9)	4.5	336	160	100	95	5	0	0	0	22	0	0	0	0	1200
VFI (VPI-5 DPA)	1	4	142	0	95	5	0	2	0	0.5	0	0	0	0.5	40
VFI (VPI-5 TBA)	1.12	20	150	0	0	50	50	2	0	0	0	0	0	0	50
SUZ-4	6.2	96	150	20	86	14	0	0	0	0	14.7	0	0	0	681

Summary

This thesis discusses the rational design of catalysts for sustainable oxidative chemistry using tailored confined spaces where molecules can react selectively. Several categories of confinement effects in each catalyst are presented, and insight is provided into the activation of molecular oxygen. The different techniques of design are applied to multiple challenges, from oxidative reactions themselves to a completely new type of catalyst.

Chapter 1 outlines the growing need for changing our global large-scale production to a more sustainable local one. The shift in production methods forces us to use different reactants, techniques and catalysts. This also opens opportunities for redesigning more sustainable processes, keeping the 12 principles of green chemistry in mind. In general, an optimal reaction has a high yield, and one can aim for this by controlling the reaction through catalysis. The need for good catalysts is especially important in the case of oxidation reactions. Oxygen is hard to activate, often leading to poor selectivity. By selecting the right oxidative agent, one can influence the control in the reaction. Oxygen is the most logical choice, being cheap, freely available and abundant. However, activating oxygen requires a catalyst. A catalyst can also influence control over reactions. We take a closer look at the types of confinements found in heterogeneous catalysts. Confinement effects can increase the activity of the catalyst in three ways; geometric, chemical and space confinement. Tuning the catalyst and oxidative agent can improve the yield of the reaction as well as the selectivity of the products.

Chapter 2 describes the allylic oxygenation of alkenes where the double bond is maintained while introducing a new alcohol or carbonyl functional moiety. It seems a straightforward reaction, requiring oxygen as a widely available reagent. However, oxygen has a high activation barrier due to a resonance stabilisation. Once this barrier is overcome, free-radical oxygen leads to unwanted over-oxidation products. We

studied the oxidation of cyclohexene with oxygen under mild conditions, screening nine different transition-metal catalysts supported on nitrogen-doped carbon (N:C). The Co/N:C and the Cu/N:C gave 70–80% conversion and 40–50% selectivity towards the cyclohexene-2-one. Optimisation of these catalysts gave >85% conversion, with >60% selectivity to the allylic ketone, at 70 °C and 10 bar oxygen pressure. Scanning electron microscopy, X-ray photoelectron spectroscopy, and X-ray diffraction studies showed that the active particles have a cupric oxide/cuprous oxide core/shell structure, with a correspondingly high TOF of ca. 1500 h^{-1}. Control experiments showed free-radical pathways for oxidation in most cases. Surprisingly, Cu/N:C did not involve free-radicals in solution during this oxidation. This gives a more selective pathway, with less over-oxidation.

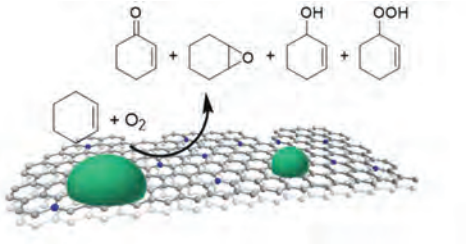

Chapter 3 shows the concept of a catalyst design inspired by nature. The heme porphyrin molecule can easily activate dioxygen, making it a near perfect oxidation catalyst, operating at ambient conditions using only a single iron atom per site. The ease of which heme activates oxygen has proven difficult to mimic in industrial catalysts. We synthesised phthalocyanines (Pcs) which are highly stable macrocycles and synthetic analogues of porphyrin. Pcs are made by cyclisation of phthalonitrile in the presence of an organic base. We present a one-step synthesis route to an empty Pc (H_2PcH_{16}), their corresponding Mn, Fe, Co, Ni, Cu and Zn complexes ($MPcH_{16}$) as well as their fluorinated analogues ($MPcF_{16}$). Furthermore, we present a new and facile protocol for making the same $MPcH_{16}$ complexes by metalation of an empty H_2PcH_{16}. The new procedure for the $MPcH_{16}$ involves the insertion of a metal ion into an empty

H_2PcH_{16}. This would be an ideal synthesis method for synthesising a variety of $MPcH_{16}$ catalysts.

These $MPcF_{16}$ are interesting because the fluorinated ring creates a 'protective shell' around the complex that can prevent its oxidation and degradation. As an added bonus, the fluorinated metal-Pc complexes are much more soluble in several organic solvents.

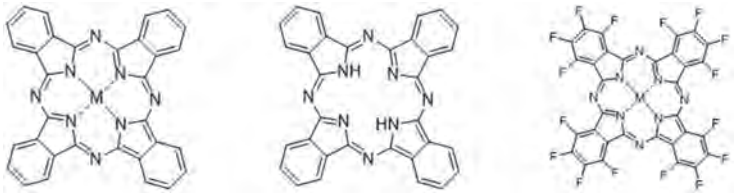

In **Chapter 4** we highlight the drawback of phthalocyanine (Pc); the problem of their multi-electron π-system causing molecular stacking, preventing access to the metal centre. This problem is addressed by polymerizing the Pc complexes.

We show the concept and application of designed materials, using Pcs as building blocks, connecting them with linkers, to create extremely well-defined catalysts. Several polymers were designed and developed, by changing the metal of the Pc and/or linkers, allowing the creation of an unique polymer with specific catalytic properties. By changing the metal used for the Pc single-atom centres and changing the linker length types, the distance is controllable between the metal sites and their surrounding environment. We control in every single step which metal is used for the Pc and the linker length used (oxalyl chloride (C_2), adipoyl chloride (C_6), terephthaloyl chloride (C_{TPA}) and sebacoyl chloride (C_{10})). This gives full control over the identity and spacing of the catalytic sites.

The new materials are used in the oxygen reduction reaction (ORR) as a case study. ORR showed that the shorter the distance between metal centres, the better the activity of the material is. This is attributed to the solvation shell. The metal ions can

polarise the water molecules to accommodate charges on the surface. The solvation shell usually has a reach of 4–5 Å, meaning that two Pcs within distance of each other, will have overlapping solvation shells. This increase in ORR activity is seen with the shorter C_0 and C_2 linkers.

Chapter 5 introduces a new challenge, the design of zeolite catalysts. These crystalline microporous materials are known for their confinement effects and are composed of T atoms, Si and Al most commonly. Millions of theoretical zeolites have been generated, however a small 300 have been synthesised. This is due to poor understanding of how they are made. An industrial partner was interested in using our previously made synthesis approach from chapter 4 for designed zeolite synthesis. However, zeolite synthesis is composed of multiple stages, involving the mixing of the reactants, forming colloids and creating a gel to obtain a crystalline zeolite. This ruled out our mix and match design approach, and so a new approach was designed.

To understand their synthesis two directions were taken. The first making a generic database containing of 76 zeolites. This is used to analyse known zeolites and gain generic synthesis results. The second direction is of a specific zeolite synthesis set.

The generic set shows us the important values in the colloid formation, showing correlations between different T atoms and the solvent and structure directing agent (SDA) amounts. Besides this, it shows the importance of the time and temperature during the synthesis. The specific set gives parameters for the synthesis of Linde Type A (LTA). Here, the mixing of the reactants is shown to be a key element in obtaining LTA and reducing or eliminating the presence of a competing phase. Our results of combined different fields within chemistry, both experimental and computational, show that together they can give us the knowledge to move forward into designing new zeolites.

Samenvatting

Dit proefschrift bespreekt het rationele ontwerp van katalysatoren voor duurzame oxidatieve chemie met behulp van op maat gemaakte ruimtes waar moleculen selectief kunnen reageren. Er worden verschillende categorieën van confinement effecten gepresenteerd, en er wordt inzicht verschaft in de activering van moleculaire zuurstof. De verschillende ontwerptechnieken voor katalysatoren worden toegepast op meerdere uitdagingen, van oxidatieve reacties tot een volledig nieuw type katalysator.

Hoofdstuk 1 schetst de groeiende behoefte om onze wereldwijde grootschalige productie te veranderen naar een duurzamere lokale productie. De verschuiving in productiemethoden dwingt ons om verschillende reactanten, technieken en katalysatoren te gebruiken. Dit biedt ook kansen voor het herontwerpen van duurzamere processen, rekening houdend met de 12 principes van groene chemie. Over het algemeen heeft een optimale reactie een hoog rendement, en dit kan worden behaald door de reactie via katalyse te sturen. De behoefte aan goede katalysatoren is vooral belangrijk bij oxidatie reacties. Zuurstof is moeilijk te activeren, wat vaak leidt tot een slechte selectiviteit. Door het juiste oxidatie middel te kiezen, kan men de controle in de reactie beïnvloeden. Zuurstof is de meest logische keuze, aangezien dit goedkoop, vrij verkrijgbaar en overvloedig is. Voor het activeren van zuurstof is echter een katalysator nodig, die de controle over de reactie kan beïnvloeden. Tevens kijken we naar de soorten confinement ruimtes die in heterogene katalysatoren worden aangetroffen. Deze confinement effecten kunnen de activiteit van de katalysator op drie manieren verhogen; geometrische, chemische en ruimtebeperking. Het afstemmen van de katalysator en het oxidatie middel kan zowel de opbrengst van de reactie als de selectiviteit van de producten verbeteren.

Hoofdstuk 2 beschrijft de allylische oxidatie van alkenen waarbij de dubbele binding behouden blijft terwijl een nieuwe alcohol of carbonyl functionele groep wordt geïntroduceerd. Het lijkt een eenvoudige reactie, waarbij vrij verkrijgbare zuurstof

nodig is reagens. Zuurstof heeft echter een hoge activeringsbarrière vanwege een resonantiestabilisatie. Zodra deze barrière is overwonnen, produceert zuurstof vrije radicalen die tot ongewenste overoxidatieproducten leiden. We hebben de oxidatie van cyclohexeen met zuurstof onder milde omstandigheden bestudeerd, waarbij we negen verschillende overgangsmetaalkatalysatoren hebben gescreend op een met nitrogen-doped carbon (N:C). De Co/N:C en de Cu/N:C gaven 70-80% omzet en 40-50% selectiviteit naar het cyclohexeen-2-on. Optimalisatie van deze katalysatoren gaf> 85% omzet, met> 60% selectiviteit voor het keton, bij 70 ° C en 10 bar zuurstof. Scanning-elektronenmicroscopie, röntgenfoto-elektronspectroscopie en röntgen-diffractie studies toonden aan dat de actieve deeltjes een cuprioxide/cupro-oxide kern/schilstructuur hebben, met een overeenkomstig hoge TOF van ongeveer 1500 h^{-1}. Controle-experimenten laten zien dat in de meeste gevallen vrije radicalen voor oxidatie zorgen. Verrassend genoeg betrof Cu/N: C geen vrije radicalen in oplossing tijdens deze oxidatie. Dit geeft een meer selectieve route, met minder overoxidatie.

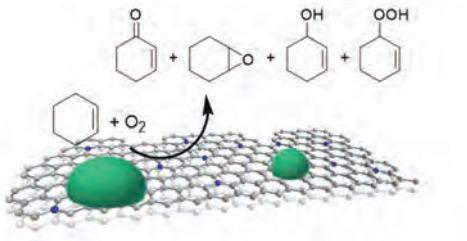

Hoofdstuk 3 toont het concept van een katalysator ontwerp geïnspireerd door de natuur. Het heem porfyrine molecuul kan gemakkelijk zuurstof activeren, waardoor het een bijna perfecte oxidatie katalysator is, die bij milde omstandigheden werkt met slechts één ijzeratoom als actief deeltje. Het gemak waarmee heem zuurstof activeert, is moeilijk na te bootsen in industriële katalysatoren. We hebben ftalocyanines (Pcs) gesynthetiseerd, wat zeer stabiele macrocycli en synthetische analogen van porfyrine zijn. Pcs worden gemaakt door cyclisatie van ftalonitril in aanwezigheid van een organische basis. We presenteren een eenstaps synthese route naar een lege Pc (H_2PcH_{16}), hun overeenkomstige Mn, Fe, Co, Ni, Cu en Zn-complexen ($MPcH_{16}$) en hun gefluoreerde analogen ($MPcF_{16}$). Verder presenteren we een nieuw en gemakkelijk protocol voor het maken van dezelfde $MPcH_{16}$-complexen door een metaal te zetten

in een lege H_2PcH_{16}. Dit zou een ideale route zijn voor het synthetiseren van een breed scala aan $MPcH_{16}$-katalysatoren.

Deze MPcF16 zijn interessant omdat de gefluoreerde ring een 'beschermende schil' rond het complex vormt die oxidatie en degradatie kan voorkomen. Als extra bonus zijn de gefluoreerde MPc complexen veel beter oplosbaar in verschillende organische oplosmiddelen.

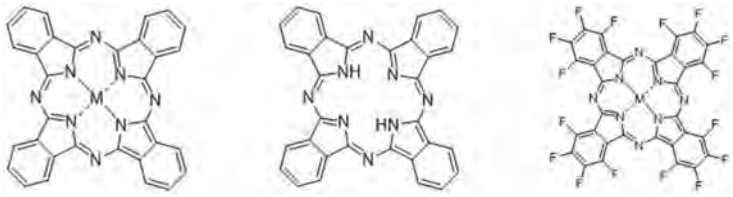

Hoofdstuk 4 belicht het nadeel van ftalocyanine (Pc); het probleem van hun multi-elektronen π-systeem dat moleculaire stapeling veroorzaakt en toegang tot het metalen centrum verhindert. Dit probleem wordt aangepakt door de Pc complexen te polymeriseren.

We laten het concept en de toepassing van ontworpen materialen zien, waarbij Pcs als bouwstenen worden gebruikt en ze met linkers worden verbonden om goed gedefinieerde katalysatoren te creëren. Er werden verschillende polymeren ontworpen en ontwikkeld door het metaal van de Pc en/of linkers te veranderen, waardoor een uniek polymeer met specifieke katalytische eigenschappen werd gecreëerd. Door het metaal atoom te veranderen van de Pc centra en door de lengte van de linker te veranderen, is de afstand tussen de metalen en hun omgeving controleerbaar. We controleren in elke stap welk metaal wordt gebruikt voor de Pc en de gebruikte linkerlengte (oxalylchloride (C_2), adipoylchloride (C_6), tereftaloylchloride (C_{TPA}) en sebacoylchloride (C_{10})). Dit geeft volledige controle over de identiteit en de afstand tussen de katalytische centra. De nieuwe materialen worden gebruikt in de zuurstofreductiereactie (ORR) als case study. ORR toonde aan dat hoe korter de afstand tussen metaalcentra, hoe beter de activiteit van het materiaal is. Dit wordt

toegeschreven aan de solvent schil. De metaalionen kunnen de watermoleculen polariseren om ladingen op het oppervlak op te vangen. De solvent schil heeft meestal een bereik van 4–5 Å, wat betekent dat twee Pcs die op afstand van elkaar liggen, overlappende solvent schillen hebben. Deze toename in ORR-activiteit wordt gezien met de kortere C_0- en C_2-linkers.

Hoofdstuk 5 introduceert een nieuwe uitdaging, het ontwerp van zeoliten. Dit kristallijne microporeuze materiaal staat bekend om hun confinement effect en bestaat meestal uit T-atomen, Si en Al. Miljoenen theoretische zeolieten zijn gegenereerd, maar een kleine 300 zijn gesynthetiseerd. Dit komt doordat het onbekend is hoe ze precies worden gemaakt. Een industriële partner van ons was geïnteresseerd in het gebruik van onze eerder gemaakte synthese strategiën uit hoofdstuk 4 voor de zeolieten. Zeoliet synthese bestaat echter uit meerdere fasen, waarbij de reactanten worden gemengd, colloïden en een gel wordt gevormd om als laatste een kristallijn zeoliet te verkrijgen. Dit sloot onze mix en match ontwerp uit, en dus werd een nieuwe aanpak ontworpen.

Om zeoliet synthese te begrijpen, werden er twee richtingen uitgegaan. De eerste is het maken van een generieke database met 76 zeolieten. Dit wordt gebruikt om reeds bekende zeolieten te analyseren en generieke synthese resultaten te verkrijgen. De tweede richting is die van een specifieke zeoliet synthese set.

De generieke set toont ons de belangrijke waarden in de colloïdevorming en toont correlaties tussen verschillende T-atomen en de hoeveelheden oplosmiddel en structure directing agent (SDA). Daarnaast toont het het belang aan van de tijd en temperatuur tijdens de synthese. De specifieke set geeft parameters voor de synthese van Linde Type A (LTA). Hier wordt aangetoond dat het mengen van de reactanten het belangrijkste element is bij het verkrijgen van LTA en het verminderen of elimineren van de aanwezige concurrerende fases. Onze resultaten van gecombineerde verschillende velden binnen de chemie, zowel experimenteel als computationeel, laten zien dat ze ons samen de kennis kunnen geven om verder te gaan met het ontwerpen van nieuwe zeolieten.

Acknowledgements

After almost 9 years at the University of Amsterdam my time here has come to an end. In those years my passion for chemistry has only grown. I wouldn't have expected back then that I would be standing here today, holding my finished doctoral thesis. With the ending of my PhD, I must thank a few people who have helped me throughout the last four years. I wouldn't have made it to the point where I am now, and all of you have helped in some way or another in the formation of this thesis. May I have forgotten somebody, my apologies in advance.

First of all, I would like to thank my promotor Prof. **Gadi Rothenberg**, you gave me the opportunity to do a PhD in your group. I remember standing in your office during the bachelor's course, unsure if I could pass your class, and you giving me the confidence to do so. You have sparked in me an interest and passion for heterogeneous catalysis, so much so that I wanted to follow another course of yours in my masters. This led to a very successful masters project in your group, and within a month of starting that project, an offer for a PhD position. Over the years you made me challenge myself, given me the opportunity to travel the world and shaped me into a better scientist. Your dedication to your work is admirable and the number of stories you can tell is impressive. Thank you for believing in me, letting me make my own choices and giving me the freedom in my PhD to develop.

Dr. **David Dubbeldam**, even though you were more in the background, your involvement is not diminished because of it. Your critical eye on my chapters, but also the friendly words in meetings make you a good supervisor. Thank you for all the help you provided.

I want to express my appreciation to all my committee members; Prof. **E.J. Meijer**, Prof. **J.H. van Maarseveen**, Prof. **G.J.M. Gruter**, Prof. **S. Woutersen**, Prof. ir. **L. Lefferts** and Prof. **S. Calero**. Thank you for taking a detailed and thorough look at

my thesis. The comments and questions I have received will only make me a better scientist.

Amanda, Klaas Jan, Ning, **Shiju** and **Stefania**, I want to acknowledge you for all the interesting questions, guidance and useful suggestions during group meetings. You kept me on my feet and shaped me into a better scientist.

Elad Gross and **Hillel**, I want to say thank you for the pleasant and fruitful collaboration. I'm confident we will be able to publish the data soon. I enjoyed the many zoom calls we had discussing the interesting FTIR results. **Karen Wilson** and **Adam Lee** thank you for the valuable international experience. I enjoyed my time in your group a lot and was welcomed with open arms. I wish you all the best of success in your new lab with your growing group. **Raimond Bonné** and the rest of **Euro Support**, I enjoyed the small peek you gave me into the catalyst fabrication industry. I've enjoyed our conversations and very much appreciate all the useful help you offered along the way. **Ed**, thank you for going out of your way to measure my compounds. I know measuring these things wasn't easy and you always gave it your best shot!

During my PhD I had the pleasure of being in the HetCat group. I've made so many friends along the way, and I can't express my gratitude enough how supportive everybody has been along the ride. **Marjo**, I've enjoyed our conversations and all the advice you have given me. Your presence every Tuesday, and the astonishing amount of knowledge you have are missed. **Paul**, for the last few months I invaded your office and I enjoyed those last months a lot. You are warm and friendly to everybody coming in with a computer, stirring plate or other electronic problem. Besides your skills I also found out you have a great sense for humour, and I'll miss our little chit chats. **Norbert**, whatever the problem is in the lab, you can fix it just with an O-ring. You have taught me so much in the lab, or how to fix something in my house. Thank you for the amazing friendship we have developed, the different views we have gave so many interesting conversations. I will miss our jokes and talks, without you and Paul, the lab wouldn't be the same.

Jasper, you and I go way back, we met as high school students trying out a day in university (which is almost 10 years ago) and now we both finish our PhDs. I'm happy I can count you as one of my best friends, you have always supported me and helped me with everything. Thank you for everything and I hope we will stay in touch. **Maria**, I loved our little chats with some tea and a snack. I admire the calm way you approach problems. I wish you all the best in your undoubtedly great career! **Yuan**, hiding behind your computer every morning to greet me was always a highlight. I've missed our morning chats ever since you finished. **Thierry**, I don't think I have ever seen you on a bad day. You are always cheerful and ready to help anybody. Great qualities to have and I hope they get you far in life. **Pieter**, every single group meeting presentation I had, you later approached me with a paper related to what I talked about. I've enjoyed the time with you and the many great inputs you gave. **Martijn**, you were my fumehood neighbour for the last few months, and I've enjoyed our chats. **Sang Ho**, thank you for introducing me to the amazing Korean cuisine. I enjoyed the talks and many laughs I had with you. **Yiwen**, **Wei**, **Eric**, **Andreea**, **Bruno, Kamilla**, **Layla**, **Sheetal**, **Ishan**, **Johan**, **Edwin** and **Anand** thank you for the many lunches and moments we had together. I've valued all the input you gave me and the friendships developed over time. **Noë**, you have done so many projects in our group, you are part of the standard crew. Thank you for being my paranymph! The more I got the know you, the more shared interest we found to have. You are always up for a chat, a helping hand or just making me laugh.

To all my former master students; **Wowa**, I wish you all the best with your PhD. **Florentine**, I've enjoyed our time working together. Always in a good mood, happy to help with anything and try a lot of different synthesis. I know you are doing great at your PhD! **Peter**, you worked independently and smartly, and we will publish your work soon. You really went the extra mile and travelled to Israel to start the collaboration with Elad and Hillel. I cherish the friendship we have developed and I have faith you'll bring your PhD to a good end, I'll be here if you need anything! **Connor**, apologies for the many, *many* jokes you had to endure about Brexit and the

veganism. The fact you were still willing to do a PhD in our group shows the huge amount of perseverance you have in you. You are hardworking and ready to tackle any obstacle thrown your way. I cherish both the friendship we have and that you are my paranymph, I truly hope you enjoy your PhD. **Fran**, I've enjoyed our time together in the lab. Figuring out how that new rotating oven works, tackling a completely new subject together; zeolites, and then corona happened. Yet, you managed to power through and finish your masters during this weird time, and even start a PhD also within our group. Keep up the good work you have been doing so far. **Yi**, you fit right in our group and were always happy for a chit-chat. I wish you all the best in your future. **Janita**, also you were brave enough to face the zeolite challenge with me. I have immense respect for the work you have done, working independently and powering through while corona happened. Good luck finishing your masters. **Marco**, you were the company I had for the final moments in my thesis. We definitely had a lot of hiccups, but your catalysts are very promising. Keep questioning everything you do, and you will make a great scientist. To my bachelor students; **Emma**, **Michelle**, **Sebastiaan**, **Mees** and **Pim**, thank you for all the time and effort you all have put in.

Thank you to all other students, PhD friends from other groups and others. Special thanks to **Dylan**, I'm happy I can count you as a friend, we share the same type of humour and during game nights with you, Jasper and Peter, we have made some memories. Good luck in your PhD. **Erik**, we go way back to our bachelor degree, and I value our friendship. Wherever you may end up, I know you'll make the best out of it. **Evi**, **Eva**, **Xander**, **Didjay**, **Marianne**, **Lennard**, **Vikash**, **Joris**, **Koen**, **Niels S.**, **Nathan**, **Wouter**, **Pavel**, **Roelof**, **Rick, Jeremy**, **RJ** and **Stuart**. I enjoyed our friendships!

Thank you to some non-chemistry friends; **Nienke**, **Elke**, **Elena** and **Meaghan**. I'm amazed and proud where all of us have gone, and yet we managed to stay in touch. Thank you for always showing interest in my work, encouragement and love you gave, and I wish you girls all of the best.

Thanks to **my parents**, **Niels** and **family** who always gave a listening ear to whatever problems I encountered. You have made it possible for me to achieve all of this. Thank you for supporting me and always pushing me to achieve higher.

And last but not least, **Alex**; even though you haven't been present in my entire PhD, you have made a huge impact on it. Your never-ending support and belief in me helped me to keep writing this thesis. You have made me smile, helped me with my English and pushed me to stay on track. Thank you for making that final year easier for me.

List of publications

[1] Covalent structured catalytic materials containing single-atom metal sites with controllable spatial and chemical properties: concept and application, **I.M. Denekamp**, C. Deacon-Price, Z. Zhang, G. Rothenberg, *Catal. Sci. Technol.* **2020**, *10*, 6694–6700.

[2] A simple synthesis of symmetric phthalocyanines and their respective perfluoro and transition-metal complexes, **I.M. Denekamp**, F.L.P. Veenstra, P. Jungbacker, G. Rothenberg, *Appl. Organomet. Chem.* **2019**, *33*, e4872.

[3] Selective Catalytic Oxidation of Cyclohexene with Molecular Oxygen: Radical Versus Nonradical Pathways, **I.M. Denekamp**, M. Antens, T.K. Slot, G. Rothenberg, *ChemCatChem* **2018***, 10*, 1035–1041.

[4] Boosting the Supercapacitance of Nitrogen-Doped Carbon by Tuning Surface Functionalities, J. Biemolt, **I.M. Denekamp**, T.K. Slot, G. Rothenberg, D. Eisenberg, *ChemSusChem* **2017**, *10*, 4018–4024.

[5] Hyphenated and comprehensive liquid chromatography x gas chromatography x mass spectrometry for the identification of Mycobacterium tuberculosis, M.P.B. Mourão, **I.M. Denekamp**, S. Kuijper, A.H.J. Kolk, H.G. Janssen, *J. Chromatogr. A* **2016**, *1439*, 152–160.

Scientific contributions

Oral presentation, NCCC 2020, Noordwijkerhout, The Netherlands. "Designed phthalocyanine polymers as single-site catalysts".

Poster presentation, NCCC 2018, Noordwijkerhout, The Netherlands. "Air oxidation of cyclohexene: radical vs non-radical pathways".

Poster presentation, CHAINS 2018, Veldhoven, The Netherlands. "Catalytic non-radical air oxidation of cyclohexene". Received the best poster prize.

Poster presentation, NCCC 2017, Noordwijkerhout, The Netherlands. "Understanding capacitance on nitrogen-doped carbons".

Poster presentation, NanoCity 2015, Amsterdam, The Netherlands. "Can we use biomarkers in sputum for early diagnosis of Tuberculosis?".

Overview of authors' contributions

Chapter 1: Introduction

I.M. Denekamp	Wrote the chapter. Explained the need for sustainable production, by using designed catalysts for specific reactions. Describes how to optimise oxidative catalyst.
G. Rothenberg:	Reviewed the manuscript and gave suggestions and feedback for improvements.
D. Dubbeldam:	Reviewed the manuscript and gave suggestions and feedback for improvements.

Chapter 2: Selective catalytic oxidation of cyclohexene with molecular oxygen

I.M. Denekamp	Redid and improved the experimental work, processed the data, suggested mechanism and wrote the paper/manuscript.
M. Antens	Synthesised catalysts, performed experimental work.
T. Slot	Supervised M. Antens.
G. Rothenberg	Overall supervision of the project. Reviewed the manuscript and made suggestions for improvement.

Chapter 3: A simple synthesis of phthalocyanines as oxidative catalyst

I.M. Denekamp	Developed synthesis methods. Planned and performed the experiments, supervised F.L.P. Veenstra and P. Jungbacker. Processed the data and wrote the paper/manuscript.
F.L.P. Veenstra	Performed experimental work and analysis.
P. Jungbacker	Performed experimental work and analysis.
G. Rothenberg	Overall supervision of the project. Reviewed the manuscript and made suggestions for improvement.

Chapter 4: Designing catalytic polymers with controllable spatial and chemical properties

I.M. Denekamp	Developed the synthesis for the polymers. Supervised C. Deacon-Price. Analysed and processed the data and wrote the paper/manuscript.
C. Deacon-Price	Performed experimental work.
Z. Zhang	Performed EXAFS experiments.
G. Rothenberg	Overall supervision of the project. Reviewed the manuscript and made suggestions for improvement

Chapter 5: Towards rational design of zeolites

I.M. Denekamp	Performed experiments, supervised F. Pope and J. L. Vermeulen. Analysed, processed and combined the data and wrote the chapter.
F. Pope	Performed laboratorial experiments.
J.L. Vermeulen	Performed computational experiments.
G. Rothenberg	Overall supervision of the project. Reviewed the manuscript and made suggestions for improvement

Ilse Denekamp was born in Purmerend, The Netherlands in 1994. She received her BSc in Chemistry from the Vrije Universiteit and the Universiteit van Amsterdam (UvA) in 2015, followed by an MSc in Analytical Sciences in 2017. She then joined the Heterogeneous Catalysis & Sustainable Chemistry group as a PhD student under the supervision of Prof. Gadi Rothenberg and Dr. David Dubbeldam. During her PhD, the results of which are summarised in this book, Denekamp studied selective oxidative reactions and designed novel pathways to single-site catalytic materials. She also spent three months working with Prof. Karen Wilson and Prof. Adam Lee at the Royal Melbourne Institute of Technology, supported by grants from the Stichting Amsterdams Universiteitsfonds and the Catharine van Tussenbroekfonds. Denekamp's research was recognised by several publications and awards, including the Unilever Research Prize in 2017 and the Best Poster Award at CHAINS 2018.